RESEARCH

UDOT CONNECTING COMMUNITIES

Utah Department of Transportation - Research Division
4501 South 2700 West, Box 148410 - Salt Lake City, Utah 84114-8410

Report No. UT-11.16

NON-DESTRUCTIVE AND DESTRUCTIVE INVESTIGATION OF AGED-IN-THE-FIELD CARBON FRP-WRAPPED COLUMNS

Prepared For:

Utah Department of Transportation and
New York State Department of
Transportation

Submitted By:

University of Utah
Department of Civil & Environmental
Engineering

Authored By:

Chris P. Pantelides, Ph.D., S.E.
Michael E. Gibbons, M.Sc.
Lawrence D. Reaveley, Ph.D., P.E.

June, 2011

DISCLAIMER

The authors alone are responsible for the preparation and accuracy of the information, data, analysis, discussions, recommendations, and conclusions presented herein. The contents do not necessarily reflect the views, opinions, endorsements, or policies of the New York State Department of Transportation, the Utah Department of Transportation, or the US Department of Transportation. The New York State Department of Transportation and Utah Department of Transportation make no representation or warranty of any kind, and assume no liability therefore.

UDOT RESEARCH & DEVELOPMENT REPORT ABSTRACT

1. Report No. UT-11.16	2. Government Accession No.	3. Recipient's Catalog No.
4. Title and Subtitle NON-DESTRUCTIVE AND DESTRUCTIVE INVESTIGATION OF AGED-IN-THE FIELD CARBON FRP-WRAPPED COLUMNS		5. Report Date June, 2011 6. Performing Organization Code
7. Author Chris P. Pantelides, Ph.D., S.E. Michael E. Gibbons Lawrence D. Reaveley, Ph.D., P.E.		8. Performing Organization Report No.
9. Performing Organization Name and Address University of Utah Department of Civil and Environmental Engineering 122 S. Central Campus Dr. Ste. #204 Salt Lake City, Utah 84112		10. Work Unit No. 11. Contract or Grant No. 09-9230
12. Sponsoring Agency Name and Address Utah Department of Transportation 4501 South 2700 West Salt Lake City, Utah 84114-8410 New York State Department of Transportation State Campus, Albany, New York 12232-0869		13. Type of Report & Period Covered QUARTERLY Apr. 2010 – Jun. 2011 14. Sponsoring Agency Code

15. Supplementary Notes

Project is co-sponsored by the Utah Department of Transportation and the New York State Department of Transportation

16. Abstract

The common practice of applying deicing salts on highway bridges increases the potential of reinforcing steel in these structures to experience extensive corrosion in the decks as well as the substructure. A new rehabilitation method which is believed to arrest the corrosion, restore structural integrity, extend the life, and provide interim safety until replacement at a later time is FRP jacketing. In line with this concept, all the columns of the Highland Drive Bridge at I-80 in Salt Lake City were rehabilitated with carbon FRP composites in June 2000. The present project will evaluate the performance of the carbon FRP composite for two of these columns and its ability to maintain a good bond to the concrete, thus restoring and maintaining the column's capacity after exposure to field conditions for eight years. In addition, the use of a GFRP spiral as a non-corroding column tie will be examined.

17. Key Words	18. Distribution Statement	23. Registrant's Seal
Column repair, column retrofit, bond, corrosion, concrete, FRP	UDOT Research Division 4501 South 2700 West-box 148410 Salt Lake City, Utah 84114	

ACKNOWLEDGEMENTS

The authors wish to thank the Utah Department of Transportation and the New York State Department of Transportation for funding this project. Additionally, the authors would like to thank Mark Bryant, for his assistance. The authors acknowledge Wadsworth Construction for retrieving and transporting the two columns from the Highland Drive Bridge. The authors also acknowledge the contribution of FRP composite materials by Sika Inc. and Hughes Bros. Inc.

TABLE OF CONTENTS

LIST OF FIGURES

LIST OF TABLES

EXECUTIVE SUMMARY

The present research evaluated both corroded and non-corroded reinforced concrete (RC) columns in axial compression. Carbon fiber reinforced polymer (CFRP) jackets were shown to successfully rehabilitate severely corroded steel RC columns subjected to axial compression by doubling the compressive strength and quadrupling the axial strain at peak load of the non-corroded control specimens. Current design and analytical FRP confined concrete models were implemented and were found to compare well with experimental results. The closest predictions were obtained when accounting for additional confinement provided by the internal steel spiral. Other RC columns with internal reinforcing including hybrid, which is a combination of vertical steel with a GFRP spiral, and all-GFRP reinforced columns were also tested under axial compression. An evaluation of the corrosion rates showed that the hybrid RC specimens corroded at less than 1/3 the rate of the all-steel RC specimens. The hybrid RC specimens subjected to corrosion also had approximately double the axial strain at peak load of the corroded all-steel RC specimens and showed more ductility after peak load. Two bridge columns that were in service for over 40 years, with nine of those years rehabilitated with CFRP jackets, were tested to evaluate bond performance under 2,000 kip concentric and eccentric loads. It was found that the bond was maintained and the CFRP jacket performed as intended when the substrate had been the original concrete.

THIS PAGE INTENTIONALLY LEFT BLANK

1.0 INTRODUCTION

Fiber reinforced polymers (FRP) have been used in many applications and have become the ideal material choice in many fields such as the aerospace, automobile, and other industries. This is due to their light weight, high strength, rigidity, and noncorrosive properties. These properties have appealed to engineers in many fields; however, FRP composites have only recently become a main topic of research in the construction industry. This is particularly true with respect to its application to reinforced concrete (RC) members.

Steel reinforcement has been, and is currently, the material of choice for RC members. However, the drawback to reinforcing steel is its susceptibility to corrosion. Recent bridge collapses have shed light on the nation's deteriorating infrastructure, and have shown the devastating effect corrosion can have. Corrosion can occur anytime steel is exposed to moisture, oxygen, and an electrolyte—all of which are found abundantly in nature. This poses a problem for any RC member exposed to the elements. Bridge components, columns in particular, have been a major concern due to their devastating failure, which causes collapse of the structure they support.

Bridge collapse events and the deteriorating infrastructure have left researchers asking two questions. How can we repair or extend the life of existing RC columns? How can we avoid corrosion of RC columns in the future? One potential solution to these problems is FRP composites. FRP composites do not corrode and come in many different forms that lend themselves to both exterior application for rehabilitation of existing RC columns and use as internal reinforcement to extend initial design life.

Several studies have investigated the performance and application of FRP wraps to rehabilitate corrosion damaged columns. These studies have focused on different aspects of FRP wrapping including: improvement of strength and deformation characteristics; corrosion inhibiting properties of FRP; and effects of eccentric loads on

FRP wraps. FRP composites have also been investigated as internal reinforcement for concrete columns.

It has been shown that the application of FRP wraps to columns will increase their axial capacity (Bae and Belarbi, 2009; Choo et al. 2006a, 2006b; Deitz et al. 2003; Lotfy, 2006). However, the benefit of wrapping decreases as load eccentricity and slenderness increase (Ranger and Bisby, 2007). Ranger and Bisby (2007) found that even at load eccentricities of e=0.27D, where D=column diameter, there was a 50% strength increase for FRP wrapped columns compared to an unwrapped column—the test specimens used were considered "short".

Partial impermeability is another desirable property of FRP composites. FRP wraps have been shown to stop or significantly slow the corrosion rate, which is vital in rehabilitation applications (Bae and Belarbi, 2009; Tastani and Pantazopoulou, 2004). The impermeable qualities of FRP composites seem to stay constant despite continued exposure to accelerated corrosion environments. However, Bae and Belarbi (2009) observed more corrosion in wrapped columns that underwent freeze-thaw cycles and hypothesized that micro-cracks had developed in the wrap, but noted this would need to be verified by microscopic investigation.

Despite their resiliency, FRP wraps fail at lower strain levels than exhibited in their respective tensile coupon tests. This has been observed in several studies and is to be expected given that the tensile coupon test is an ideal one-dimensional test and not an accurate depiction of the load application on FRP wraps which undergo triaxial loading. Tastani and Pantazopoulou (2004) noted that the corrosion environment did not affect the confining capacity of FRP jackets and stated that failure of FRP wrapped columns was caused mainly by bar buckling that induced stress concentrations forcing the FRP jacket to rupture locally.

Previous research regarding FRP wrapped columns subjected to corrosive environments is based primarily on columns that underwent an accelerated corrosion process; this is due to the significant amount of time required for corrosion to occur

naturally. Accelerated corrosion methods differ slightly, but most include a saline type solution and an imposed electrical potential. This imposed potential or voltage causes current to flow through the steel reinforcing bars and imitates the natural corrosion process. The most common method to quantify corrosion is through Faraday's Law (Bae and Belarbi, 2009; Pantazopoulou et al. 2001; Tastani and Pantazopoulou, 2004). The amount of steel loss can be calculated given the electrical current, time interval, Faraday's constant, and atomic mass and valency of corrosion byproduct. In this study, a similar accelerated corrosion environment was created.

Another way to prevent corrosion related problems, specifically in new construction, is to use FRP composites as internal reinforcement. However, there are drawbacks such as brittle failure and lower compressive capacity of FRP reinforcement as compared to steel. Thus, internal FRP reinforcement has not replaced steel as the main material for internal reinforcement. Furthermore, one of the most significant drawbacks of FRP composites is initial cost, which prevents it from being used more widely.

The ratio of FRP reinforcement area to gross area of a member is critical in preventing sudden brittle failure. Choo et al. (2006) determined that to prevent sudden brittle failure in glass FRP (GFRP) reinforced columns, the minimum reinforcement ratio should be greater than or equal to approximately 0.6%; they also recommended using GFRP bars with ultimate compressive strains much larger than concrete. Lotfy (2006) found that increasing the GFRP reinforcement ratio increases strength and ductility of the member.

FRP composites have lower compressive capacity compared to their tensile capacity and fail in a brittle manner. Therefore, FRP composites do not increase axial capacity by being able to carry more load than the concrete, as steel reinforcement does. Deitz et al. (2003) found that GFRP bars have a modulus of elasticity that can be assumed to be the same in compression and tension. This makes it possible to calculate the compressive capacity of GFRP bars, but their contribution to axial capacity is so low that for practical purposes it can be ignored (Luca et al., 2010).

Though the characteristics of FRP jackets and FRP internal reinforcement have been investigated in the laboratory, there is still much that is unknown about their actual performance in the field. Is the wrap still effective after local damage has occurred? Will the wrap de-bond from concrete after long-term exposure to the elements? What are the advantages of using a combination of FRP bars and steel bars as internal reinforcement? FRP composite technologies are continually evolving, meaning there are many products and applications that have yet to be studied such as FRP spirals used as internal confining reinforcement.

In this study, the use of carbon FRP (CFRP) jackets to rehabilitate corroded columns is evaluated. Long term field performance and practical application of FRP jackets in the field were investigated by evaluating two columns that were rehabilitated while in use in the field. The use of GFRP spirals as internal ties versus steel spirals or hoops was also investigated. To fulfill these objectives two tasks were performed. Medium-scale specimens that were built with different reinforcing materials, including GFRP spirals, were corroded and tested under axial compression; some of the corroded columns were wrapped with a CFRP composite jacket. Two 40-year old corroded bridge columns that were rehabilitated in June 2000 with CFRP wraps and then aged in the field for the last nine of those 40 years were examined and tested under concentric and eccentric axial compression.

THIS PAGE INTENTIONALLY LEFT BLANK

2.0 RESEARCH METHOD

2.1 Objectives

The objectives of this research are:

1. Investigate how corrosion affects performance of steel RC columns under axial compression.
2. Investigate the performance of CFRP wraps for rehabilitating RC columns with corroded steel bars under axial compression.
3. Investigate the performance of hybrid reinforced concrete columns (using both steel and GFRP as internal reinforcement) under axial compression.
4. Investigate the performance of corroded RC columns with vertical steel bars and GFRP spirals under axial compression.
5. Compare the performance of corroded columns with CFRP jackets and three internal reinforcement options, all-steel reinforcing bars, steel verticals with GFRP spirals, and all-GFRP reinforcing bars, under axial compression.
6. Compare test results with predictions from the ACI 440 (2008) Committee Recommendations for predicting the capacity of FRP wrapped concrete, and explore modifications including accounting for corrosion of the spiral reinforcement to predict accurately the capacity of wrapped columns with corroded internal steel reinforcement.
7. Evaluate two full size field corroded concrete columns that were rehabilitated with a CFRP jacket. In particular the following two topics will be investigated:

a. Long term CFRP bond to concrete and to the repair grout under high axial load
b. Corrosion effects on the long term performance of CFRP repaired columns

2.2 Description and construction of medium-scale specimens

The medium-scale columns were 10 in. in diameter and 28 in. tall. All medium-scale specimens were cast from the same mix on August 21, 2009 to minimize differences in concrete strength. Concrete cylinders, 4 in. x 8 in., were made from the same mix at the time of casting and were crushed on the day the specimens were tested giving an average concrete compressive strength of 5,200 psi. All specimens and cylinders were de-molded three days after casting and were dry cured inside the Structures Laboratory.

Dry curing can cause micro-cracks in the concrete allowing water and electrolytes to penetrate the concrete cover quickly, thus making corrosion start quickly and continue at a faster rate. This was a desirable effect because the research objective was to subject some of the specimens to corrosion; in addition, dry curing often takes place in the field.

The medium-scale columns were constructed with three different internal reinforcement types or variations consisting of all-steel, steel vertical with GFRP spiral, and all-GFRP vertical and spiral. Table 2.1lists the 14 medium-scale specimens tested in this study according to their identification, with a description of each specimen and a list of applicable descriptive figures.

Eight specimens were made with all-steel reinforcement. Specimens #7SCOREX and #8SCOREX, were used to evaluate the corrosion environment to determine how long the remaining specimens subjected to corrosion should stay in this environment. Specimens #1SCTL and #2SCTL were not subjected to corrosion and were kept as controls. Specimens #3SCOR and #4SCOR were subjected to corrosion for 11

weeks and tested in axial compression six months after they were removed from the corrosion environment. Specimens #5SCORW and #6SCORW were subjected to corrosion for 11 weeks and then wrapped with CFRP composite jackets one month before they were tested in axial compression.

Four hybrid specimens with steel vertical bars and GFRP spirals as hoop reinforcement were constructed. Specimens #11HYBCOR and #12HYBCOR were subjected to corrosion before axial compression testing; specimens #9HYBCTL and #10HYBCTL were not subjected to corrosion and were tested as controls.

Specimens #13GLCTL and #14GLCTL were constructed with all-GFRP reinforcement. These columns were not placed in the corrosion environment because this would have had little effect on the GFRP bars.

For steel reinforced columns, four #4 steel bars were used as vertical reinforcement and #3 steel spirals spaced at 3 in. on center were used as hoop reinforcement as shown in Figure 2.1. The CFRP wrapped specimens had the same internal reinforcement as the all-steel reinforced columns, but were wrapped after being subjected to corrosion as shown in Figure 2.2. The hybrid columns had the same vertical reinforcement as the all-steel columns and a #3 GFRP spiral spaced at 3 in. on center as shown in Figure 2.3. The all-GFRP columns had four #5 vertical bars and a #3 GFRP spiral spaced at 3 in. on center as shown in Figure 2.4. The reinforcement was kept uniform in size and spacing to the extent possible to allow for a comparison between GFRP and steel internal reinforcement. The only size difference was the #5 vertical GFRP bars in the all-GFRP specimens versus #4 steel bars. However, any additional capacity due to this size difference would be minimal because GFRP bar's compressive strength is very low and can be neglected because the modulus of elasticity of GFRP bars is similar to that of concrete. It is also important to note that though the size and spacing of the spiral GFRP reinforcement is the same as the steel the GFRP will have less effective confinement due to GFRP's lower modulus of elasticity of 5,920 ksi, versus 29,000 ksi for steel. Therefore, GFRP spiral confined concrete columns would need 4.9

times more spiral reinforcement than a steel spiral reinforced column to achieve the same confining performance.

Table 2.1: Specimen Identification Summary

Specimen	Description	Figures
#1SCTL	All-steel internal reinforcement (control)	2.1 & 2.6a
#2SCTL	All-steel internal reinforcement (control)	2.1 & 2.6a
#3SCOR	All-steel internal reinforcement exposed to corrosion for 11 weeks	2.1 & 2.6c
#4SCOR	All-steel internal reinforcement exposed to corrosion for 11 weeks	2.1 & 2.6c
#5SCORW	All-steel internal reinforcement exposed to corrosion for 11 weeks and then wrapped with two layers of CFRP	2.2 & 2.6c
#6SCORW	All-steel internal reinforcement exposed to corrosion for 11 weeks and then wrapped with two layers of CFRP	2.2 & 2.6c
#7SCOREX	All-steel internal reinforcement corroded-Used as trial corrosion specimen	2.1 & 2.6c
#8SCOREX	All-steel internal reinforcement corroded-Used as trial corrosion specimen.	2.1 & 2.6c
#9HYBCTL	Hybrid internal reinforcement, steel verticals and GFRP spiral, (control)	2.3 & 2.6a
#10HYBCTL	Hybrid internal reinforcement, steel verticals and GFRP spiral, (control)	2.3 & 2.6a
#11HYBCOR	Hybrid internal reinforcement exposed to corrosion for 11 weeks	2.3 & 2.6b
#12HYBCOR	Hybrid internal reinforcement exposed to corrosion for 11 weeks	2. 3 & 2.6b
#13GLCTL	All-GFRP internal reinforcement (control)	2.4 & 2.6a
#14GLCTL	All-GFRP internal reinforcement (control)	2.4 & 2.6a

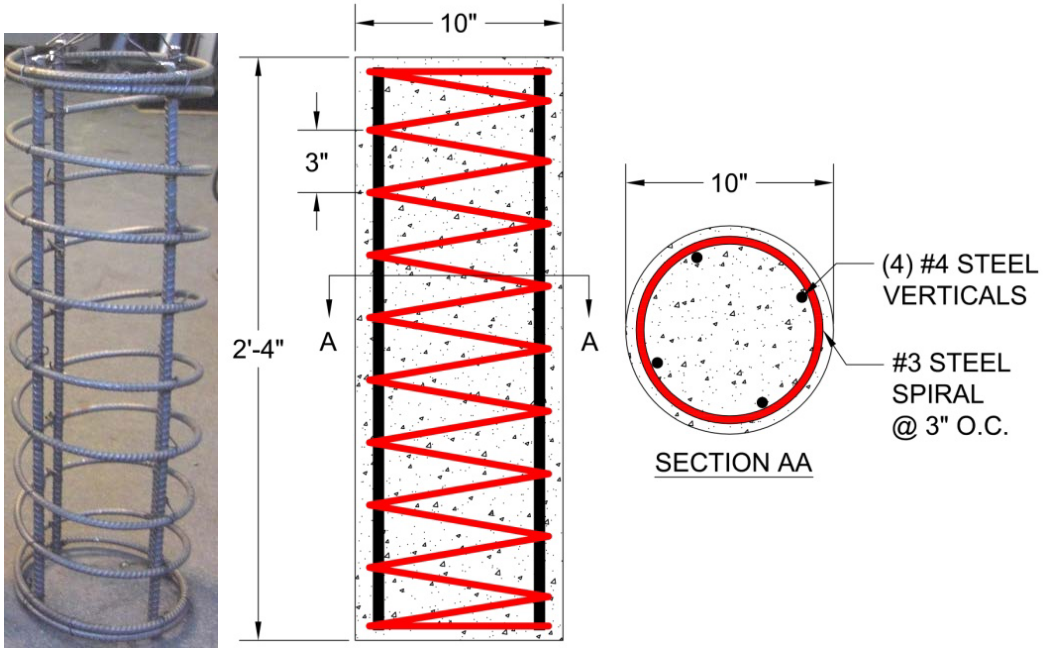

Figure 2.1: Steel reinforced columns

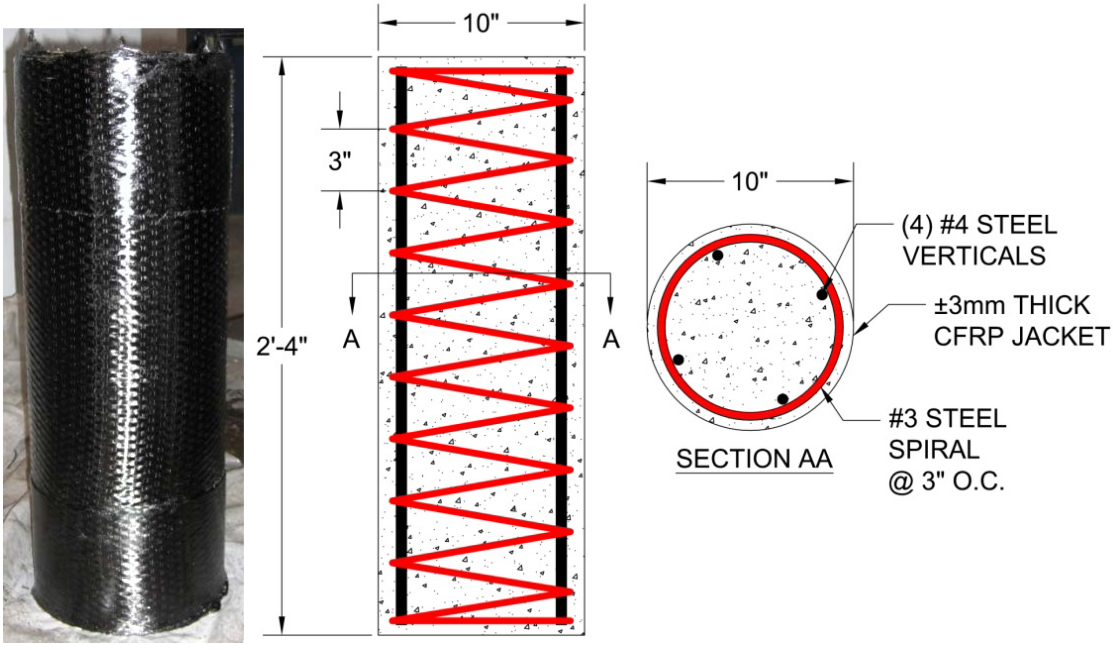

Figure 2.2: Steel reinforced columns wrapped with CFRP

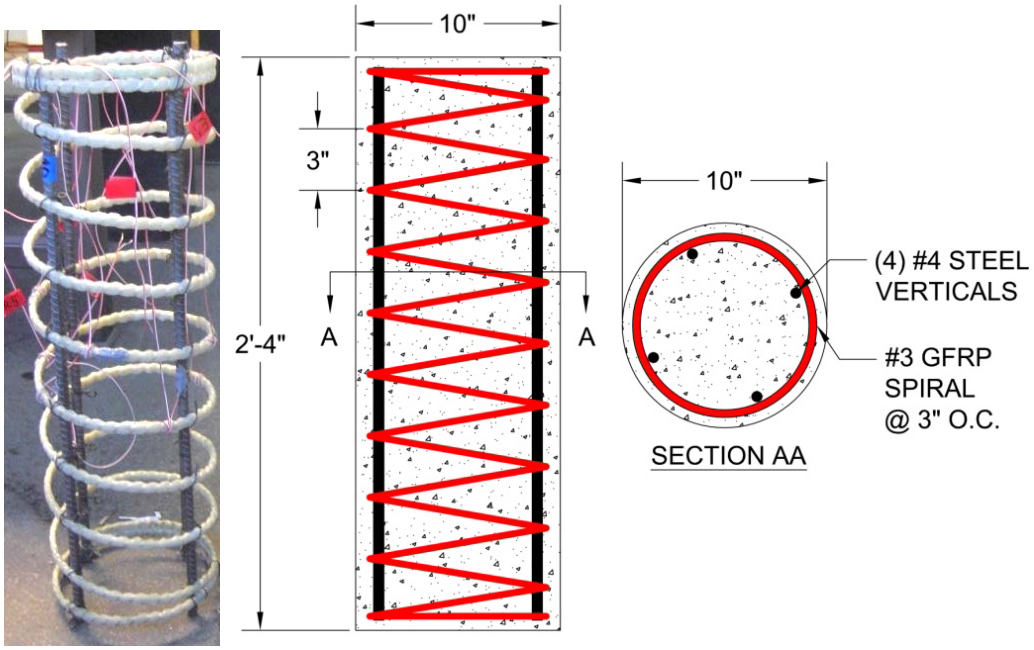

Figure 2.3: Hybrid (steel and GFRP) reinforced columns

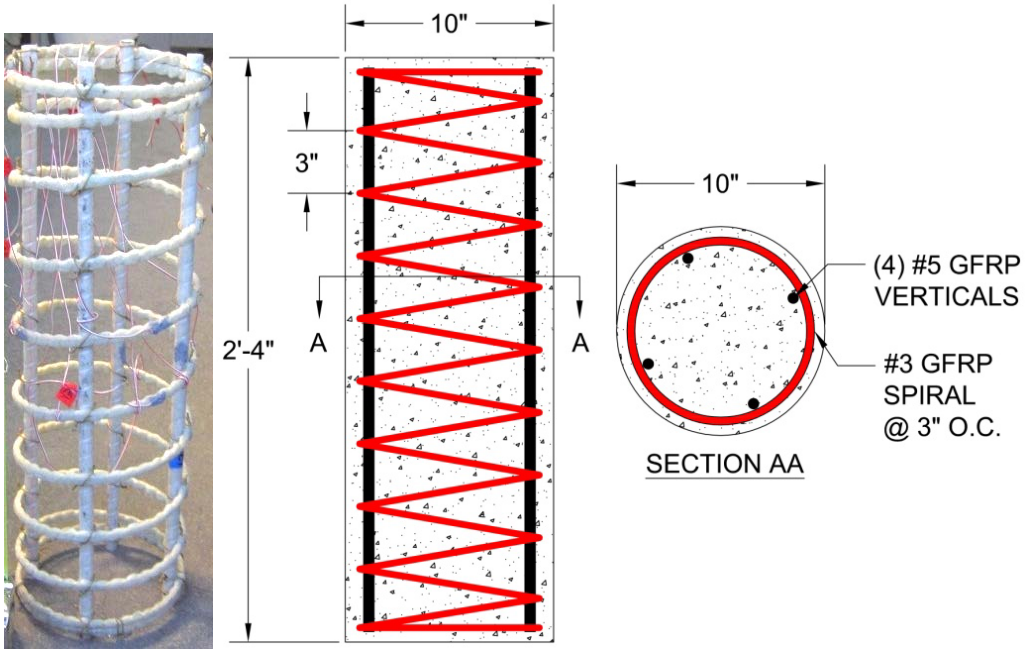

Figure 2.4: GFRP reinforced columns

2.3 Design and construction of the corrosion environment

The first step in preparation for testing was to subject the columns to corrosion. The corrosion system for the medium-scale specimens was based on the Florida Method of Test for an Accelerated Laboratory Method for Corrosion Testing of Reinforced Concrete Using Impressed Current (Florida DOT, 2000). This method consists of using a saltwater solution and an impressed voltage to accelerate the corrosion process. However, the actual corrosion rate and amount of voltage to be used for the specimens was not known for application in this study; therefore, two trial corrosion columns, #7SCOREX and #8SCOREX, were used to determine these unknowns.

A power supply with a maximum capacity of 12 volts (12V) and 3 amps (3A) was used to supply a constant voltage to the two specimens. The specimens were placed in a tank with 5% salt solution by weight, as shown in Figure 2.5. The tank was filled with the salt water solution p to approximately half the height of the medium-scale columns, or 14 in. In order to induce the current, a metal grate was placed at the bottom of the tank to receive the current leaving the specimens, thus completing the circuit. The induced voltage and completed circuit causes an electric current to flow through the rebar and accelerates the corrosion process. The two trial corrosion specimens were constructed with steel vertical bars and steel hoops as described previously. Figure 2.6 shows a comparison of the visual appearance of the columns subjected to corrosion while the process was underway and the condition of the control specimens.

The power supply was initially set at a constant voltage of 6V and the corrosion process was initiated on September 17, 2009. Voltage measurements were taken across shunts that connected the circuits. The shunts have a known resistance of 0.01 ohms and thus current can be calculated from the voltage measurements by dividing the voltage measured by the resistance; readings were taken daily. The specimens had developed cracks within one week of initiating the corrosion environment. This became evident by a jump in the current for each specimen and was later confirmed by visual observation.

After starting the corrosion process a few changes were made to the corrosion system used during the trial period. The steel grate at the bottom of the tank was a different grade steel than the steel rebar so it was replaced by several pieces of steel rebar placed around each of the specimens. The power supply was unable to maintain a constant voltage of 6.0V due to the increase in current exceeding its 3.0A capacity. Therefore, the constant voltage was adjusted from 6.0V to a voltage ranging from 3.0V to 5.0V over a period of four weeks. The ideal voltage was determined to be 5.0V for the existing power supply; this was the highest constant voltage that kept the amount of current under the maximum capacity of the power supply.

The two specimens were observed visually on a weekly basis and pictures were taken. One of the two preliminary corrosion specimens, #7SCOREX, was removed from the corrosion environment on Oct. 23, 2009 (after five weeks) and is shown in Figure 2.7(a). Column #8SCOREX was removed on Nov. 27, 2009 (after ten weeks) and is shown in Figure 2.7(b). Cracks were measured and documented as shown in Table 2.2. It is important to note that these cracks developed while the specimen was cycled in the corrosive environment at room temperature and that no freeze thaw cycles were applied.

Corrosion of the remaining six medium-scale columns was initiated in March of 2010. Four of the six columns had all-steel reinforcing bars and spirals and two had steel vertical bars with glass fiber reinforced polymer (GFRP) spirals. The columns were placed in the corrosion tank with 5% salt water solution by weight, and were allowed to soak in the solution for one week before the power supply was connected on March 24, 2010 (see Figure 2.8). Three DC power supplies were required to implement corrosion of the six medium-scale columns. Each power supply was connected to two columns and supplied a constant 5.0V potential across each vertical rebar. The 5.0V potential was checked with a voltmeter after initial set up and every time readings were taken to ensure it stayed constant at 5.0V throughout the corrosion process.

Initial voltage readings were taken right after the 5.0V potential was applied. Subsequently, readings were taken frequently in the beginning, on March 25, 26, 29, 30,

31, and April 1, 2, and 7 to ensure the corrosion process was running correctly. From this time onwards readings were taken weekly up to 11 weeks.

Table 2.2: Crack Measurements

#7SCOREX			#8SCOREX		
Crack #	Size (in.)	Length (in.)	Crack #	Size (in.)	Length (in.)
1	0.013	4	1	.016 to .02	5
2	0.01	10	2	.007 to .013	9
3	0.007 to .03	31	3	.003 to .01	11.5
4	0.003	4	4	.007 to .026	15.5
5	0.01	6.5	5	.005 to .025	13
6	0.009	8.5	6	.005 to .016	31
7	0.007	4	7	.009 to .04	15
8	0.003	3			
9	0.016	13			
10	0.009	14			

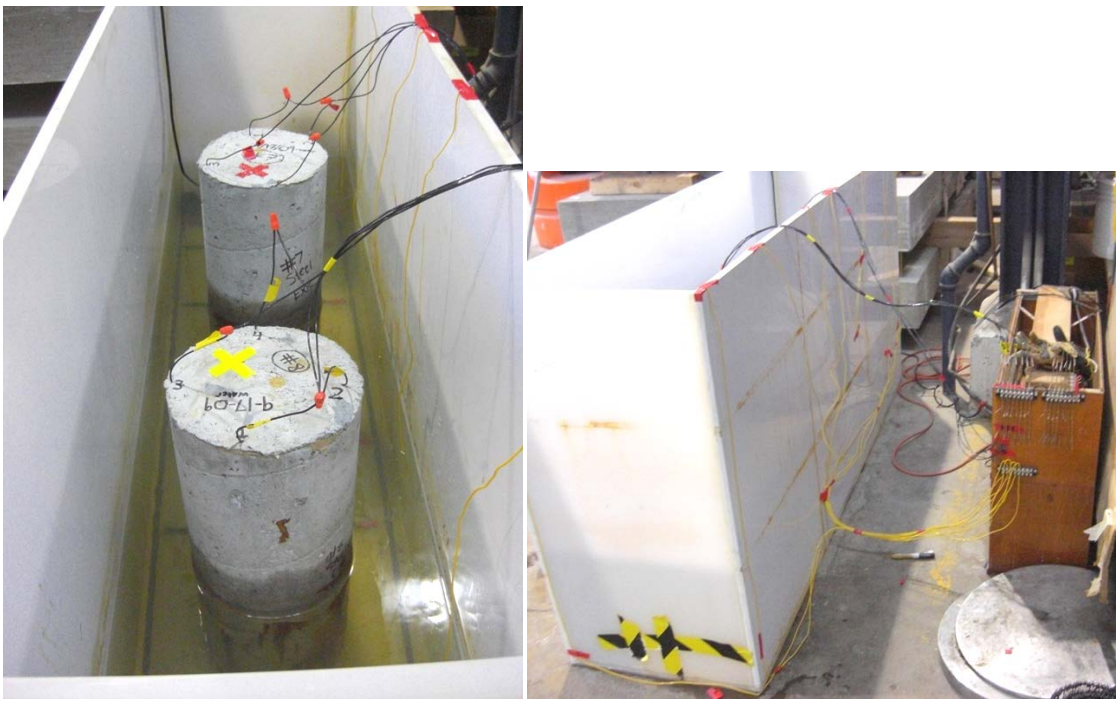

Figure 2.5: Corrosion system for #7SCOREX and #8SCOREX

(a) (b) (c)

Figure 2.6: Condition comparison: (a)Typical control specimen (b) Typical hybrid corrosion specimen (c) Typical steel corrosion specimens

(a) (b)

Figure 2.7: Trial corrosion specimen comparison (a) #7SCOREX after 5 weeks of corrosion (b) #8SCOREX after 10 weeks of corrosion

Figure 2.8: Corrosion system for medium-scale RC columns

2.4 Carbon fiber composite jackets

Columns #5SCORW #6SCORW were wrapped with *SikaWrap Hex 103C*, a high-strength unidirectional carbon fiber fabric with epoxy resin after being subjected to corrosion. This CFRP wrap has a tensile strength of 177 ksi, tensile modulus of 12.6 Msi, and an ultimate tensile strain of 0.014 in./in. The surface of the columns was roughened using a grinder with a metal diamond embedded grinding disc before being wrapped as shown in Figure 2.9. Roughening the surface of the columns removes any loose concrete cover and laitance and provides a better surface for the resin to bond. After being roughened, the columns were coated with epoxy resin and then wrapped with resin impregnated CFRP sheets. The entire column was wrapped with two layers of CFRP made up of two separate sheets with approximately 8 in. lap splices. The top and bottom 6 in. were then wrapped with an additional two layers to prevent premature end crushing during loading. The final product is shown in Figure 2.10.

Figure 2.9: Roughened surface of Columns #5SCORW and #6SCORW

Figure 2.10: CFRP wrapped column

2.5 Column instrumentation

Four linear variable displacement transformers (LVDTs) were placed at 90 degrees around all columns during testing to measure vertical displacement; a 2,000 kip load cell was used to measure the load on all columns. Figure 2.11 shows how the LVDTs were placed on the columns. Thus, vertical strain and stress applied could be measured for all specimens. However, there were some differences in gauging.

Control specimens that were not corroded, had internal gauges placed on their rebar cages before they were cast (see Figure 2.12). One gauge was placed on each of the four vertical bars at mid-height. Five gauges were placed on the spiral reinforcement. The spiral gauges were placed at every 90 degrees making a full circle of the specimen and ending with two gauges in the same quadrant but at different heights due to the spiral shape. The spiral gauges were placed at approximately the mid-height of the columns; these nine gauges, four vertical and five radial, allowed both vertical and radial strains of the column reinforcement to be recorded during testing. Figure 2.13 shows the protective coating applied to the internal reinforcement gauges to avoid damage during casting.

The specimens subjected to corrosion did not have internal gauges because the corrosion environment would have made any possible readings unreliable due to the extent of the corrosion. Concrete gauges were not placed on the columns subjected to corrosion to prevent unreliable data from being recorded due to excessive cracking and the high likelihood of a gauge being placed over a crack. However, CFRP wrapped specimens had four gauges placed at mid height on the external surface of the column bonded to the carbon fiber to measure radial strain in the CFRP jacket.

Figure 2.11: LVDT placement and steel confinement collars

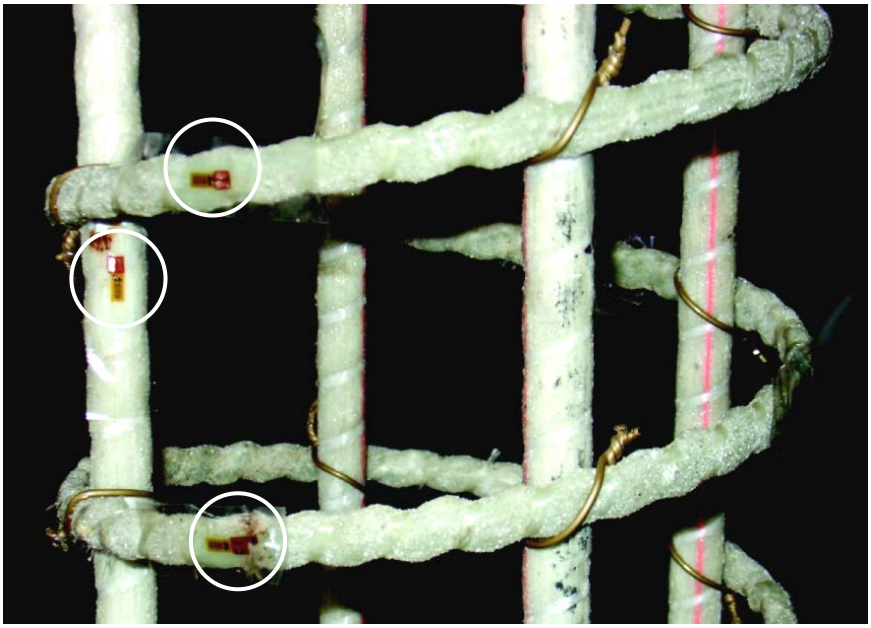

Figure 2.12: Internal strain gauge placement

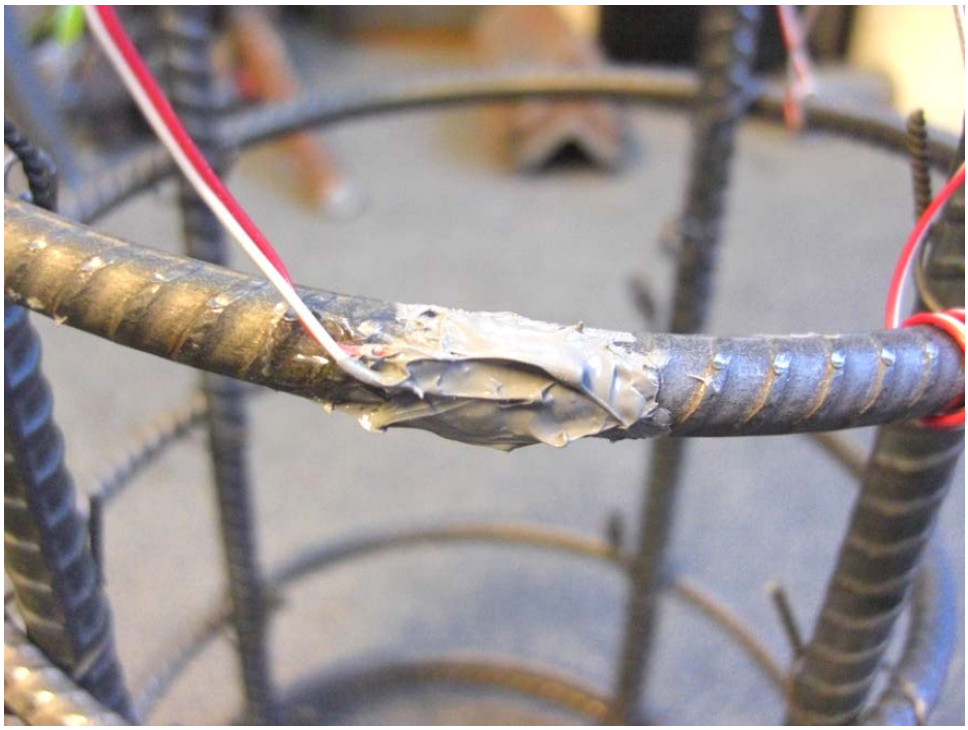

Figure 2.13: Internal strain gauge protective coating

2.6 Test preparation and protocol

To test the columns a large steel W14x342 column was attached to the base of the hydraulic actuator and this steel column applied the load to the medium-scale RC columns. Figure 2.14 shows the swivel base plate that was used during testing to reduce possible eccentricities in the system.

The columns were tested under displacement controlled monotonic axial compression. A loading rate of 0.02 in. per minute was selected for these tests. This rate was slow enough to avoid dynamic effects on the results of the tests. A Temposonic LVDT controlled the displacement of the actuator.

Steel collars were built to confine the top and bottom of the columns to prevent premature end crushing. The collars were fabricated from a 10 in. diameter by1/2 in. thick pipe that was cut into two 6 in. long sections. These sections were cut in half and then angles with bolt holes were welded to the two halves. This made it possible to bolt the collars around the top and bottom of the specimens as shown in Figure 2.11. Great care was taken not to crush any strain gauge wires in the process.

Hydrostone, a high strength plaster, was used to cap the columns to provide a level and smooth top surface. The plaster mix used a 32% water to Hydrostone ratio by weight. This was fluid enough to self level and leave a smooth surface, but also had a compressive strength at least 2,000 psi higher than the concrete. Figure 2.15 shows the columns after Hydrostone was applied.

A VISHAY data acquisition system was used to obtain and record the data from LVDT's and/or strain gauges during the tests.

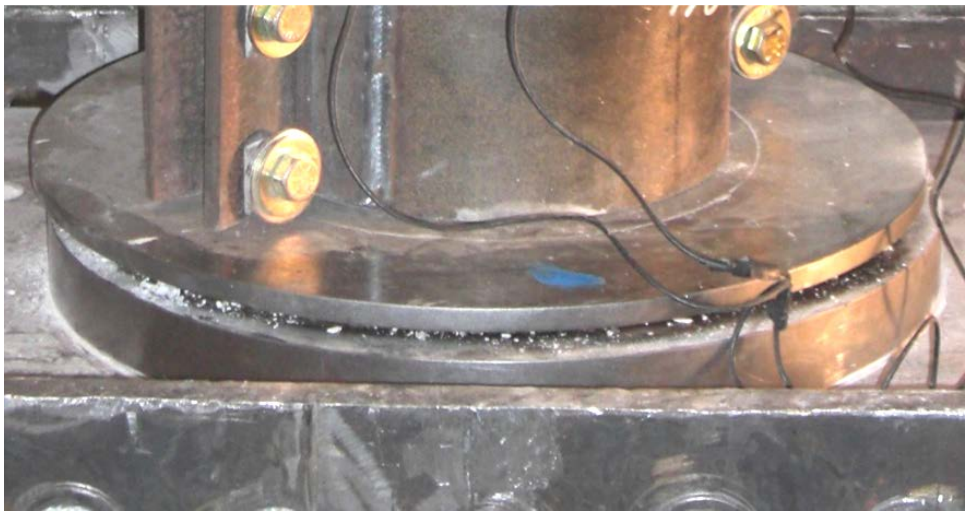

Figure 2.14: Swivel base plate

Figure 2.15: Hydrostone caps

THIS PAGE INTENTIONALLY LEFT BLANK

3.0 EXPERIMENTAL AND ANALYTICAL RESULTS

This section presents and discusses the results from the corrosion environment, compressive load tests, and design and analytical models. Methods used to interpret the experimental results and calculations performed will also be discussed.

3.1 Test preparation and protocol

For specimens #3SCOR, #4SCOR, #5SCORW, #6SCORW, #11HYBCOR, and #12HYBCOR, as described in Table 2.1, the accelerated corrosion process began on May 24, 2010. The accelerated corrosion process was terminated on June 9, 2010, after approximately 11 weeks. This amount of time was determined from the trial corrosion test specimens, columns #7SCOREX and #8SCOREX. A high amount of corrosion was desired in order to show more drastic differences when comparing columns with different types of internal reinforcing bars and also to demonstrate the effectiveness of CFRP jackets in repairing corroded columns with significant steel corrosion.

The amount of corrosion, in terms of mass loss, was estimated using the imposed current values obtained from the voltage measurements taken throughout the corrosion process and Faradays law as follows:

(3.1)

where is the amount of steel loss in grams; which is the atomic mass of iron; which is the valency of the assumed corrosion product, $Fe(OH)_2$; which is Faraday's constant; and is the time interval over which , the average current, is applied.

Mass loss values were then converted to percent steel loss by dividing the mass loss by the original steel mass. The final values after 78 days of corrosion are

summarized in Table 3.1. It is important to note that this is an indirect method of calculating steel mass loss because current not actual mass loss was being measured. In the all-steel reinforced concrete columns it was apparent that most of the corrosion occurred in the steel spiral, as observed in the large field specimens. This is to be expected because the hoops have the least amount of concrete cover. In all tests of the corroded columns, the hoop steel was corroded to the point that it provided little confining support and resulted in sudden brittle failures as shown in Figure 3.1. The vertical bars were also affected by the corrosion, but not as significantly as the steel spirals. In some cases the vertical steel had only minor corrosion as shown in Figure 3.1.

Hybrid specimens #11HYBCOR and #12HYBCOR, which had vertical steel bars and GFRP spirals as hoop reinforcement, had less than half the amount of corrosion as the all-steel RC columns in terms of percent steel loss. As a result, #11HYBCOR and #12HYBCOR had much less cracking which helped keep the rate of corrosion lower than the all-steel RC columns. Figure 3.2 shows the difference in corrosion rate, by the amount of current measured, in the all-steel specimens versus the hybrid specimens over time. From the beginning of corrosion to the end, it is clear that the rate of corrosion of the all-steel RC columns was three to four times that of the hybrid columns.

Figure 3.2 also shows that there was an initial jump in corrosion rate, but then the corrosion rate began to drop off. This was likely due to their being less steel to corrode, and because the corrosion byproducts began blocking the gaps and cracks that had formed. The build-up of corrosion byproduct slowed the flow of salt water solution to the steel. This conclusion was drawn from the noticeable second jump in the graph just before 60 days into the corrosion process. During this time the salt water solution was replaced and the columns were cleaned off. Therefore, the jump came as a result of cleaning off the corrosion build-up around the columns. Figure 3.3 shows the amount of total steel loss over time. It is clear that the hybrid columns had approximately only 1/3 the total percent steel loss of the all-steel reinforced columns.

The rate of corrosion increases when cracks form, because cracks allow a more rapid flow of water and electrolytes to the steel bars. Thus, cracking increases the corrosion rate. Another reason less cracking was observed in #11HYBCOR and #12HYBCOR was that the vertical steel was enclosed by the GFRP spiral which helped to hold the tensile forces produced by the expansion of the corrosion reaction. Figure 3.4 shows the buildup of corrosion byproducts along the cracks in the columns. Note that the hybrid columns have very little to no cracking and corrosion buildup.

Table 3.1: Corrosion Summary

Specimen	Total Mass Loss (g)	Steel Loss (%)
#3SCOR	478	16.3
#4SCOR	515	17.6
#5SCOR	457	15.6
#6SCOR	491	16.7
#11HYBCOR	91	7.0
#12HYBCOR	87	6.7

Figure 3.1: Effects of corrosion on steel spiral

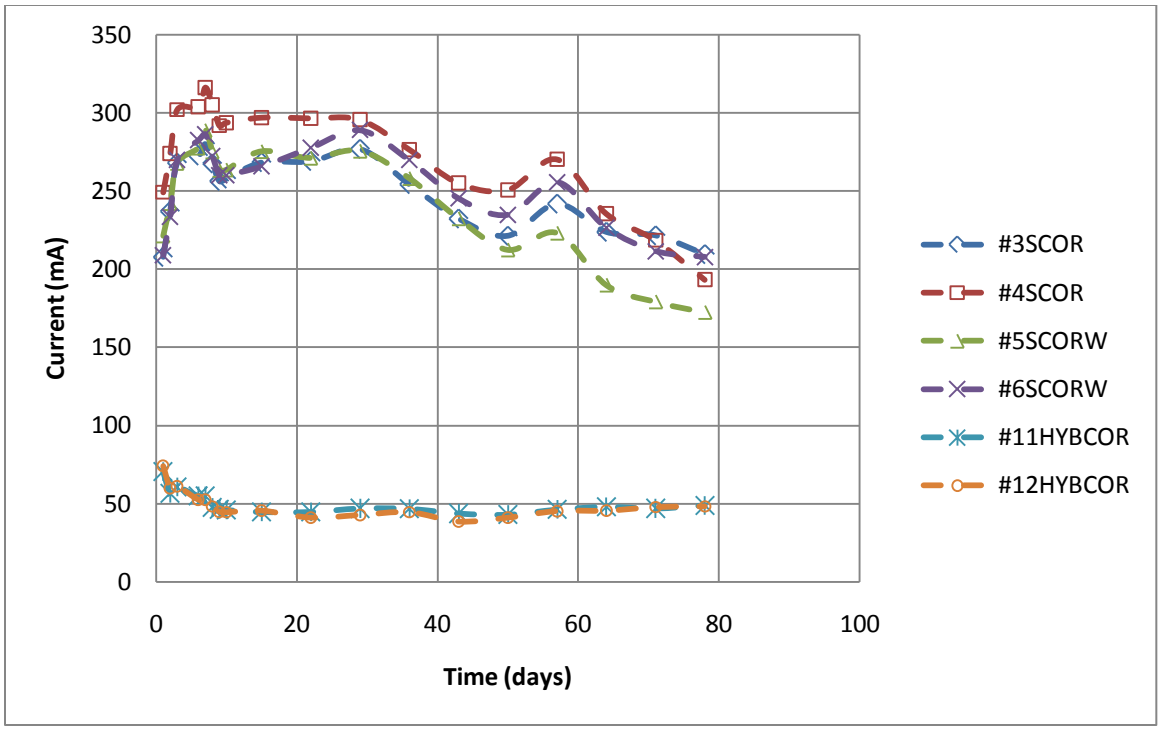

Figure 3.2: Corrosion rate over time

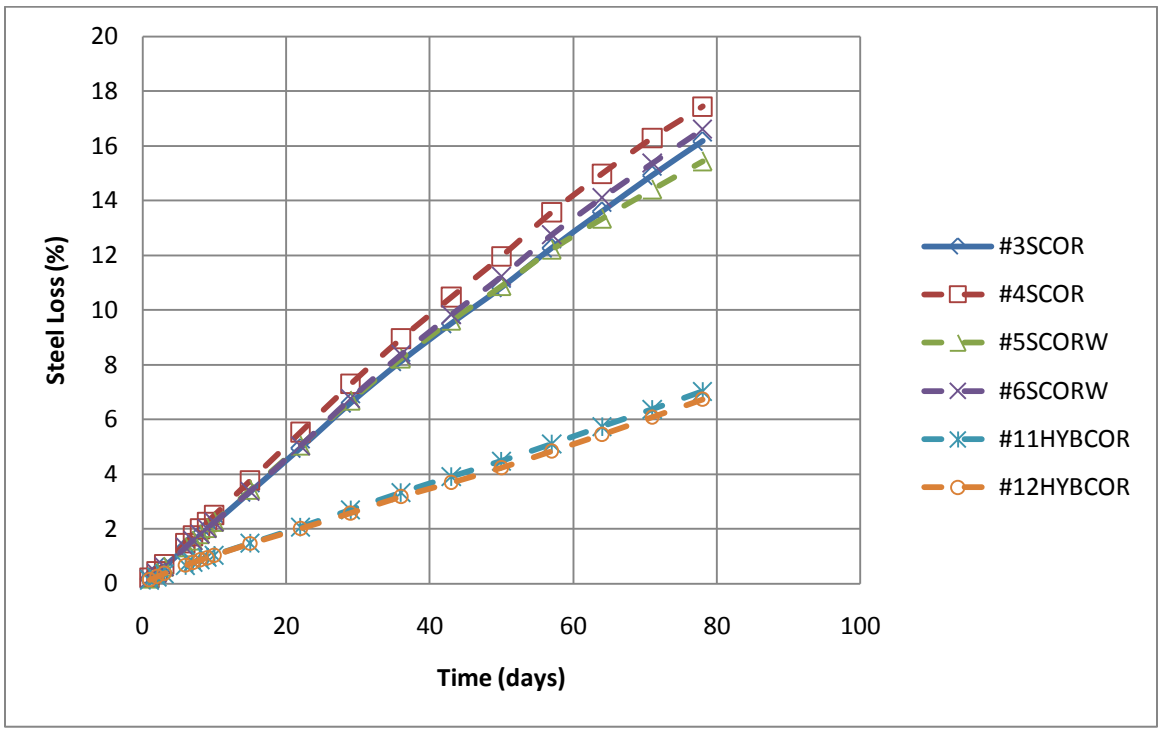

Figure 3.3: Total percent steel loss over time

#11HYBCOR #5SCORW #4SCOR

#3SCOR #12HYBCOR #6SCORW

Figure 3.4: Corrosion build up along cracks

3.2 Results of load tests

The most common way of evaluating the performance of columns under axial compression is through their stress versus strain curve. The stress values were calculated by dividing the load measured by the load cell by the total area of the column, , to get the stress in psi. The overall average strain of the columns was calculated by taking the average of the displacements measured by the four LVDTs and dividing them by the gauge length to get the strain.

The control specimens also had strain gauges placed on the internal reinforcement on each vertical bar and five places on the spiral, as described in Section 2.5. Graphs of stress versus radial and axial strain for control specimens and the CFRP wrapped specimens are shown in the Figures A.1-A.7 of the appendix. Graphs of axial stress versus strain in the vertical reinforcing bars of control specimens are shown in Figures A.8-A.12 of the appendix.

Control specimens #1SCTL and #2SCTL, with all-steel internal reinforcement, were tested under uniaxial compression to establish a baseline capacity for the columns. However, in testing #1SCTL it became apparent that collars were needed to keep premature end crushing from occurring where the load was applied (See Figure 3.5). Therefore, #1SCTL did not provide correct results and was excluded from the study. However, specimen #2SCTL used the steel collars described earlier, as shown in Figure 2.11, and produced a proper failure (see Figure 3.6). This test showed that the compressive capacity of specimens that were not subjected to corrosion was approximately 500 kip or 6400 psi. The test results including axial load, axial stress, and axial strain are summarized in Table 3.2; Figures 3.7-3.18 show the failures of all medium size columns. In Figure 3.19 the stress-strain curves of each specimen type were averaged to show an overall comparison of the axial compression performance for each type. Note that the wrapped specimens had more than doubled the axial capacity and ultimate strain of the other specimens including the control, #2SCTL, which was not subjected to corrosion.

Corroded specimens #3SCOR, #4SCOR, and #8SCOREX show the detrimental effects of corrosion in RC columns. These specimens had a 13% average decrease in compressive strength, a 23.5% average decrease in axial strain at peak, and a 30.7% average decrease in axial strain at break; break being defined as a 20% drop in load. These results show that corrosion decreases both the axial capacity and ductility of RC columns. The ductility at failure had the most drastic reduction; this coincides with visual observations during the tests. The medium-scale columns subjected to corrosion failed suddenly; shortly after reaching peak capacity the load dropped at once instead of slowly decreasing as was the case for the control specimens; this occurred because much of the corrosion occurs in the hoops resulting in a drastic loss of confinement that makes the column fail similarly to an unreinforced concrete cylinder. Figure 3.20 shows a comparison of the stress-strain curves of all specimens with all-steel internal reinforcement including #5SCORW and #6SCORW which were wrapped with carbon fiber sheets after being corroded.

Figure 3.20 shows that wrapping the columns subjected to corrosion with CFRP jackets significantly increased the axial compressive strength and ultimate strain compared even to the columns not subjected to corrosion. The wrapped column's average compressive capacity was approximately 2.4 times that of the control specimen, and the average axial strain at peak axial load was over 4.5 times that of the control specimen. The significant increase in compressive strength and ductility shows that CFRP jackets can successfully rehabilitate corroded columns.

Hybrid specimens #11HYBCOR and #12HYBCOR showed no changes in overall capacity due to corrosion as shown in Figure 3.21, which shows all columns that had GFRP spirals. In fact, the peak load and strain at peak load were higher than the hybrid control specimens #9HYBCTL and #10HYBCTL. Specimens #11HYBCOR and #12HYBCOR, compared to the non-corroded all-steel control, had only a 4.9% average decrease in axial capacity versus the 13.3% average decrease in axial capacity exhibited by the hybrid control specimens. Therefore, it appears that there were no detrimental effects due to corrosion for these specimens. However, during the corrosion process the

columns were once again introduced to water allowing the unreacted cement to hydrate and increase the compressive strength of the concrete. Therefore, there was likely a difference in concrete strength between columns subjected to corrosion and the control specimens.

To investigate this possibility of strength gain in the concrete, six concrete cylinders from the same mix and post curing environment as the medium-scale specimens were put into a moist concrete curing room for 11 weeks and were then compression tested. The result of the concrete cylinder test revealed that there was a significant change in concrete strength from 5,200 psi to 6,700 psi. The difference in concrete strength was accounted for in the methods used for prediction of capacity that will be discussed later in this chapter. However, this is still a good representation as to what occurs in the field. The concrete strength of columns exposed to weather, and thus water, allows for continued curing and concrete strength increase over time. This increase in concrete strength over time is not taken into account during the design process. Therefore direct comparison of load capacity between control and corroded specimens subjected to corrosion is still valid.

The average overall capacity of the control hybrid columns, #9HYBCTL and #10HYBCTL, was lower than the all-steel control columns, as shown in Figure 3.22, and was approximately the same as the specimens reinforced with all-steel subjected to corrosion, but had only an 8.2% average decrease in axial strain at break versus the 30.7% average decrease for #3SCOR, #4SCOR, and #8SCOREX. The strain at peak load and load at break was nearly double for #11HYBCOR and #12HYBCOR versus #3SCOR, #4SCOR, and #8SCOREX, as shown in Figure 3.23.

The increased strain at peak load and slower decrease in capacity after peak load means the hybrid columns had a more ductile failure. Excessive damage was more evident before total collapse because there was more cracking and cover falling off before failure. However, #3SCOR and #8SCOREX in particular, showed little to no sign of cracking or cover loss and suddenly lost all load capacity shortly after peak (see Figure

3.20). One reason for the sudden brittle failure was the extensive corrosion in the hoops. What remained of the hoop steel after the corrosion process had become brittle and failed catastrophically simultaneously all around the column. The hybrid column's GFRP hoops failed in specific locations but, due to the spiral still being intact, the column was able to carry some load by redistributing the dilational forces. Figures 3.8-3.12 of the corroded steel columns show how entire sections of the hoop fell off; whereas, Figures 3.15-3.16 show the GFRP spiral was still attached after the initial break and continued to brake in different places as the load was redistributed.

An interesting observation regarding the hybrid columns is that hybrid columns subjected to corrosion had a more ductile failure than the control hybrid columns as shown in Figures 3.19 and 3.21. Columns #9HYBCTL and #10HYBCTL still showed cracking and cover loss before failure, but lost all load in a sudden drop instead of a slow steady drop in load observed in #11HYBCOR and #12HYBCOR. A possible explanation for this is the corrosion process may have altered the performance of the GFRP spirals or the effect of corroded and cracked concrete allowed the GFRP hoops to be less affected by the concrete cover and thus not fail suddenly when the concrete failed.

Columns #13GLCTL and #14GLCTL, with all-GFRP reinforcement, had a 15.7% lower average axial capacity and 13% lower average axial strain value at break compared to the all-steel reinforced control (see Figure 3.22). As expected, this shows that the all-GFRP reinforcement gives less capacity and lower ductility than the columns with comparable steel reinforcement. The hybrid columns subjected to corrosion, #11HYBCOR and #12HYBCOR, had higher axial capacity and axial strain at break than the all-GFRP columns. However, when comparing the hybrid control to the all-GFRP specimens there was only a slight improvement of 3% in axial capacity and 5.2% in axial strain at break. Therefore, in terms of control specimens there was minimal difference in the all-GFRP reinforced to the hybrid columns. However, the hybrid columns would be a more economical choice initially due to the current cost of GFRP bars, but it is important to remember that lower initial cost does not always translate to life cycle cost. GFRP bars may have a higher initial cost, but may increase the design life, which can more than

make up for the initial cost at time of construction. Nevertheless, hybrid columns would be preferable in seismic regions for ductility.

The specimens that were repaired with CFRP wraps, columns #5SCORW and #6SCORW, had 2.4 times the axial capacity of the control specimens that were not subjected to corrosion, and 4.5 times the axial strain at peak load (See Figures 3.19-20). Therefore, the rehabilitation of these columns was successful at increasing both the vertical load and strain capacities of the columns to the point they surpassed their initial strength and strain values. Though the stress and strain capacities were greatly enhanced, these CFRP wrapped specimens had explosive failures. In these explosive failures, the load dropped directly from peak to zero suddenly and without warning. However, sudden failure and drop in load was also observed for #3SCOR, #4SCOR, and #8SCOREX. Therefore, not wrapping these columns means lower capacity and still a dangerous brittle failure at a much lower load. In fact, if these columns were designed correctly with built-in safety factors and loading of the columns was not increased it is very unlikely wrapped columns would ever reach the axial load necessary to fail them in field applications. The importance of CFRP wraps is even greater when considering seismic loads, since the axial strain is greatly increased.

Figure 3.5: #1SCTL premature end crushing

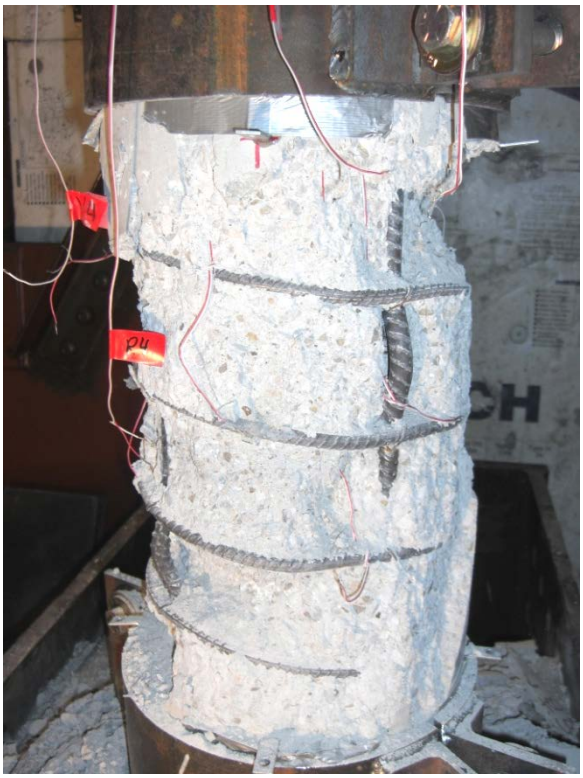

Figure 3.6: #2SCTL proper failure

Figure 3.7: #2SCTL

Figure 3.8: #3SCOR

Figure 3.9: #4SCOR

Figure 3.10: #5SCORW

Figure 3.11: #6SCORW

Figure 3.12: #8SCOREX

Figure 3.13: #9HYBCTL

Figure 3.14: #10HYBCTL

Figure 3.15: #11HYBCOR

Figure 3.16: #12HYBCOR

Figure 3.17: #13GLCTL

Figure 3.18: #14GLCTL

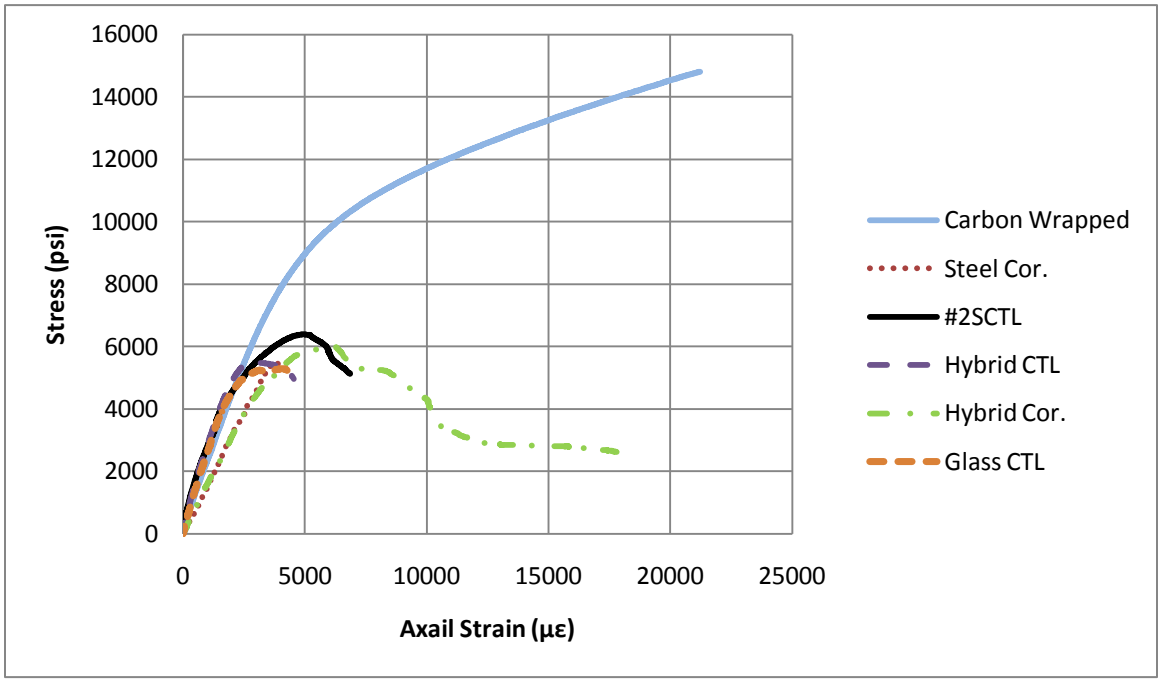

Figure 3.19: Averaged stress-strain curves for each specimen type

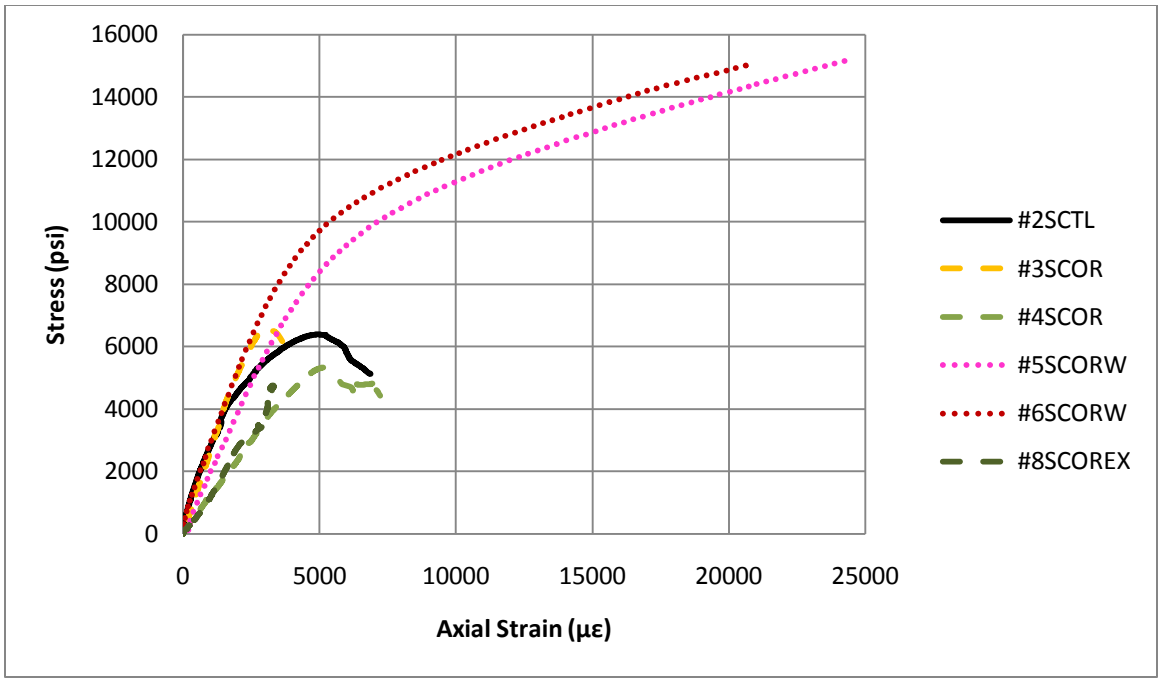

Figure 3.20: Stress-strain curves of specimens with all-steel reinforcement

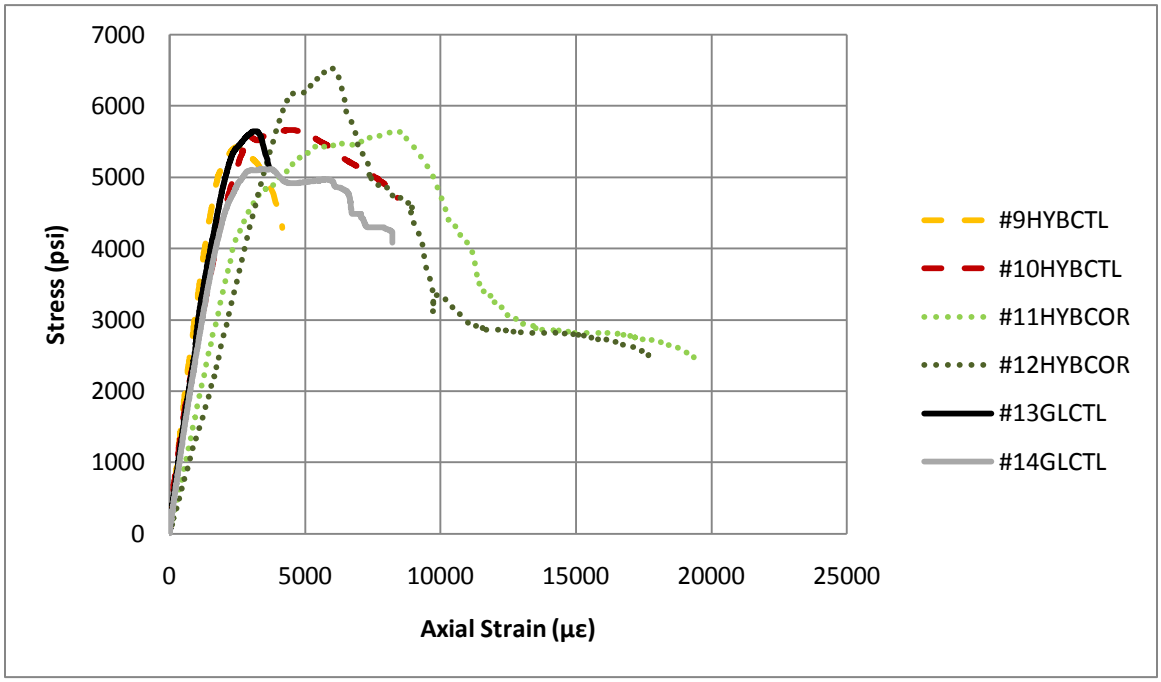

Figure 3.21: Stress-strain curves of all specimens with GFRP spiral

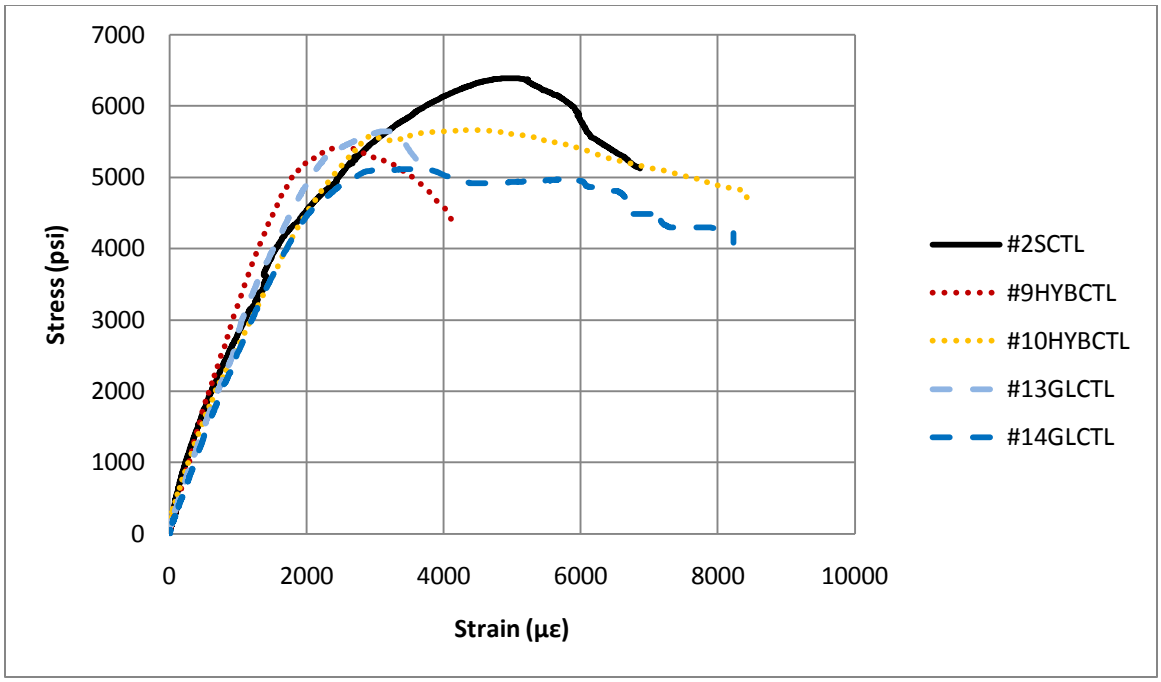

Figure 3.22: Stress-strain curves of all control specimens

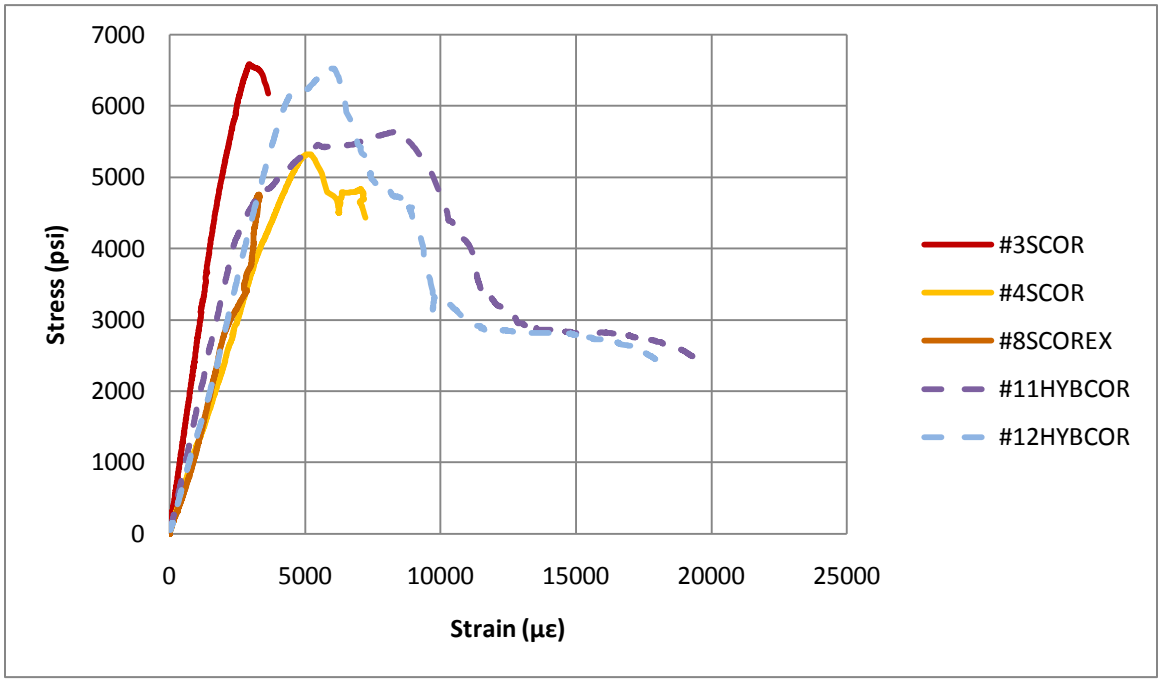

Figure 3.23: Stress-strain curves of all unwrapped corroded specimens

3.3 Analytical results

The test results for the medium-scale columns were compared with axial strength and axial strain values calculated by two different FRP confined concrete strength prediction models and an internal steel spiral confinement model. The method discussed in section 12.1 of the ACI 440 (2008) recommendations and the method developed by Moran and Pantelides (2002) were modified to account for additional confinement provided by the steel spiral. They were additionally modified to calculate the effective amount of steel spiral loss in the columns subjected to corrosion. The modified equations could also be used to predict the capacity of a corroded column wrapped or unwrapped if the amount of effective steel spiral loss were known or could be estimated.

3.3.1 *Capacity prediction*

The general equation to calculate the capacity of a confined column under pure axial compression is presented in section 12.1 of the ACI 440 (2008) recommendations:

(3.2)

where = axial capacity, = confined concrete compressive strength, = gross column area, = total vertical steel area, and = steel yield strength. The additional reduction factor of 0.85 outside of the brackets is to account for incidental moments.

The same general equation, (3.2), was used to calculate the capacity for both section 12.2 of ACI 440 (2008) and the Moran-Pantelides (2002) Model (M-P Model). However, ACI 440 (2008) section 12.2 and the M-P Model offer different ways of calculating .

In section 12.1 of ACI 440 (2008), is based on the unconfined concrete strength (and the confinement pressure ( ) provided by the FRP jacket and is given by the following equation.

(3.3)

where = 0.95 an additional reduction factor based on the committee's judgment, and = a shape efficiency factor (1.0 for round columns). The equation to calculate the confining pressure is given by:

(3.4)

where = FRP composite tensile modulus, = thickness of FRP wrap, and = diameter of column, and = effective strain level in FRP composite at failure.

In the M-P Model is given by:

(3.5)

where = the normalized FRP jacket stiffness given by:

(3.6)

The method described in section 12.1 of ACI 440 (2008) is a design oriented model that is simple and conservative in nature. However, the M-P Model is an analytical model that is not as conservative and tries to model the experimental capacity of the column. Therefore, one would expect the ACI 440 (2008) to conservatively under predict actual strength values and for the M-P Model to be closer but possibly slightly over predict the actual strength at times. The major difference between these equations comes down to the different empirical factors applied in the equations. Both methods calculate the confined concrete strength which is then multiplied by the area of concrete and added to the axial capacity of the vertical steel bars in the column to get the overall capacity of the column in equation (3.2). However, equation (3.3) does not account for the confining pressure provided by the internal steel spiral.

Therefore, when calculating the expected capacities of the columns the was corrected to account for the confinement provided by the steel spiral using the following equation developed by Mander et al. (1988):

(3.7)

where = spiral confined concrete strength and given by:

(3.8)

where = Area of steel spiral, = inside diameter of spiral reinforcement, = confinement effectiveness coefficient = 0.95 for round spirals, and = vertical spacing of spiral reinforcement.

Equations (3.7) and (3.8) were used to calculate the capacity of the unwrapped specimens. The calculated capacity for the control specimens was 495 kip and the actual control, column #2SCTL, reached 502 kip; thus, the percent difference between calculated and actual capacity was -1.4%. Therefore, Equations (3.7) and (3.8) would effectively predict the actual capacity of the medium-scale specimens subjected to corrosion if adjusted for concrete strength and steel spiral corrosion. These were corrected by using the adjusted f'c of the corroded columns in Eq. (3.7) and by using an effective steel spiral area instead of the initial steel spiral area in Eq. (3.8). These modifications yield the following equation for :

(3.9)

where .

After the spiral confined concrete strength ( ) was calculated it is used to replace in equations 3.3, 3.5, and 3.6. The predicted capacities of uncorroded columns and the percent loss in capacity due to corrosion are listed in Table 3.3. Table

3.3 shows that the ACI 440 method significantly under-predicted the actual capacity of the specimens, because the corroded specimens had higher capacity than the ACI 440 Method's calculated value for uncorroded specimens. Thus, the amount of steel spiral loss necessary to obtain the drop in capacities shown in Table 3.3 were calculated using only the M-P Model and Mander's Model.

The amount of steel spiral area loss was calculated by making the capacity a function of steel spiral corrosion. Thus, it is possible to calculate the capacity of a steel spiral reinforced column wrapped or unwrapped with any given amount of corrosion. The effect of vertical steel bar loss was neglected in these calculations because it was visually confirmed that most of the corrosion occurred in the steel spirals and because of the small amount of vertical steel, . Additionally, with increasing confining stress, the vertical steel's effective contribution to capacity decreases, where effective contribution can be defined as .

The calculated capacity of both wrapped and unwrapped columns were plotted versus amount of corrosion in the steel spiral in Figure 3.24. The capacities in Figure 3.24 were divided by their individual calculated capacities when not subjected to corrosion to enable comparison of columns of different concrete strength, the control specimens where f'_c = 5,200 psi and the specimens subjected to corrosion where f'_c = 6,700 psi. Therefore, from Figure 3.24 we see that if one of the unwrapped specimens had lost all spiral reinforcement to corrosion it would drop to 0.71, or 71%, of its uncorroded capacity whereas the wrapped specimen would drop to only 87% of its uncorroded capacity.

The horizontal lines in Figure 3.24 represent the actual experimental capacities obtained divided by their corresponding calculated uncorroded capacities using the M-P Model. Note that the capacity of the control specimen #2SCTL is close to 1 as expected because it was not subjected to corrosion. Whereas, the average capacities of the specimens subject to corrosion are both below 1, and, both cross their respective calculated capacities at about the same amount of spiral steel loss, 73% for unwrapped

and 76.7% for wrapped, giving an average effective spiral steel loss of approximately 75%. The close correlation of percent steel area loss in the spirals between the unwrapped and wrapped specimens helps to validate that the models are accurately predicting the effective amount of steel spiral loss. However, as presented earlier in Table 3.1 the maximum amount of mass loss calculated from Faradays Law using Eq. 3.1was 17.6%. The maximum steel spiral loss would be 31.7% if all the corrosion had occurred in the spiral instead of being evenly distributed between the vertical and spiral steel.

Despite the fact that the maximum mass loss of steel spirals was only 31.7% this also assumes even distribution of corrosion throughout the spiral, and corrosion of RC columns is never uniform. In particular, areas near the water line experience more corrosion because of wetting and drying and because they are nearest an abundant supply of oxygen. Therefore, a 31.7% of total mass loss means that there was likely at least 75% of steel spiral loss in certain sections of the spiral, and this was confirmed by post test visual observation of the specimens subjected to corrosion. In fact Figure 3.25 shows a piece of steel spiral that has a spot where more than 75% of the area was lost due to corrosion. It is important to remember that the 75% calculated corrosion is the effective amount of corrosion and not the actual corrosion in the entire spiral. Rather the specimens subjected to corrosion behaved as if they had lost 75% of their spiral reinforcement due to corrosion, and actually had more or less than 75% of corrosion along its length.

3.3.2 *Strain prediction*

Both the ACI 440 Method and the M-P Model predict the ultimate strain as well as ultimate strength. The maximum compressive strain was calculated using the ACI 440 Method modified to account for spiral confined concrete and corrosion using the following equation:

(3.10)

where = 0.002, strain at maximum compressive stress of unconfined concrete, = 1.0 for round columns, geometry efficiency factor, = maximum confining pressure from Eq.3.4 except using in place of , = spiral confined concrete strength calculated by using equations 3.9 and 3.7, and = effective strain in FRP wrap at failure. Note the value (0.00948) used was the average actual radial strain at failure recorded by radial strain gauges that were placed on the CFRP jackets. This equates to using the ACI 440 Method for computing where the ultimate tensile strain, = 0.014 obtained from coupon tests, is multiplied by a reduction factor 0.677. The reduction factor accounts for the wrap failing before reaching its ultimate tensile strain due to the tri-axial loading the jacket experiences versus pure tension exhibited in tensile coupon tests. Values for in the ACI 440 range from 0.57 to 0.61. However, it is likely that these values are conservative and that the CFRP composite used to calculate these values was different than the one used in this research. Therefore, it is best to use the actual recorded values for the effective strain to get a more accurate prediction of ultimate compressive strain of a CFRP composite wrapped column, when available.

The M-P Model uses a process of three equations after calculating , the jacket stiffness, to calculate ultimate compressive strain. First the plastic dilation rate ( ), which relates change in radial strain to change in axial strain, and the ultimate radial strain ratio ( ) are calculated. Then the ultimate axial strain ( ) can be calculated.

(3.11)

(3.12)

(3.13)

where and are defined previously and = radial strain corresponding to taken as 0.0005 in./in.

The actual ultimate compressive strains of the CFRP wrapped specimens, #5SCORW and #6SCORW, were 0.0243 in./in. and 0.0208 in./in. respectively, making the average ultimate compressive strain of the CFRP wrapped specimens equal to 0.02255 in./in. However, these specimens were subjected to corrosion and therefore, the above equations were adjusted by using the corrosion adjusted , strength of spiral confined concrete, to calculate the ultimate compressive strain. The calculated ultimate compressive strain using the ACI 440 Method and the M-P Model considering 75% steel spiral loss were 0.02259 in./in. and 0.02469 in./in. respectively giving a percent difference from average actual ultimate compressive strain of 0.2% and 9.5%, respectively. These results show that the ACI 440 Method better predicted the average ultimate compressive strain compared to the M-P Model. However, the M-P Model had only a 1.6% difference when compared to the higher value of the two wrapped specimens.

3.3.3 *Stress-strain models*

Stress-strain models were developed to compare with the actual stress versus strain data of the CFRP wrapped specimens. Stress-strain plots of FRP wrapped columns are bilinear in nature and thus usually require a piecewise function or combination of two functions to model them. In this study the following equations were used to develop the stress-strain graphs. It is important to note that the inputs to the following equations determine the shape of the graph; therefore, each graph is independent from the other and portrays an accurate representation of the method they are modeling.

The equations used to develop the stress ( ) versus strain ( ) plots were:

(3.14)

(3.15)

where = slope/modulus of the second linear portion of the graph, = transition strain, = unconfined concrete modulus which are given by:

(3.16)

(3.17)

(3.18)

Figure 3.26 shows the graphs of the stress-strain models developed using values obtained from the ACI 440 Method assuming 75% spiral steel loss, the M-P Model assuming 75% spiral steel loss, and the recorded test values for the wrapped specimens #5SCORW and #6SCORW. Figure 3.26 confirms the previous stated conclusions that the M-P Model more accurately predicts the compressive strength of the columns while the ACI 440 method better predicts the average axial strain of the specimens.

Figure 3.27 shows the graphs of the stress-strain models developed using values obtained from the ACI 440 Method and the M-P Model assuming no steel loss, and the recorded test values for the wrapped specimens #5SCORW and #6SCORW. Figure 3.27 shows that the corrosion affected the end result or performance of the columns more than the initial performance considering the models more accurately predict the behavior of the columns before ultimate strength is reached when not considering the corrosion, but are more accurate in predicting the ultimate compressive strength and strain when corrosion is considered.

Figure 3.28 shows the graphs of the stress-strain models developed using values obtained from the ACI 440 Method and the M-P Model not accounting for the steel spiral, and the recorded test values for the wrapped specimens #5SCORW and

#6SCORW. Figure 3.28 illustrates the importance of taking the steel spiral into account. The equation proposed in ACI 440 (2008) currently neglects the effects of the internal hoop reinforcement. However, as shown in the Figure 3.28 this is likely overly conservative.

Table 3.2: Test Results Summary

Specimen	Max Load (kip)	Max Stress (psi)	Axial Strain at Max Load (με)	Axial Strain at Break (20% drop in load) (με)
#1SCTL	NA	NA	NA	NA
#2SCTL	502	6392	5000	6900
#3SCOR	517	6583	3000	3800
#4SCOR	418	5322	5100	7300
#5SCORW	1190	15152	24300	24300
#6SCORW	1182	15050	20800	20800
#7SCOREX	NA	NA	NA	NA
#8SCOREX	375	4775	3300	3200
#9HYBCTL	426	5424	2600	4200
#10HYBCTL	445	5666	4500	8400
#11HYBCOR	443	5640	8400	10300
#12HYBCOR	512	6519	6000	7300
#13GLCTL	444	5653	3200	3700
#14GLCTL	402	5118	3400	8200

Table 3.3: Calculated Non-corroded Capacity and Actual Corroded Capacity

Method	Calculated Non-corroded Capacity (kip)	Experimental Capacity (kip)	% Capacity Loss (%)
ACI 440	1138	1186	4.0
M-P Model	1310	1186	-10.5
Mander's Model (Steel spiral only)	586	468	-25.2

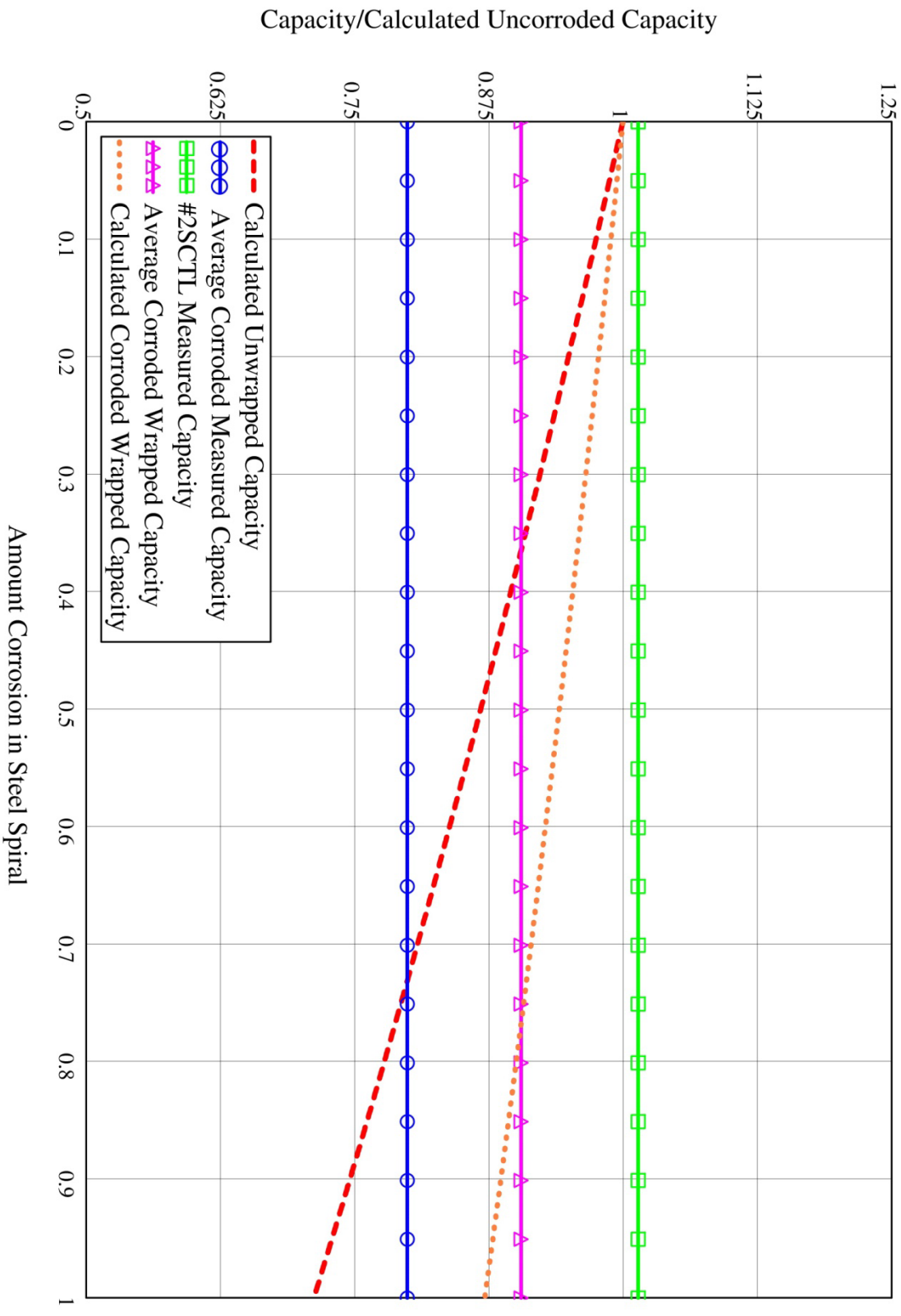

Figure 3.244: Axial capacity versus corrosion

Figure 3.25: Section of spiral with more than 75% steel loss

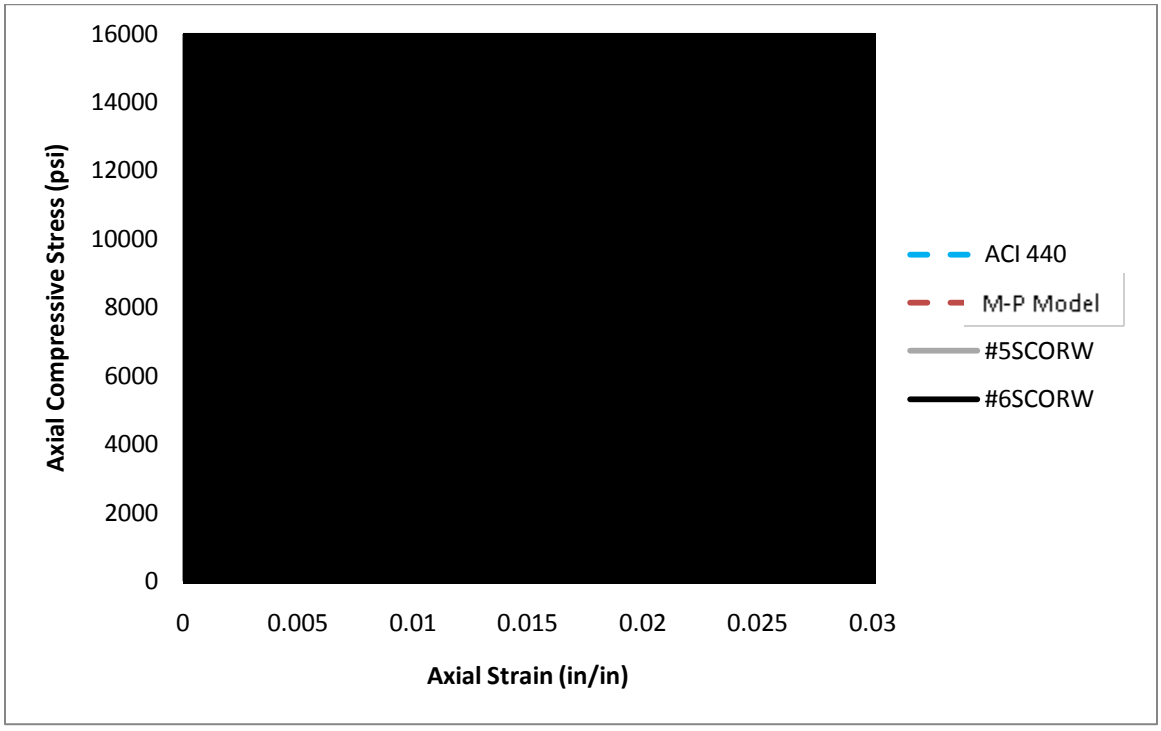

Figure 3.26: Stress-strain models assuming 75% spiral steel loss

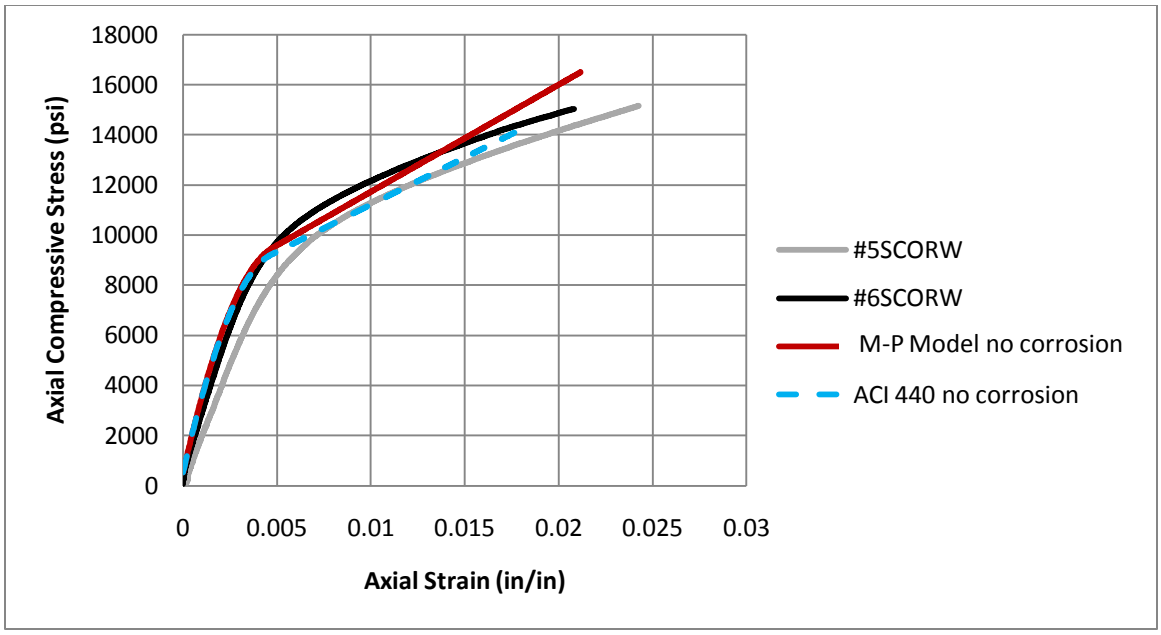

Figure 3.27: Stress-strain models assuming no spiral steel loss

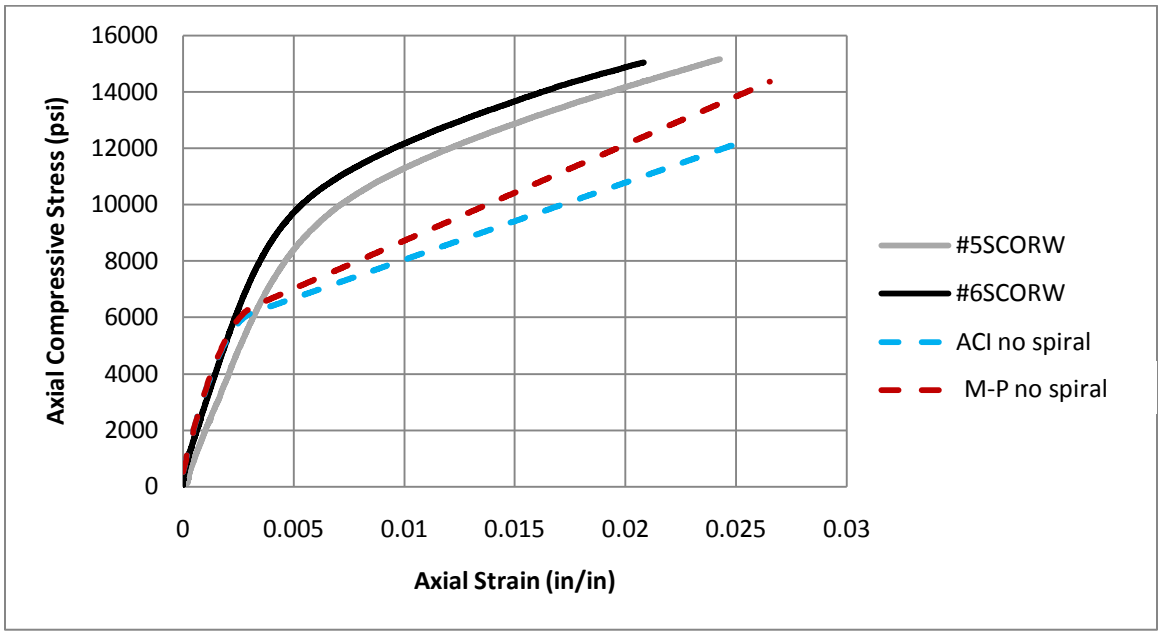

Figure 3.28: Stress-strain models not accounting for steel spiral

THIS PAGE INTENTIONALLY LEFT BLANK

4.0 FIELD APPLICATION TESTS

This chapter presents testing conducted on two actual bridge columns from the Highland Drive bridge that was built in 1965 on I-80 in Salt Lake City, Utah. The bridge was rehabilitated in June 2000 with CFRP wraps. Two of the bridges columns that were rehabilitated with CFRP jackets in June 2000, and had been in service for approximately 9 years in their rehabilitated condition, were retrieved from the bridge in 2009 when the bridge was demolished. These columns were loaded up to 2,000 kips in the load frame shown in Figure 4.1. Both columns were loaded concentrically as well as eccentrically.

4.1 Instrumentation

Electrical strain gauges were placed at eight locations, spaced every 45° around the perimeter of the column, at the mid height of the columns. At each location, one strain gauge was placed to measure radial strain and a second to measure vertical strain. Four Linear Variable Differential Transducers (LVDTs) were also placed every 90° around the mid-height of the column and spanned a minimum vertical distance of 2 ft to measure axial deformations. The applied axial load was measured using a load cell with a capacity of 2,000 kip. A diagram showing the arrangement of the electrical strain gauges and LVDTs is provided in Figure 4.2.

Strain values were taken directly from the readings of the electrical strain gauges. Vertical strain was calculated using the vertical LVDTs by recording the change in length and dividing it by the original gauge length. Axial stress values were calculated by dividing the force reading of the load cell by the cross sectional area of the column.

Figure 4.1: Column in load frame

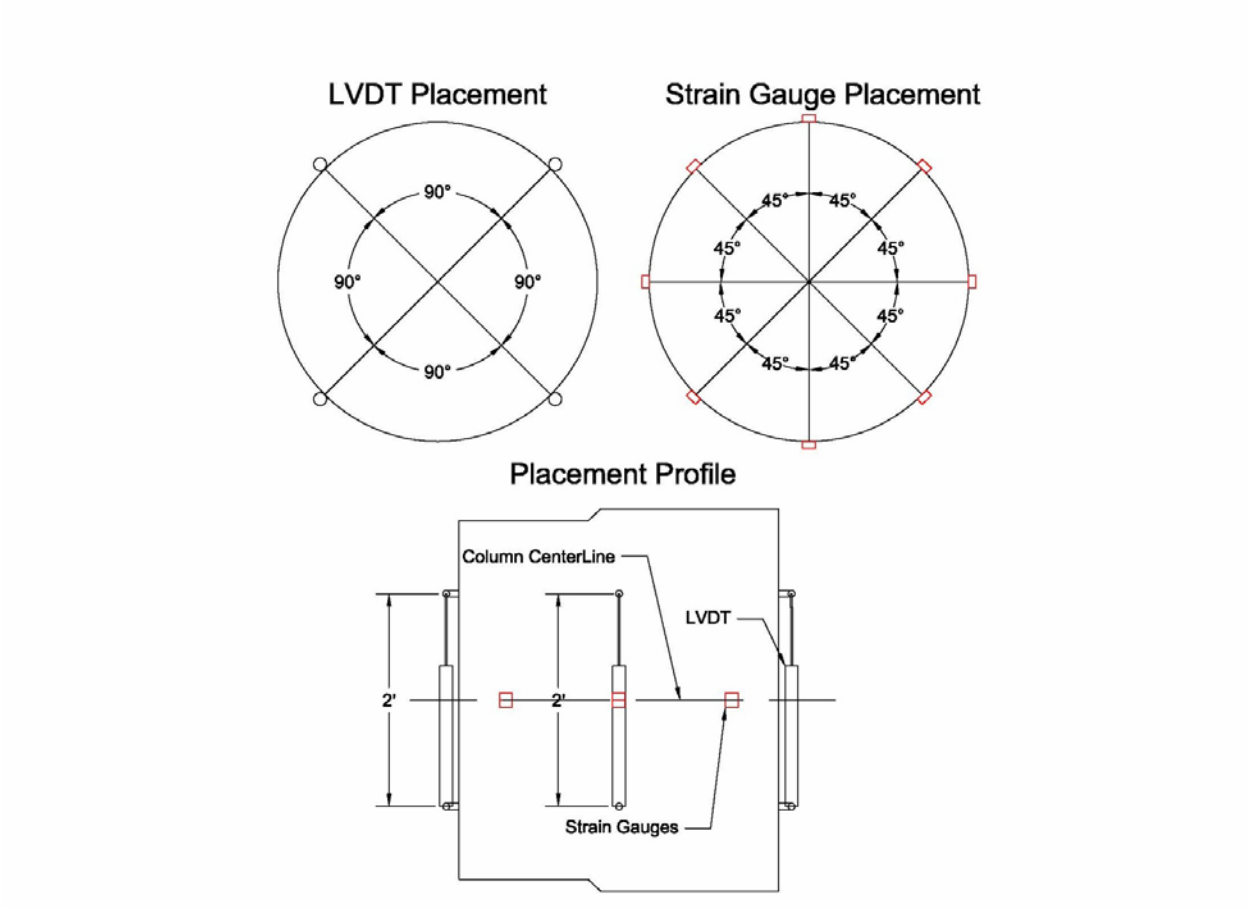

Figure 4.2: Instrumentation diagram

4.2 Test method and observations

Both columns, LG1 and LG2, underwent eight (8) load tests as shown in Table 4.1. Each test was performed using ten half-cycles in load control mode: two half-cycles for each at each 400 kips increment up to 2,000 kips as shown in Figure 4.3. Steel plates, measuring 1 in. thick, were used to achieve three different eccentricities; two of the steel plates were 6 in. wide by 42 in. long and the other two were 12 in. wide by 42 in. long. The plates were placed in-between two 40 in. by 40 in. by 3 in. thick plates that were located at the base of the load frame, as shown in Figure 4.4.

All plates remained in place during the concentric load test, but for each eccentric test, a plate on the south side was removed until only Plate 4 remained. These four tests (concentric, eccentric 1, 2, and 3) were then repeated for each column after two vertical slits, approximately 1/8 in. wide and completely severing the FRP jacket, were cut on the compression (north) and tension (south) sides of the column by use of a mini-grinder. A listing of all the performed tests can be found in Table 4.1.

When cutting the CFRP jacket of column LG2, the carbon fibers began to burst open once the majority of the outer fibers were cut. In column LG2 this occurred on both the compression and tension sides of the column. For column LG1 this only occurred at the very top of the column on the compression side. This behavior may be due to a small amount of corrosion occurring after application of the carbon fiber jacket, and/or could have been caused by continued creep of the column. Therefore, volumetric expansion of the rusting steel reinforcement and/or creep effects in this area induced a prestressing force in the jacket prior to testing, and delaminated some of the repair grout from the original concrete. Once the CFRP jacket was cut, the prestressing force was released and allowed the repair grout to pull away from the original concrete causing a 0.04 in. wide crack shown in Figure 4.5. Column LG2 had more delamination than column LG1 because it had a greater area of repair grout. It is important to note that some corrosion

likely occurred during time that columns were stored outside the laboratory with unwrapped cut ends exposed to rain and snow.

A ‘Tap Test’ consisting of sounding the FRP surface with a quarter coin, was conducted on the CFRP jacket of column LG1 after the first four load tests were completed and before the jacket was cut, and no delamination was audibly detected. Thus, the CFRP jacket was effective in keeping the cracks between the repair grout and the original concrete closed until the jacket was cut.

As testing continued, the cracks widened and the repair grout continued to delaminate from the original concrete; this decreased the effective confinement of the CFRP jacket. Figure 4.6 shows the strain values measured by the eight radial gauges versus axial load after the CFRP jacket was cut.

As axial load increased, delamination reached Gauge 7 and actually caused the strain gauges to report negative values, which indicates they experienced compressive strain due to the release in tensile stress from the jacket. However, after each test, the gauges were manually reset to zero which made delaminated areas show zero strain for subsequent tests as shown in Figure 4.7. Figure 4.7 shows there was significant delamination in column LG2 near the cuts (Gauge 2 and Gauge 6). The typical observed localized concrete bond failure can be seen in Figures 4.8 and 4.9. The radial strain graphs for all tests performed on both LG1 and LG2 are shown in figures A.13 to A.28 of the appendix.

Table 4.1: Tests Performed for Columns LG1 and LG2

Test Number	Test Name/Type	Plates Removed	Support Length Removed	Bottom Eccentricity
1	Concentric	None	None	None
2	Eccentric 1	Plate 1	12 in.	4.5 in.
3	Eccentric 2	Plates 1 and 2	18 in.	7.6 in.
4	Eccentric 3	Plates 1,2, and 3	24 in.	11.0 in.
5	Jacket CUT Concentric	None	None	None
6	Jacket CUT Eccentric 1	Plate 1	12 in.	4.5 in.
7	Jacket CUT Eccentric 2	Plates 1 and 2	18 in.	7.6 in.
8	Jacket CUT Eccentric 3	Plates 1,2, and 3	24 in.	11.0 in.

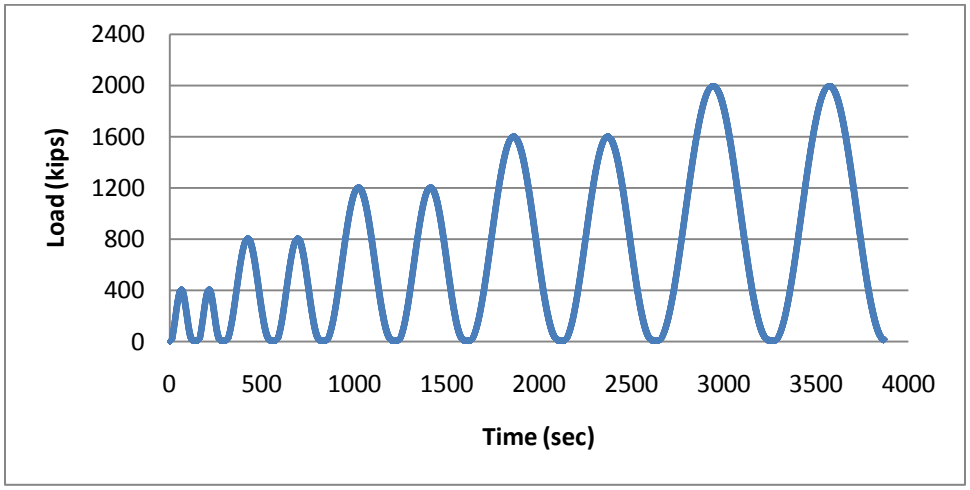

Figure 4.3: Load cycles for LG1 and LG2

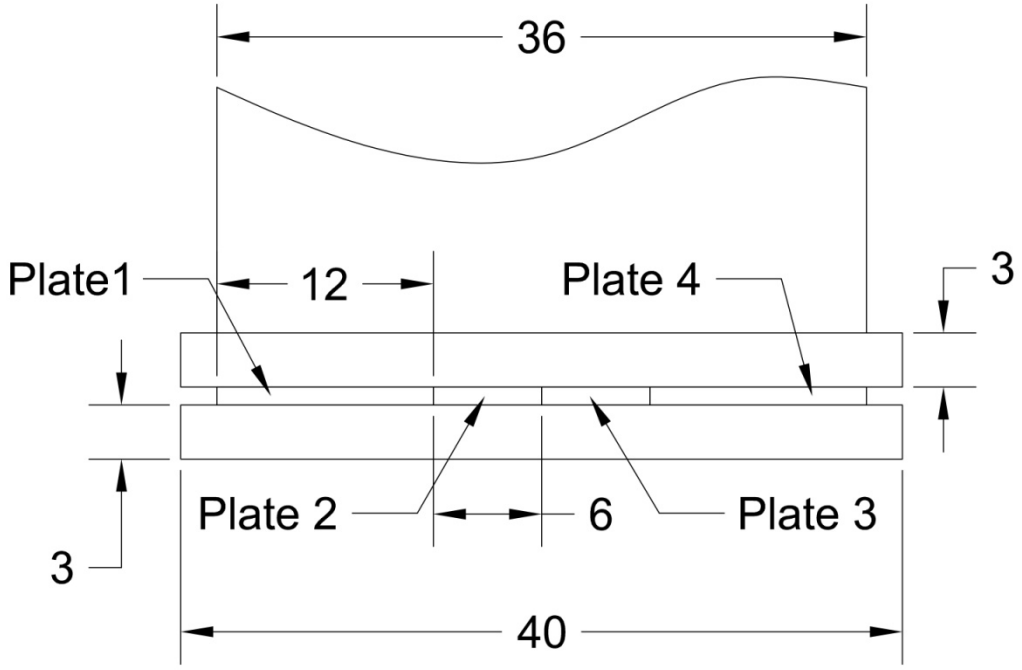

Figure 4.4: Eccentricity diagram

Figure 4.5: Original crack after jacket was cut

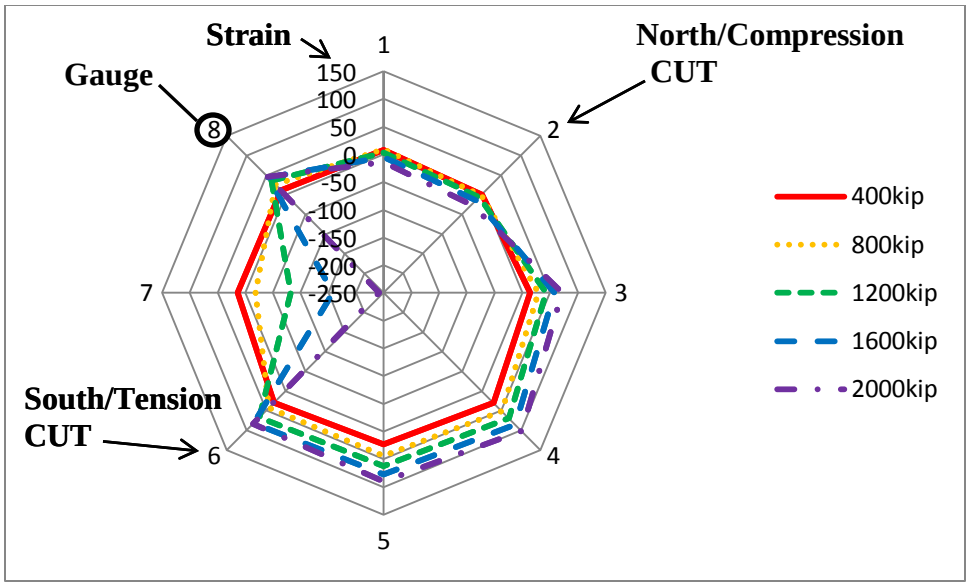

Figure 4.6: Radial micro-strain for column LG2 during CUT concentric test

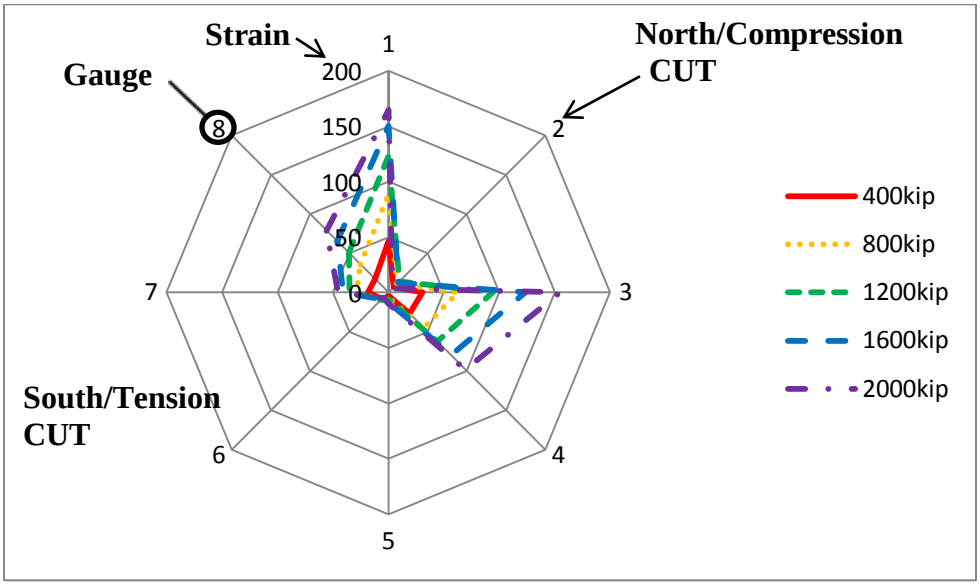

Figure 4.7: Radial micro-strain for column LG2 during CUT eccentric 3 test

Figure 4.8: Delamination cracking at end of LG1 CUT eccentric 3 test

Figure 4.9: Picture of delamination of LG1 after testing

4.3 Axial stress versus axial and radial strain graphs

The graphs presented in Figures 4.10 through 4.17 show the measured axial and radial strains due to an applied vertical stress. The radial strain values for the following graphs were calculated by averaging the strain values on the compression side (Gauges 1, 2, and 3) and the gauges on the tension side (Gauges 4, 5, and 6). The axial strain values are an average of the calculated strain of the two vertical LVDTs on each respective side. These strain values were taken at the peak of the 2nd half-cycle for each given load level. The axial stress was calculated by taking the measured axial load and dividing it by the cross-sectional area.

Figures 4.10, 4.12, 4.14, and 4.16 show that as the eccentricity increases the north/compressive axial strain increases and the radial tensile strain increases. Figures 4.11, 4.13, 4.15, and 4.17 show that as the eccentricity increases the south/tensile side show a decrease in compressive axial strain, in addition to a radial tensile strain decrease. When comparing Figures 4.10 and 4.12, we see there is a slight increase in axial strain and a slight decrease in radial tensile strain after cutting the CFRP jacket. However, the difference between Figures 4.14 and 4.16 is minimal and in some cases reversed.

Table 4.2 shows the axial displacement of the columns on both the north/compression and south/tension side at 2,000 kips load. The displacement values were calculated by taking the strain values calculated from the vertical LVDTs and multiplying them by the total length of the column. Table 4.2 shows how the eccentricity increases the north displacement and decreases the south displacement. For column LG1, comparing the concentric to the eccentric 3 test, the column's axial displacement on the north side of the column doubled, and on the south side it decreased substantially. For column LG2, comparing the concentric to the eccentric 3 test, the column's axial displacement on the north side of the column almost doubled and on the south side it decreased. These results are compatible with the radial strain readings.

Table 4.2 also shows that cutting the CFRP jackets did not significantly affect the displacement values when placed under a 2,000 kips load. However, it is expected that at loads higher than 2,000 kips more significant differences would be observed; the jacket would become more engaged and thus more of a factor at higher loads/displacements.

Table 4.2: Axial Displacement Values at 2,000 kips Load

Test	Calculated From LVDT Readings	
	North Axial Displacement	South Axial Displacement
(Name)	(in.)	(in.)
LG1 Concentric	0.07448	0.06545
LG1 CUT Concentric	0.07992	0.05970
LG1 Eccentric 3	0.14573	0.00559
LG1 CUT Eccentric 3	0.15069	0.00525
LG2 Concentric	0.07624	0.06432
LG2 CUT Concentric	0.06365	0.07393
LG2 Eccentric 3	0.12254	0.01165
LG2 CUT Eccentric 3	0.12227	0.01198

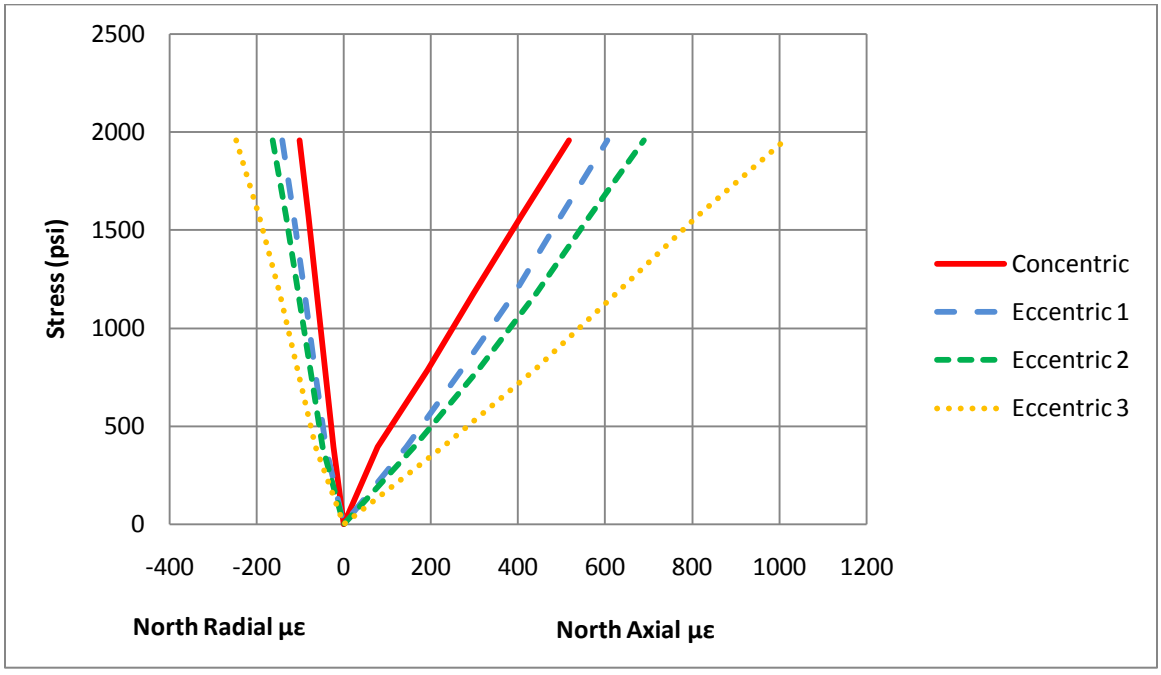

Figure 4.10: LG1 north/compressive side axial stress versus strain

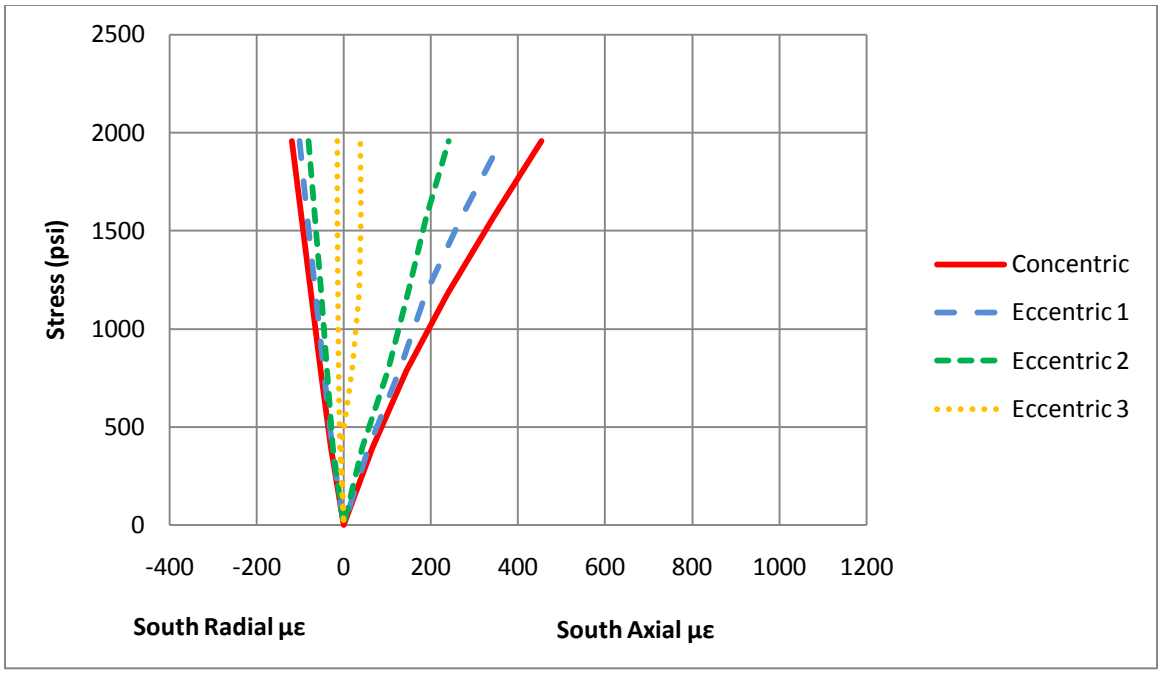

Figure 4.11: LG1 south/tensile side axial stress versus strain

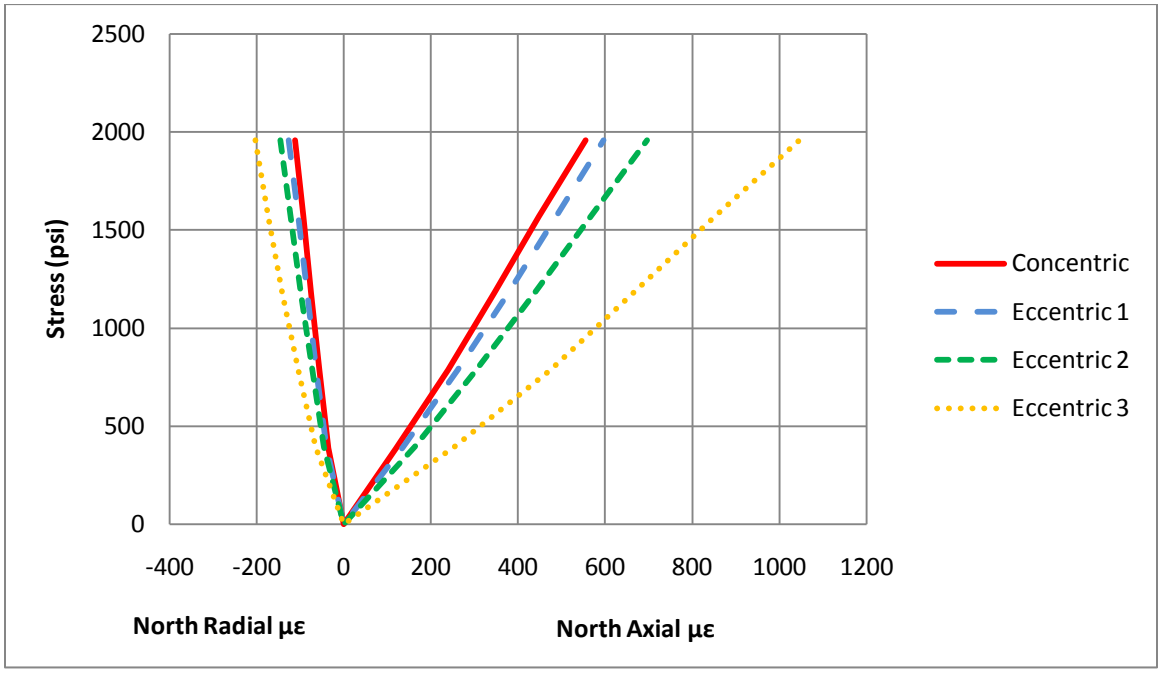

Figure 4.12: CUT LG1 north/compressive side axial stress versus strain

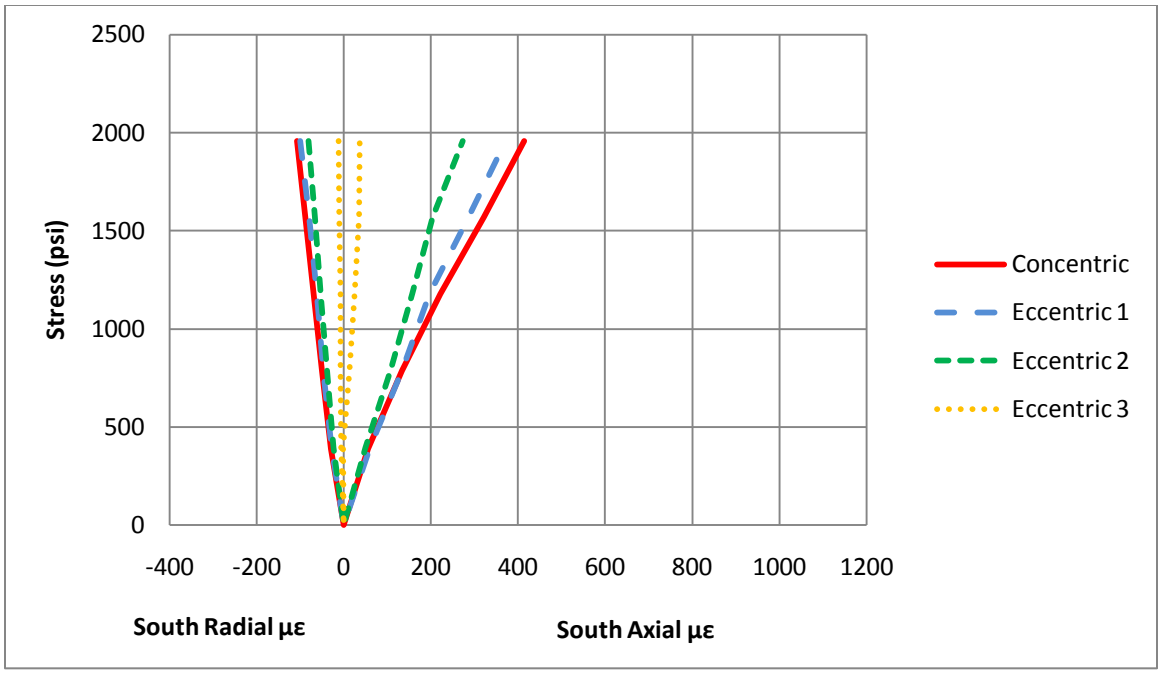

Figure 4.13: CUT LG1 south/tensile side axial stress versus strain

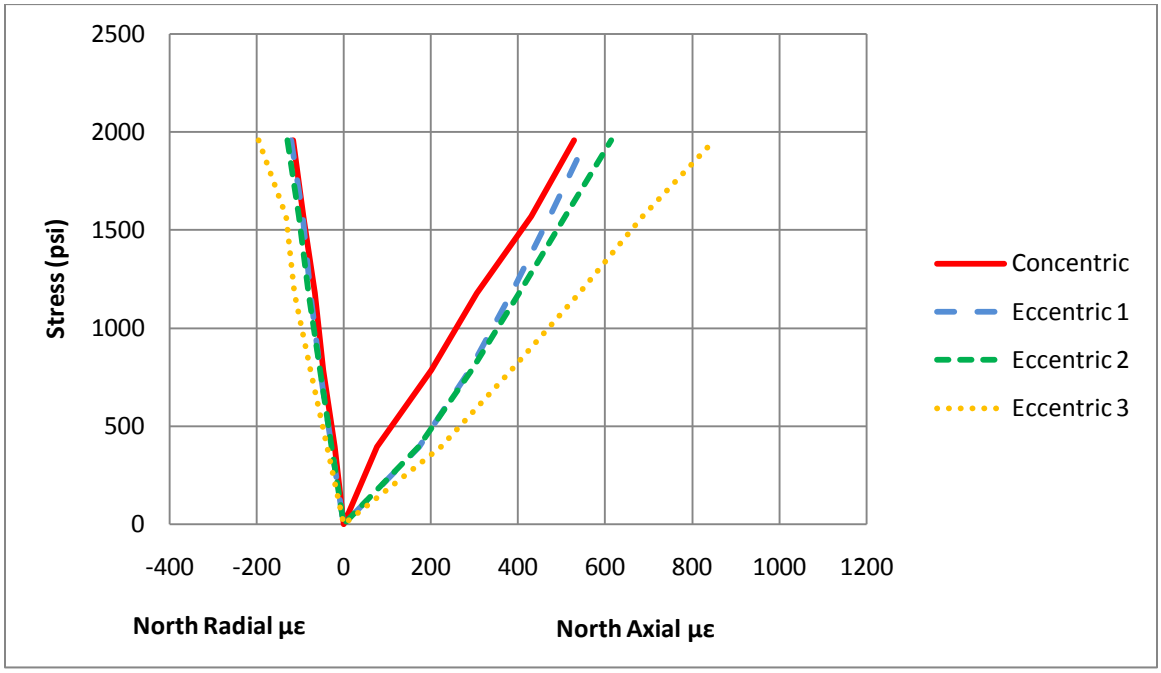

Figure 4.14: LG2 north/compressive side axial stress versus strain

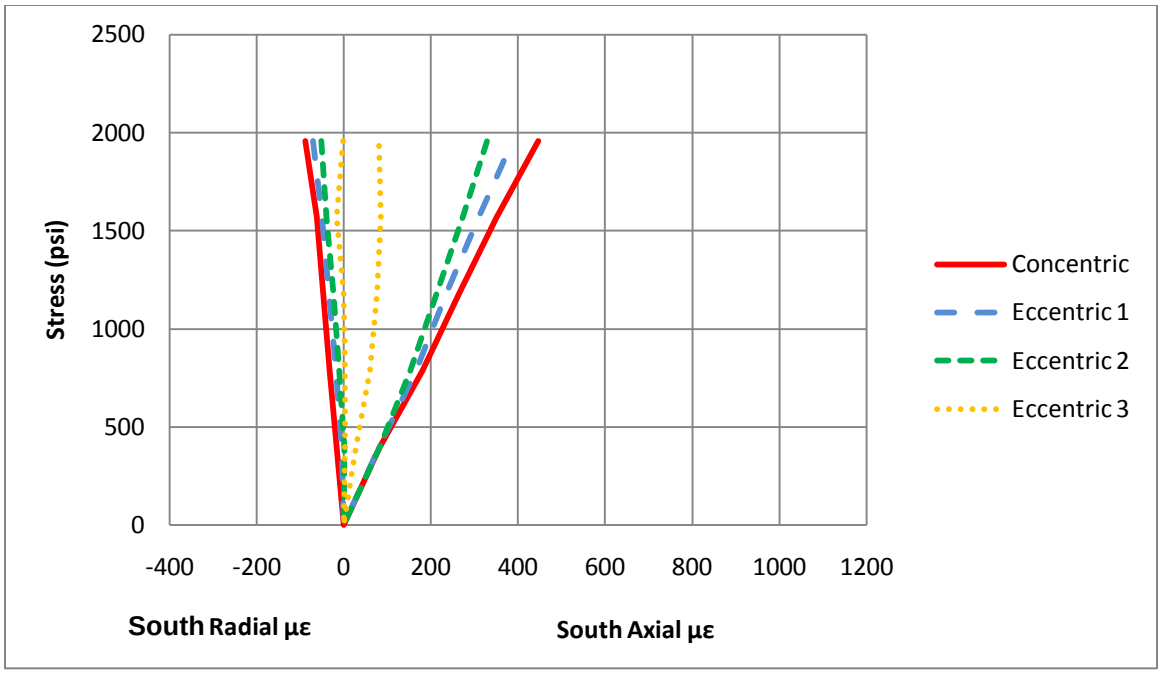

Figure 4.15: LG2 south/tensile side axial stress versus strain

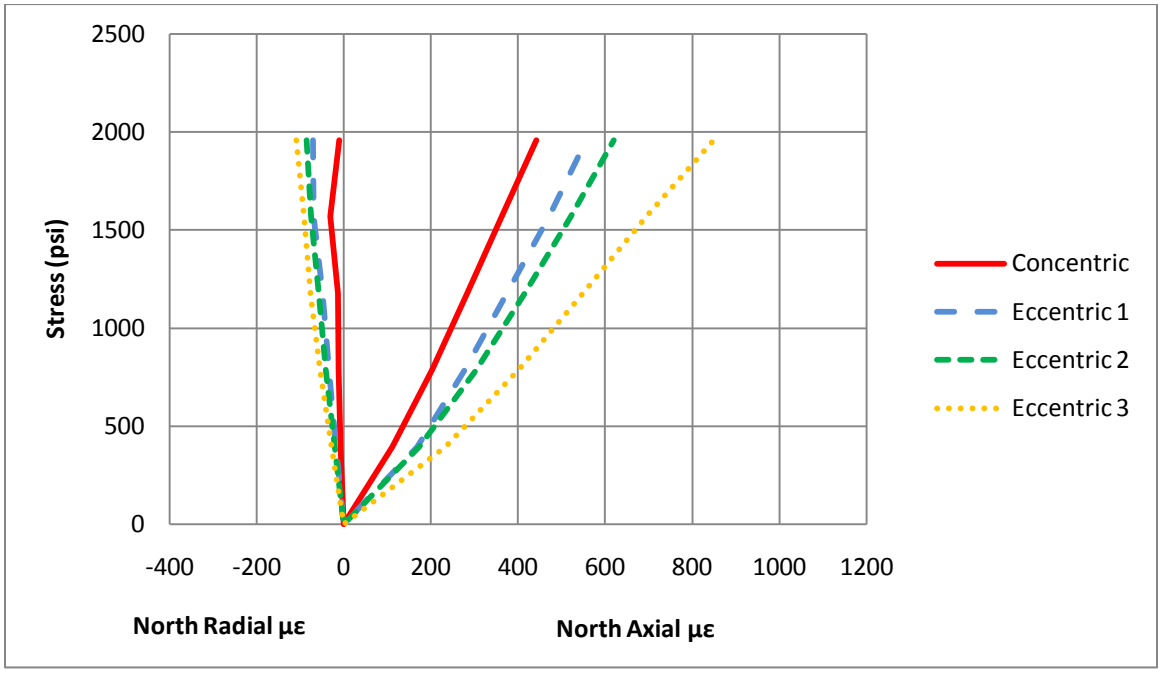

Figure 4.16: CUT LG2 north/compressive side axial stress versus strain

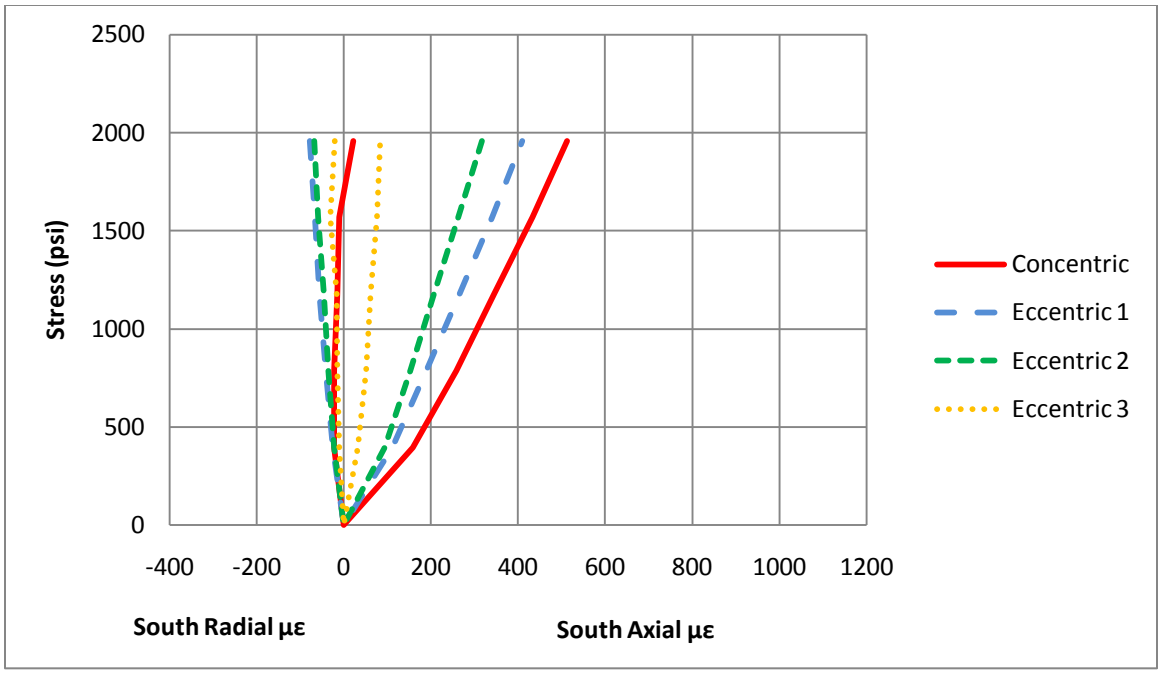

Figure 4.17: CUT LG2 south/tensile side axial stress versus strain

4.4 Delamination and bond analysis

Post test observation of the tested columns showed that none of the cracks went significantly deeper than the concrete cover, leaving the entire concrete core basically intact. In fact, most of the cracking was found at the interface between repair grout and original concrete, or completely within the repair grout. It appears that the delamination of the CFRP jacket after it was cut was not due to lack of bond between the concrete and the jacket, but due to delamination between the grout and the original concrete, as shown in Figure 4.18.

There appeared to be a good bond between the repair grout and the jacket. Figure 4.19 shows a large piece of the jacket, about 2 ft tall and stretching around one half of the column that was torn off by the chain used to lay the column on its side after removing it from the testing frame. Note that in Figure 4.19 a significant portion of the CFRP jacket was bonded to the repair grout and not to original concrete. Adhesion tests were performed to determine if the CFRP jacket was bonded to the original concrete and not just the repair grout. The adhesion tests were performed using an Elcometer Model 106 Adhesion Tester, shown in Figure 4.20. Adhesion tests were performed in various places on both columns LG1 and LG2 in areas that had not delaminated during testing.

The Elcometer tests in regions of repair grout usually indicated a good bond between the CFRP jacket and the grout because grout was removed, as shown in Figure 4.21. However, due to the fracturing of the grout prior to the pull off test, or weakness in the grout itself, the stress required to remove the CFRP sections from the grout was about 200 psi or less. In areas where the CFRP jacket was bonded to original concrete, the adhesive applied to the column at the time of application of the CFRP jacket often failed before the concrete layer, as shown in Figure 4.22. This could be due to an initial installation problem. The bond stress measured when the adhesive failed varied between 200 – 400 psi.

Figure 4.23 shows small sections of the CFRP jacket that could be peeled off near areas that were damaged from the demolition of the Highland Bridge and transportation of the columns from the Highland Bridge to the laboratory prior to testing. The peeled off sections were not adequately bonded to the concrete. This is likely because the damage allowed moisture to enter and degrade the bond, or perhaps the full bond between the original concrete and the CFRP jacket was not adequate due to an installation issue.

Overall, the rehabilitation of these columns was successful, because the CFRP jacket gave additional reinforcement to the columns and did not fail under the 2,000 kip load tests. Areas of the jacket that had been damaged before testing did not show any additional damage as a result of loading the column to 2,000 kips. Though the bond between the jacket and original concrete of the column was not strong enough to fail the concrete, it is not as critical to have good concrete bond with circular columns as long as the bond in the jacket splice is sufficient.

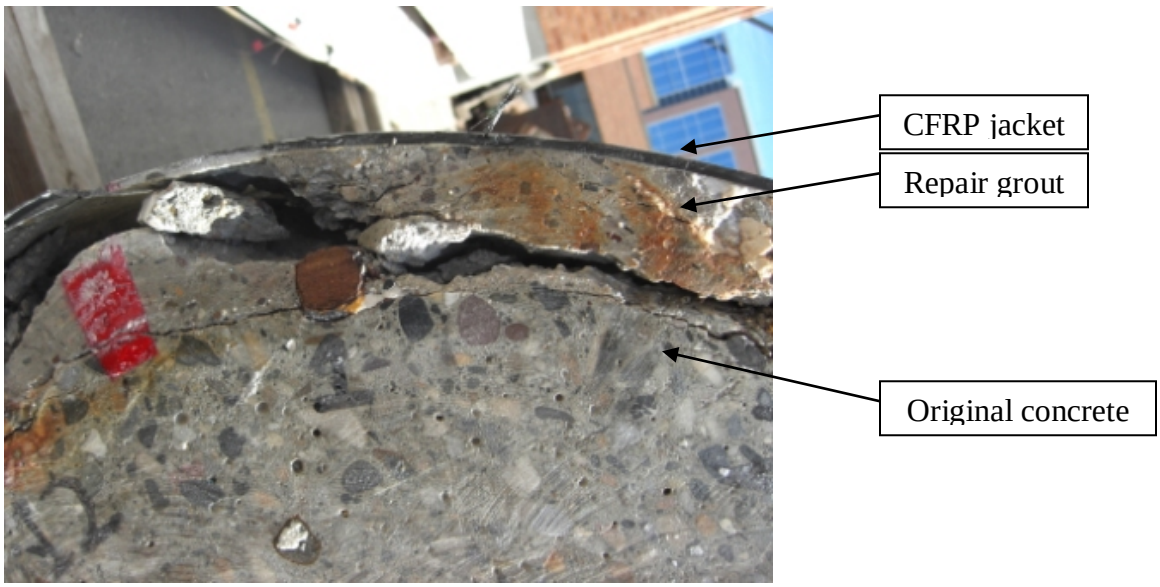

Figure 4.18: Debonding of repair grout and original concrete

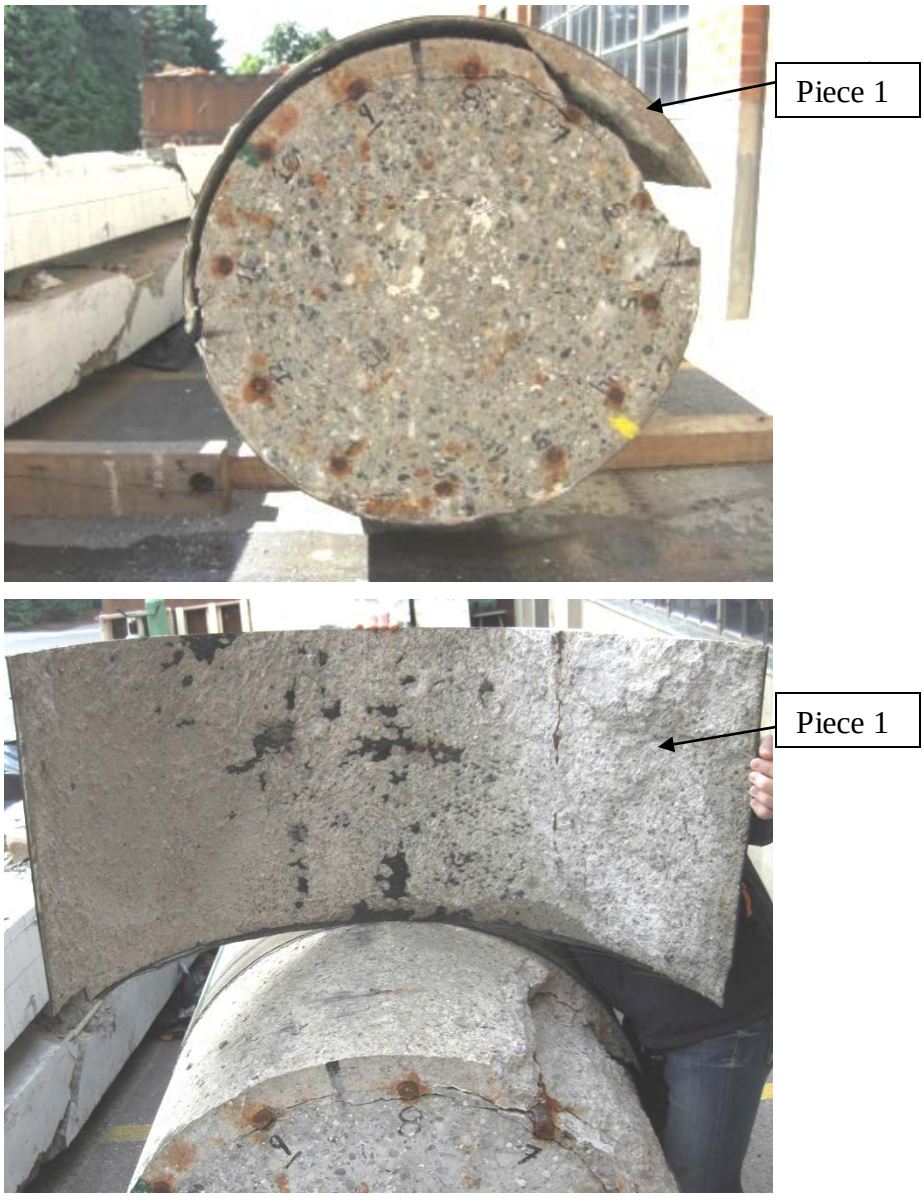

Figure 4.19: CFRP Jacket-concrete bond – Piece 1 removed from column

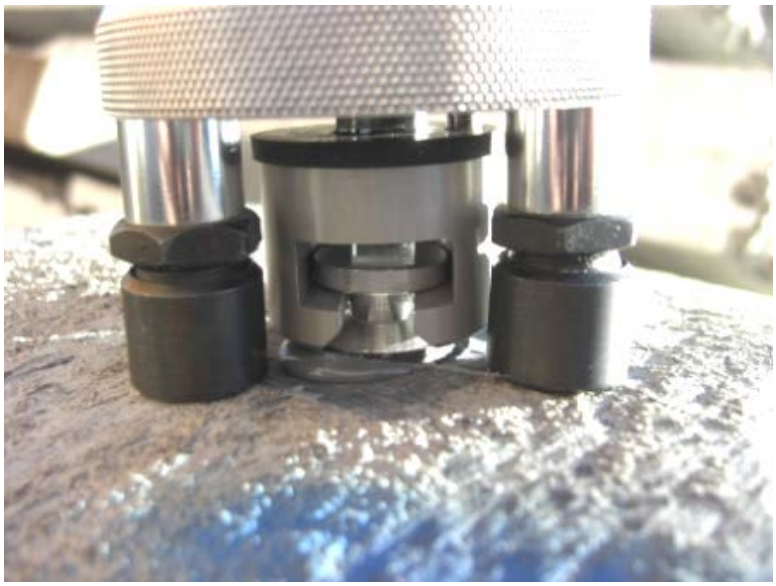

Figure 4.20: Elcometer Model 106 Adhesion Tester

Figure 4.21: Grout region bond test

Figure 4.22: Original concrete region bond test

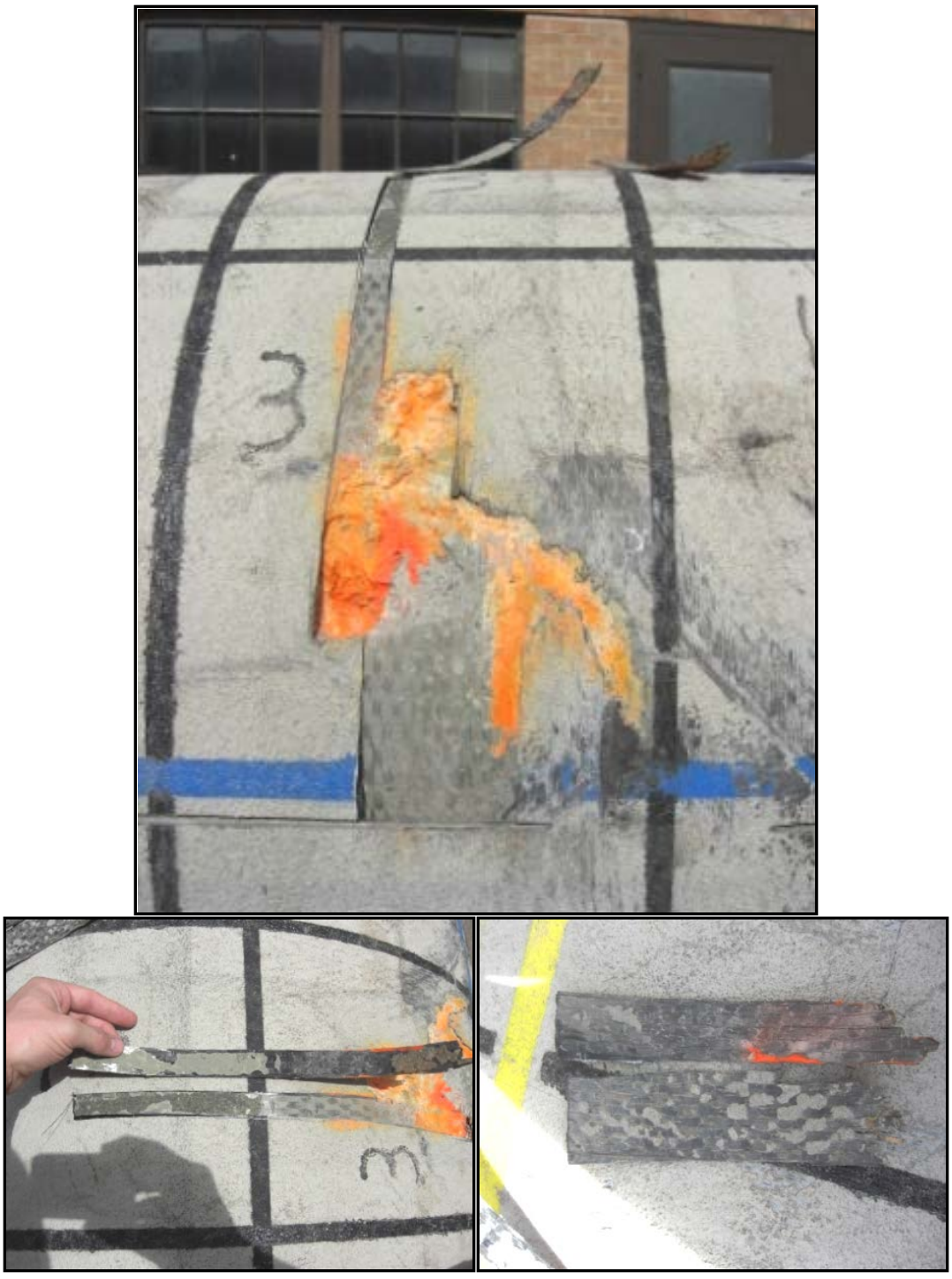

Figure 4.23: LG1 Damaged section (Top) sections that were peeled off (Bottom Left and Right)

THIS PAGE INTENTIONALLY LEFT BLANK

5.0 CONCLUSIONS

This chapter presents the conclusions that were drawn as a result of this research. The conclusions are summarized in two categories: Section 5.1 regarding the medium-scale specimens and Section 5.2 for the full-scale columns from the field.

5.1. Medium-scale specimens

The medium-scale columns were constructed with three different internal reinforcement types or variations consisting of all-steel, steel vertical with GFRP spiral (hybrid), and all-GFRP vertical and spiral. Eight columns were subjected to corrosion. Two of the all-steel reinforced concrete specimens that were subjected to corrosion were wrapped with CFRP composite jackets. All columns were tested in axial compression and the following conclusions can be drawn:

1. CFRP jacketing is an effective method for rehabilitating corrosion damaged columns. CFRP jackets slow the corrosion process and increase the ultimate strength and ultimate strain of the columns. Despite the rehabilitated columns' explosive failure, the ultimate strength and ultimate strain increase would provide a sufficient factor of safety to abate such concerns. This is particularly true in the case of severely corroded columns where the hoop steel has been compromised and brittle failure occurs at much lower load and strain levels compared to the non-corroded specimens.

2. From the test results of this study it appears that there were no detrimental effects due to corrosion on the hybrid specimens which had vertical steel bars and GFRP spirals. However, the overall load capacity of the columns was lower than the all-steel control, and was approximately the same as the all-steel reinforced

specimens subjected to corrosion. The axial strain at peak axial load was nearly double for hybrid specimens subjected to corrosion versus all-steel reinforced specimens subjected to corrosion. The tests showed that hybrid columns have an overall more ductile failure compared to severely corroded all-steel RC columns and all-GFRP RC columns. Excessive damage was evident before total failure because of more cracking and cover falling off before failure for the hybrid columns subjected to corrosion.

One interesting observation regarding hybrid columns is that the hybrid columns subjected to corrosion had a more ductile failure than the control hybrid columns. The control hybrid columns still showed cracking and cover loss before failure, but lost all load suddenly instead of a slow steady crumble and steady drop in load observed for the columns subjected to corrosion.

3. The hybrid columns subjected to corrosion had less than half the amount of corrosion, in terms of percent steel loss, as the all-steel reinforced columns. The GFRP spiral helps to restrain the tensile forces produced by the corrosion reaction and prevent cracking. As a result, the hybrid columns had much less cracking which helped keep the rate of corrosion to lower than 1/3 the rate of the all-steel columns. It is important to note that the hybrid columns had less total steel than the all-steel reinforced columns; this is the reason for 1/2 the percent steel loss, but 1/3 the rate of mass loss.

   Additionally, most of the corrosion in all-steel RC columns occurs in the spiral or hoop reinforcement. This can be a significant concern, because if the hoops become severely corroded the columns loose ductility and have sudden brittle failures. Using GFRP spirals my help avoid these potential problems.

4. For columns not exposed to corrosive environments, steel internal reinforcement provides the best performance with columns achieving higher axial capacity and

ductility. However, in applications where corrosion is possible, hybrid reinforcement using steel vertical bars and GFRP spirals may be a good choice. The GFRP spirals help increase the concrete cover to vertical steel and can reduce the corrosion rate to less than 1/3 the rate of comparable all-steel RC columns by reducing cracking in the concrete cover, while still providing some additional strength and ductility compared to all-GFRP columns and severely corroded steel reinforced columns.

The initial cost for hybrid columns would also be lower than all-GFRP columns considering the current cost of GFRP reinforcement. Another option is to use all-steel reinforcement, and if corrosion becomes a concern to rehabilitate the columns with CFRP wraps. This option has found wide acceptance in many areas of the world. The rehabilitated columns in this research had more than twice the ultimate axial strength and four times the ultimate axial strain before failure than the non-corroded control specimens.

Columns with all-GFRP reinforcement provide assurance that no corrosion will occur, and thus may be good for extreme corrosion environments, but they should not be used in areas where seismic loads are a concern.

5. Neglecting the contribution of the steel spiral when calculating the axial strength was found to underestimate the axial compressive strength and overestimate the ultimate axial strain. The ACI 440 method and the M-P Model more accurately predicted the actual specimen capacities and results when modified to account for additional confinement provided by the steel spiral. Despite accounting for the contribution of the steel spiral, the design oriented ACI 440 Method was still conservative and in all cases under-predicted actual capacities. It is possible that these models could also be used to predict the capacity of a corroded column

wrapped or unwrapped if the amount of effective steel spiral loss could be determined or estimated.

5.2 Full-scale columns with CFRP jackets

Two full-scale columns 12 ft tall and 3 ft in diameter were tested; they were in service for forty years, nine of which were after being rehabilitated with CFRP jackets. The two columns were tested in axial compression for evaluating the FRP to concrete bond strength. From these tests the following conclusions can be drawn regarding CFRP bond and corrosion effects on CFRP rehabilitated columns under field conditions:

1. The CFRP jacket was not effectively bonded to non-grouted regions at the time of testing as shown by failure in the adhesive applied to the columns instead of failure of concrete during adhesion tests. This was likely due to an installation related issue, or the effects of several years of exposure to the weather and moisture.

   In terms of pull out strength, no significant difference was observed between grouted and non-grouted regions. However, in most cases grout was removed when adhesion tests were performed instead of the adhesive failing. This could mean there was better adhesion of the CFRP jacket in grouted regions, or that the grout was weaker in tension than the original concrete.

2. A small amount of corrosion continued to occur in the column reinforcement and as a result it prestressed the CFRP jacket. This was made evident when cutting the CFRP jacket of the full scale columns. The CFRP composite began to burst open once the majority of the outer fibers were cut. This behavior can be explained by the fact that a small amount of corrosion occurred after application of the carbon fiber jacket.

The volumetric expansion of the rusting steel reinforcement in this area induced a prestressing force in the jacket prior to testing, and delaminated some of the repair grout from the original concrete. Once the CFRP jacket was cut, the prestressing force was released and allowed the repair grout to pull away from the original concrete causing cracks. The effect of prestressing the CFRP jacket would be similar to using expansive grout in CFRP jacket applications. Therefore, a small amount of corrosion after application is not a particular concern.

The rehabilitated columns performed well under a 2,000 kip axial load in both the concentric and eccentric tests and no delamination or failure in the jackets occurred until the jackets were manually cut and retested. After the jacket was manually cut it began to delaminate when loaded to 2,000 kips concentrically and continued to delaminate more as the eccentricity was increased. This shows that the previous tests, before the jacket was cut, significantly engaged the jacket and the jackets did not fail.

THIS PAGE INTENTIONALLY LEFT BLANK

6.0 RECOMMENDATIONS AND IMPLEMENTATION

The present study evaluated both corroded and non-corroded reinforced concrete (RC) columns in axial compression. Carbon fiber reinforced polymer (CFRP) jackets were shown to successfully rehabilitate severely corroded steel RC columns subjected to axial compression by doubling the compressive strength and quadrupling the axial strain at peak load of the non-corroded control specimens. Two bridge columns that were in service for over forty years, with nine of those years rehabilitated with CFRP jackets, were tested to evaluate bond performance under 2,000 kip concentric and eccentric loads. It was found that the bond was maintained and that the CFRP jacket performed as intended when the substrate had been the original concrete. It is therefore recommended that CFRP jackets can be used to rehabilitate corrosion damaged or even severely corroded columns. Appropriate caution should be used to ensure that all the loose material is removed before actual implementation of the CFRP jacket.

Other RC columns with internal reinforcing including hybrid, which is a combination of vertical steel with a GFRP spiral, and all-GFRP reinforced columns were also studied. An evaluation of the corrosion rates showed that the hybrid RC specimens corroded at less than 1/3 the rate of the all-steel RC specimens. The hybrid columns subjected to corrosion had less than half the amount of corrosion, in terms of percent steel loss, as the all-steel reinforced columns. The hybrid RC specimens subjected to corrosion also had approximately double the axial strain at peak load of the corroded all-steel RC specimens and showed more ductility after peak load. It is clear that in applications where corrosion is possible, hybrid reinforcement using steel vertical bars and GFRP spirals may be a good choice for possible implementation.

THIS PAGE INTENTIONALLY LEFT BLANK

APPENDIX

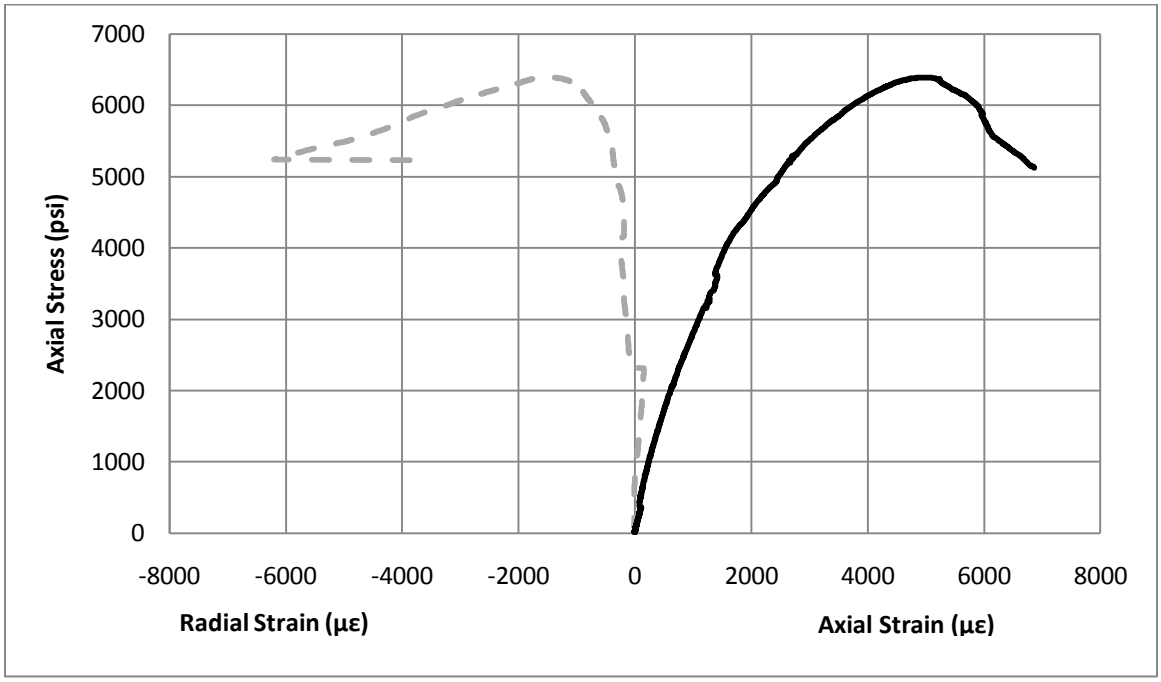

Figure A.1: #2SCTL axial stress versus radial and axial strain

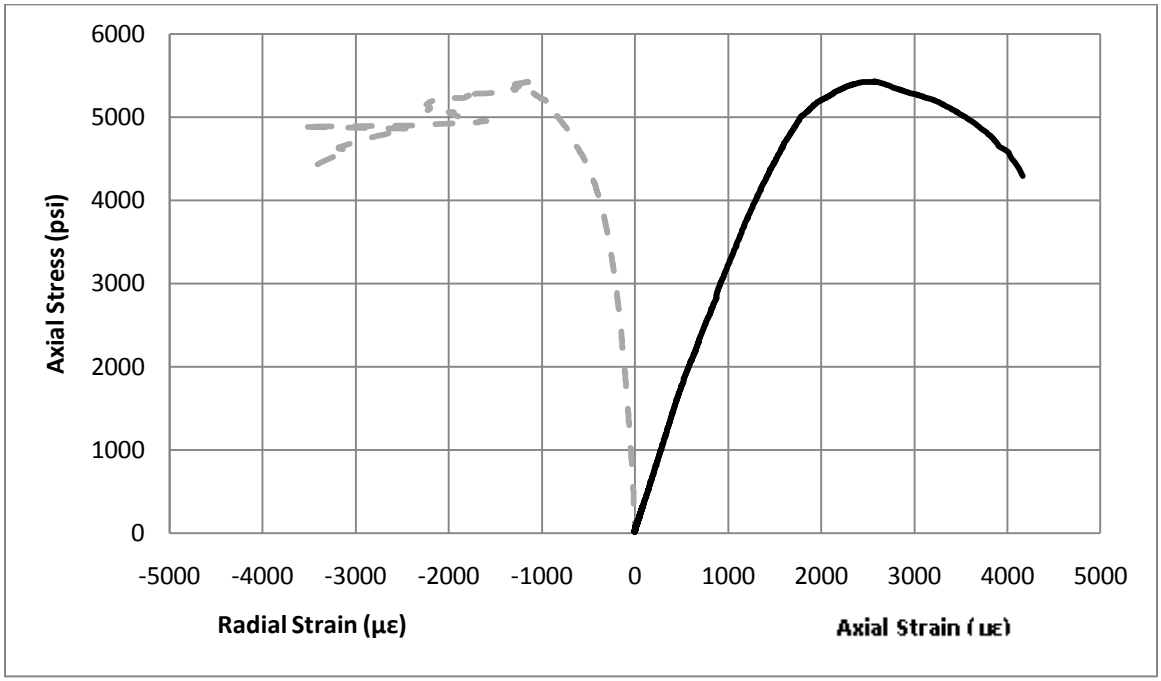

Figure A.2: #9HYBCTL axial stress versus radial and axial strain

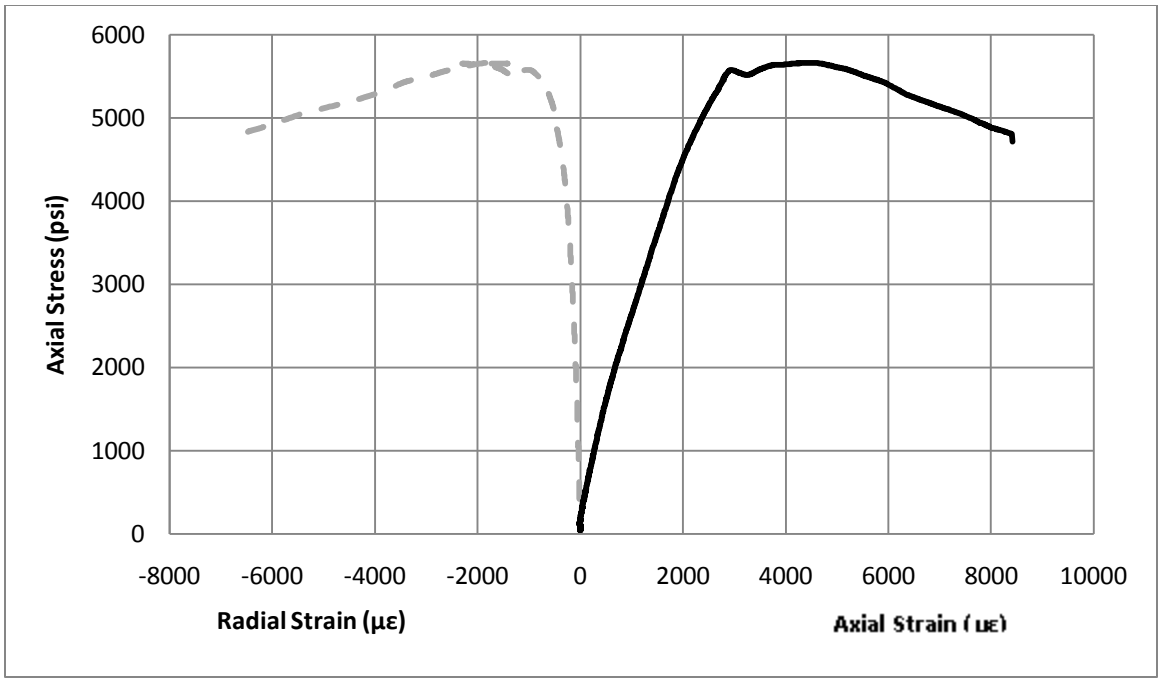

Figure A.3: #10HYBCTL axial stress versus radial and axial strain

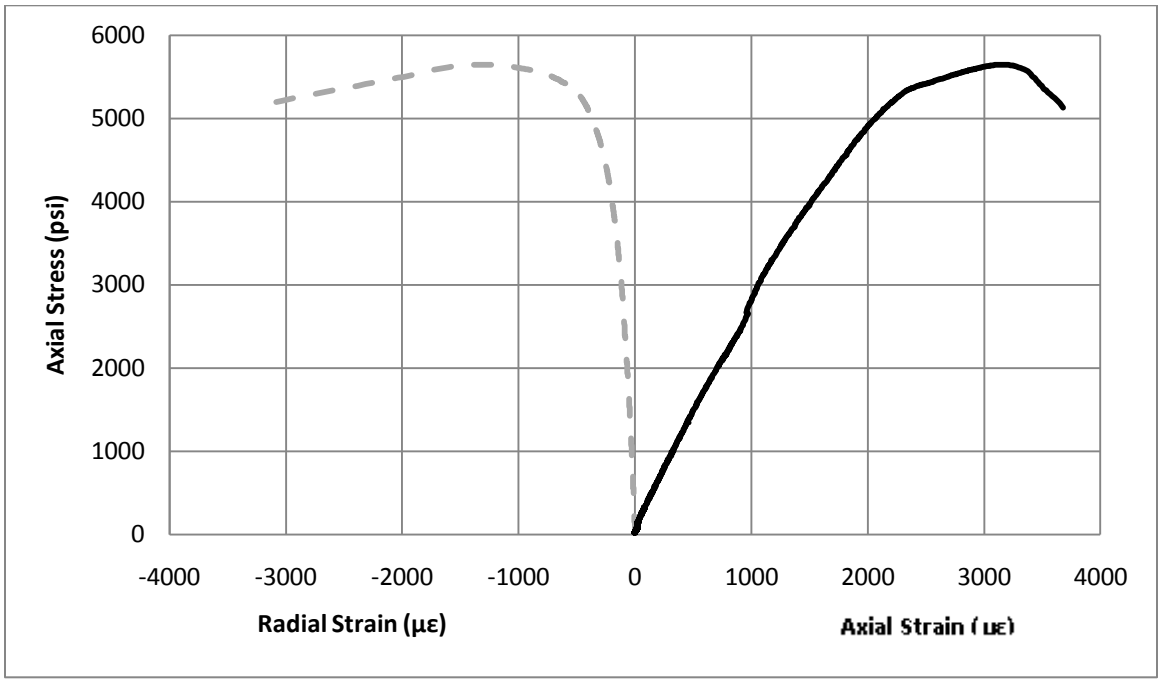

Figure A.4: #13GLCTL axial stress versus radial and axial strain

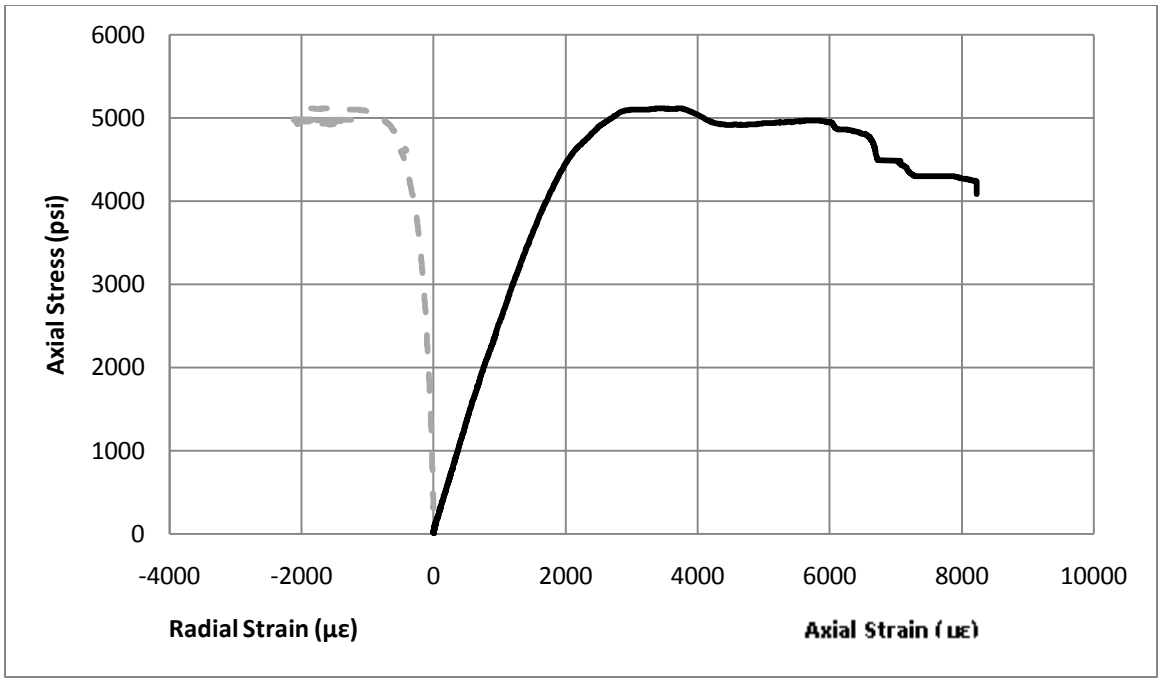

Figure A.5: #14GLCTL axial stress versus radial and axial strain

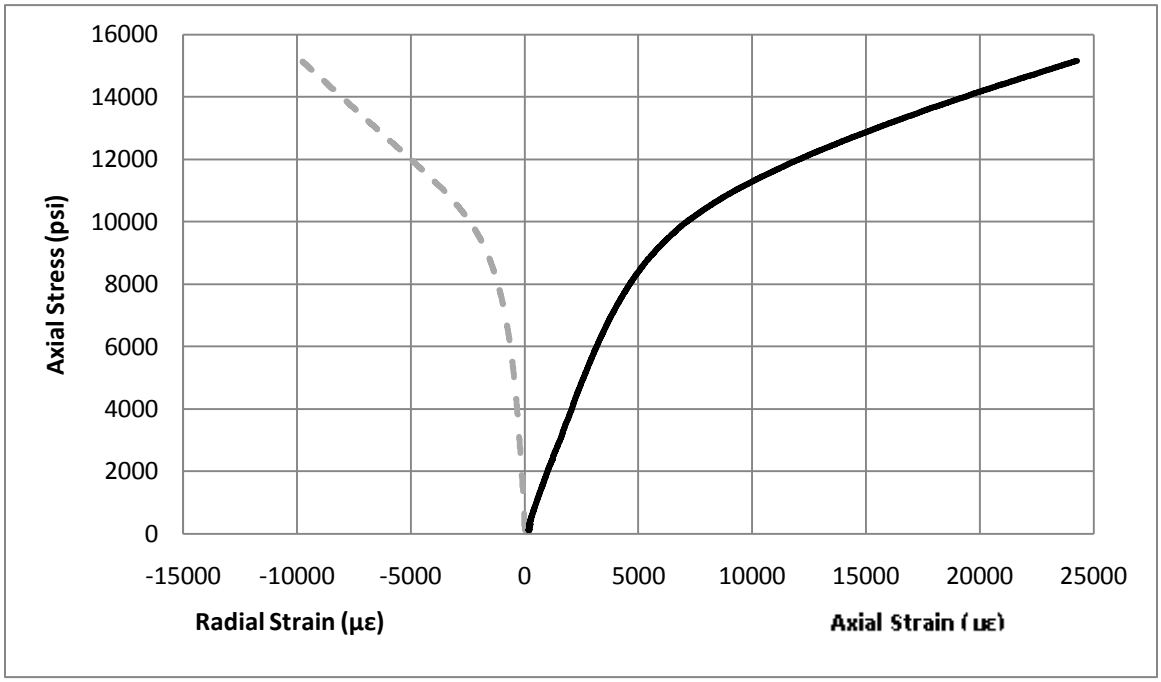

Figure A.6: #5SCORWR axial stress versus radial and axial strain

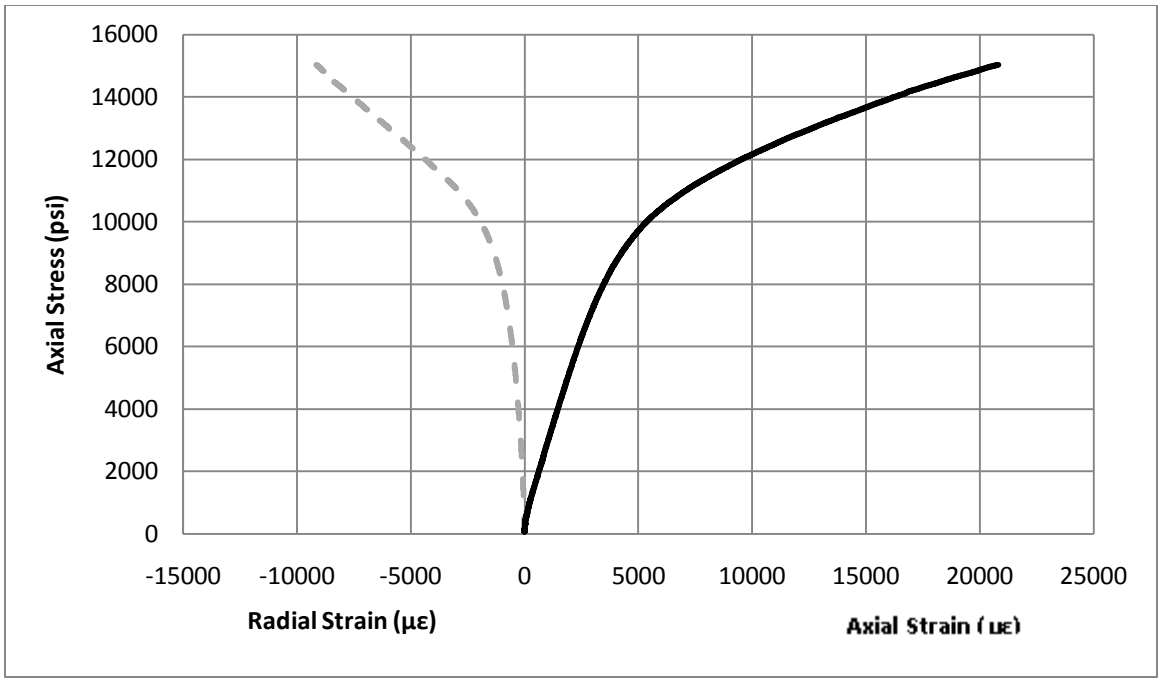

Figure A.7: #6SCORWR axial stress versus radial and axial strain

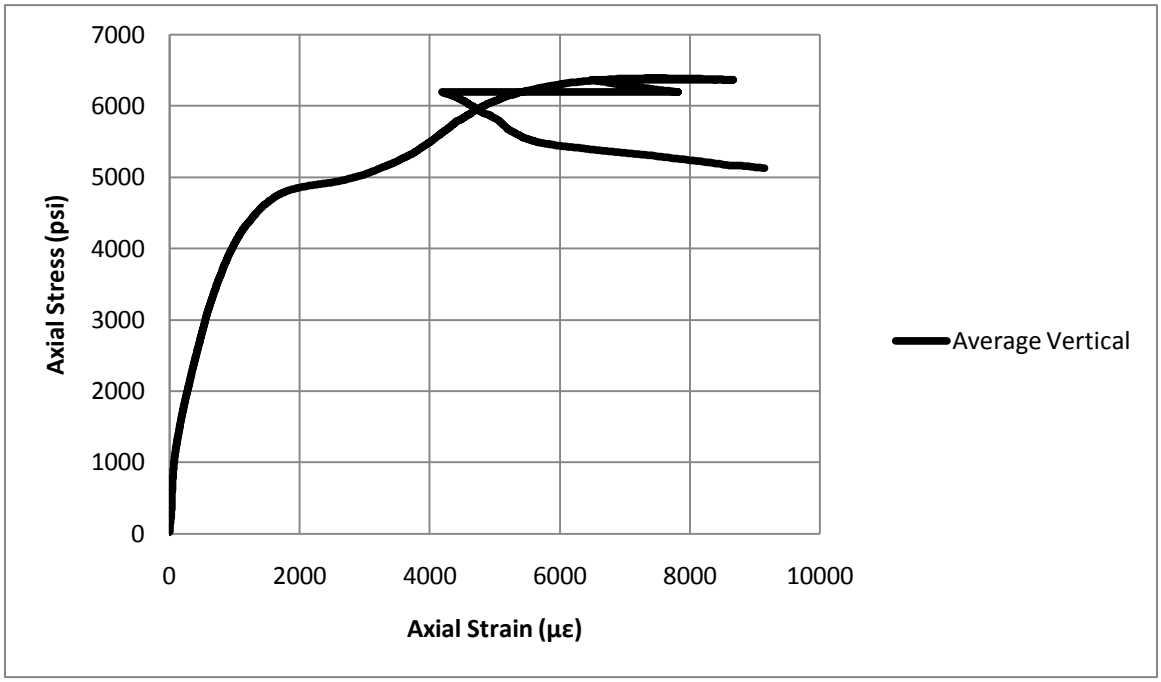

Figure A.8: #2SCTL axial stress versus axial strain in vertical bars

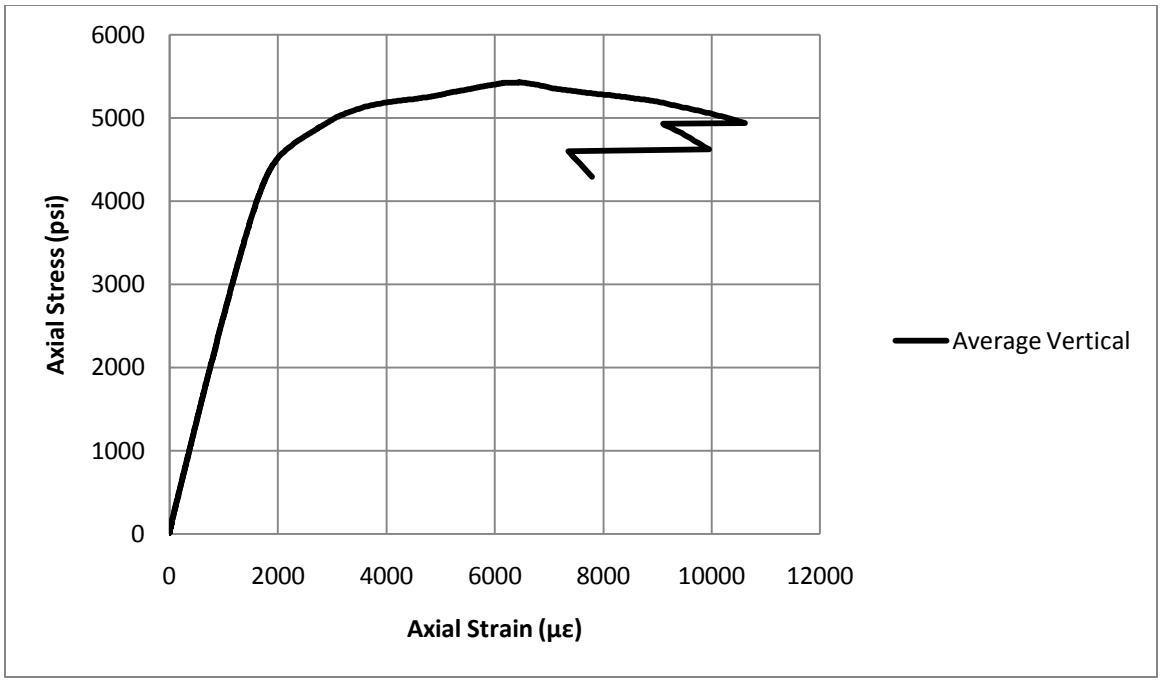

Figure A.9: #9HYBCTL axial stress versus axial strain in vertical bars

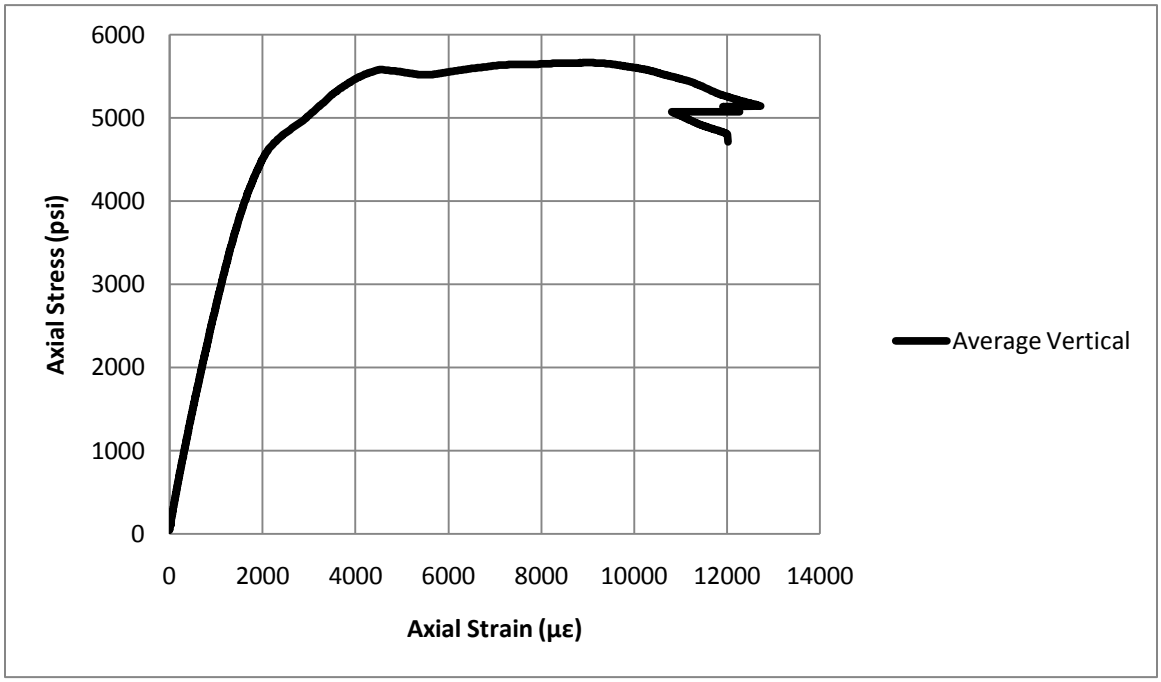

Figure A.10: #10HYBCTL axial stress versus axial strain in vertical bars

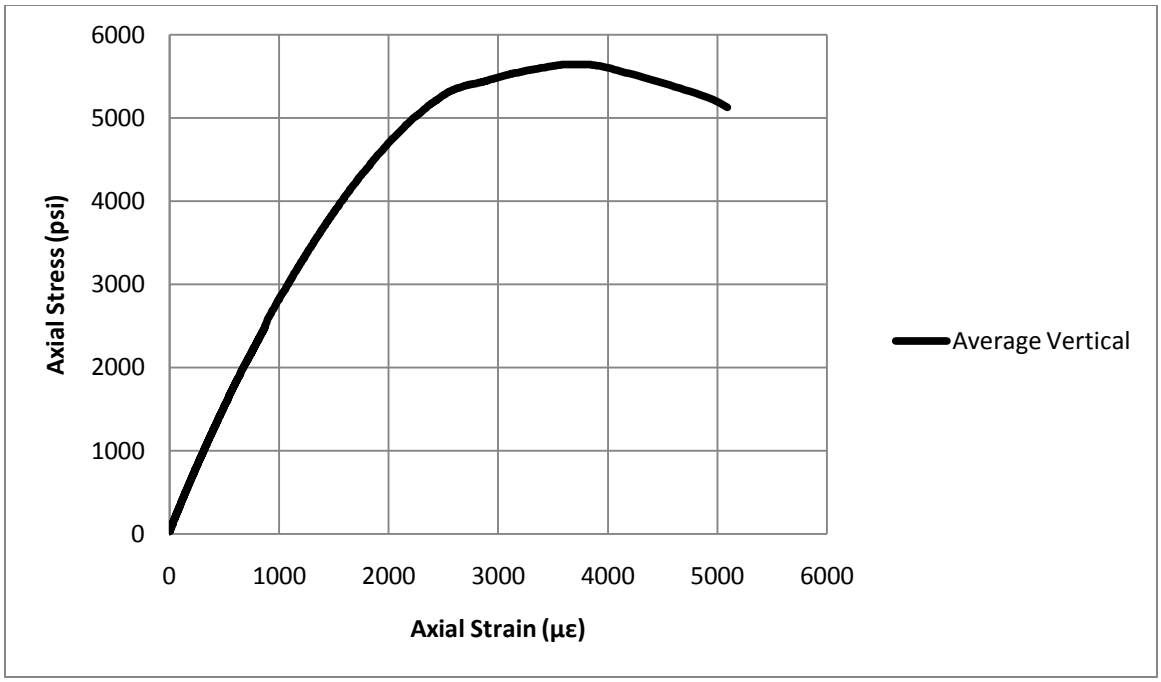

Figure A.11: #13GLCTL axial stress versus axial strain in vertical bars

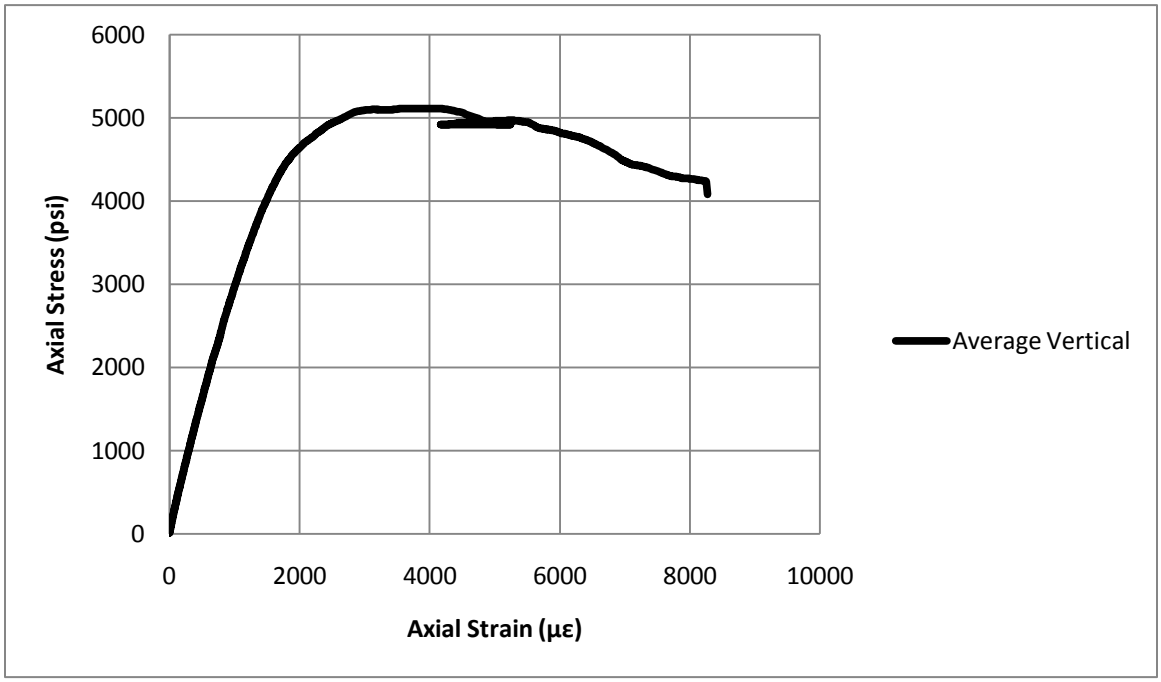

Figure A.12: #14GLCTL axial stress versus axial strain in vertical bars

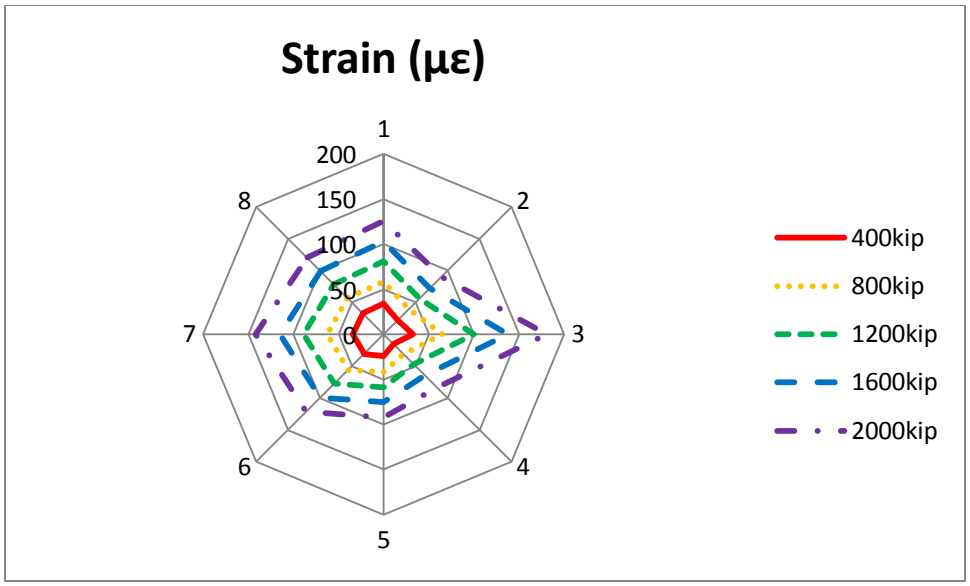

Figure A.13: LG1 radial strain for concentric test

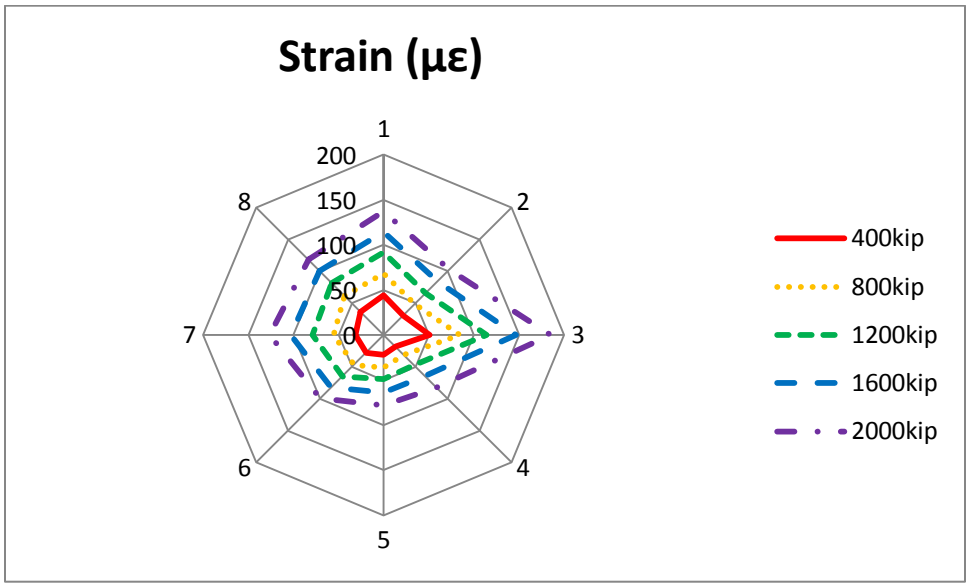

Figure A.14: LG1 radial strain eccentric 1 test

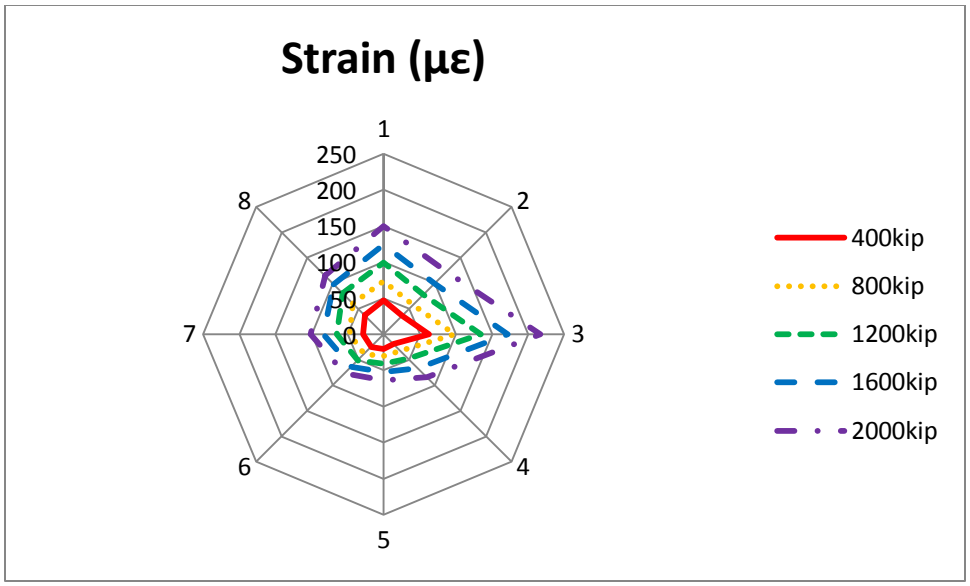

Figure A.15: LG1 radial strain eccentric 2 test

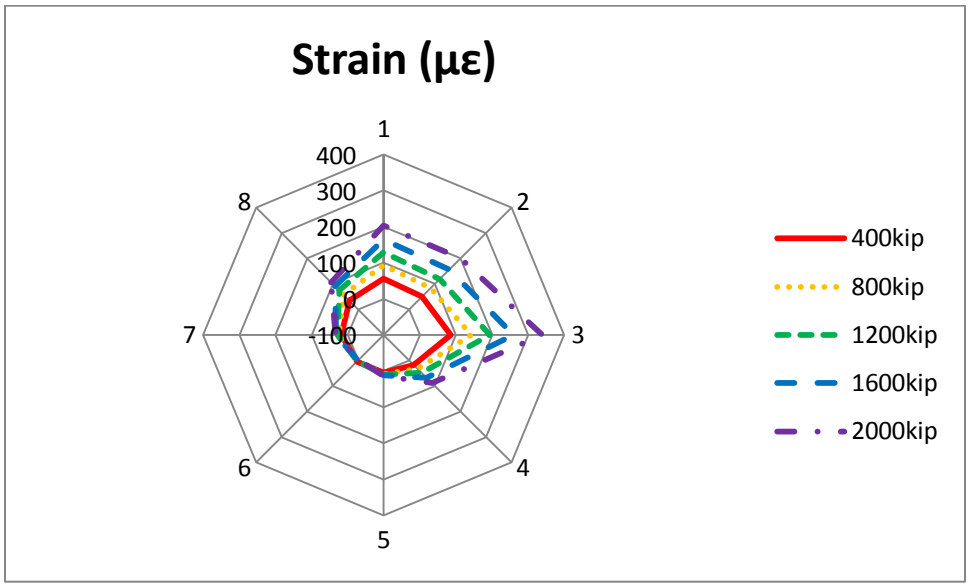

Figure A.16: LG1 radial strain eccentric 3 test

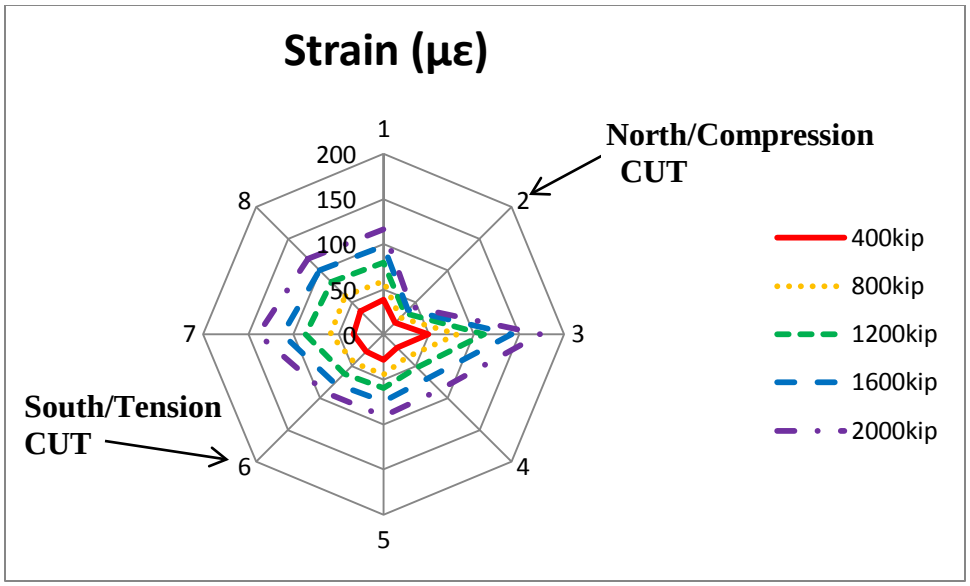

Figure A.17: LG1 radial strain cut concentric test

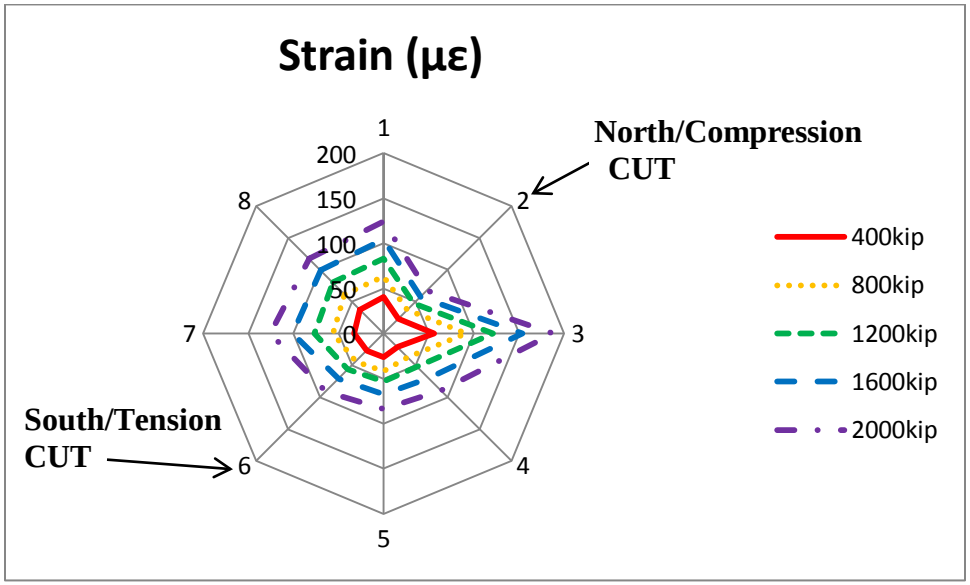

Figure A.18: LG1 radial strain cut eccentric 1 test

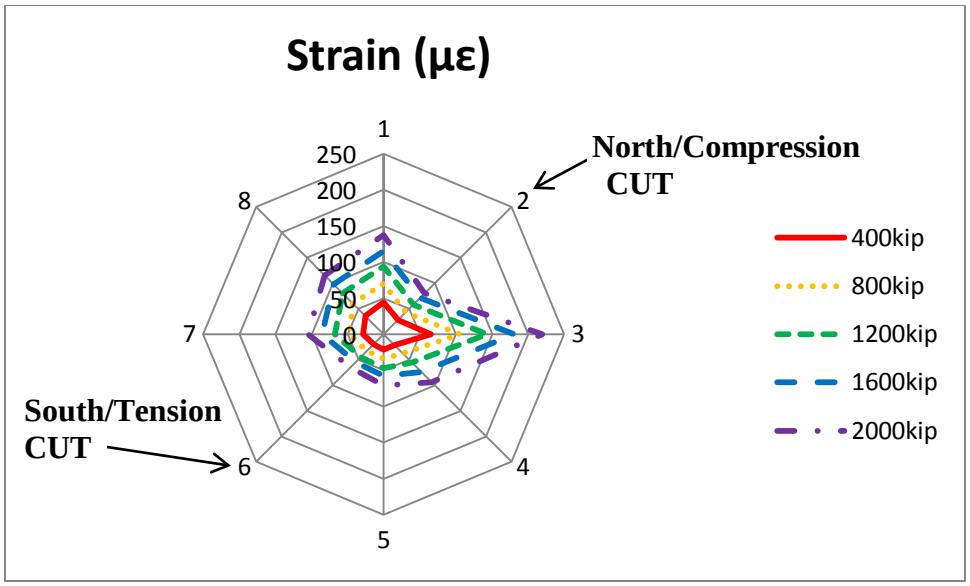

Figure A.19: LG1 radial strain cut eccentric 2 test

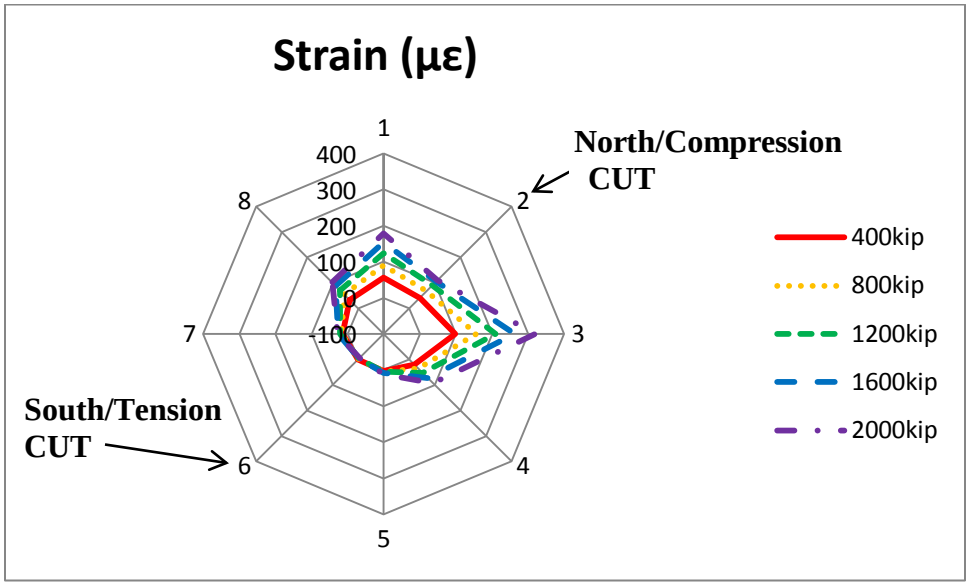

Figure A.20: LG1 radial strain cut eccentric 3 test

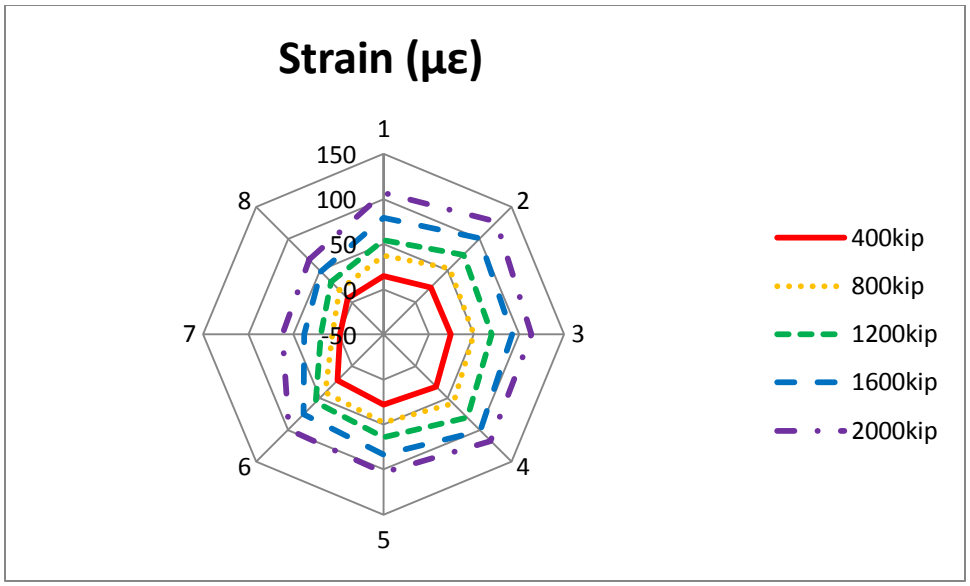

Figure A.21: LG2 radial strain concentric test

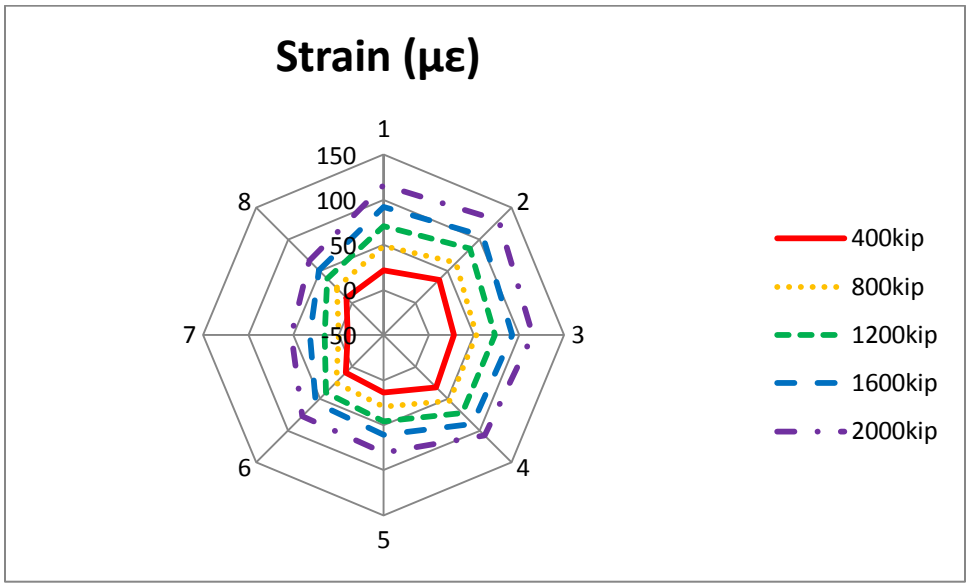

Figure A.22: LG2 radial strain eccentric 1 test

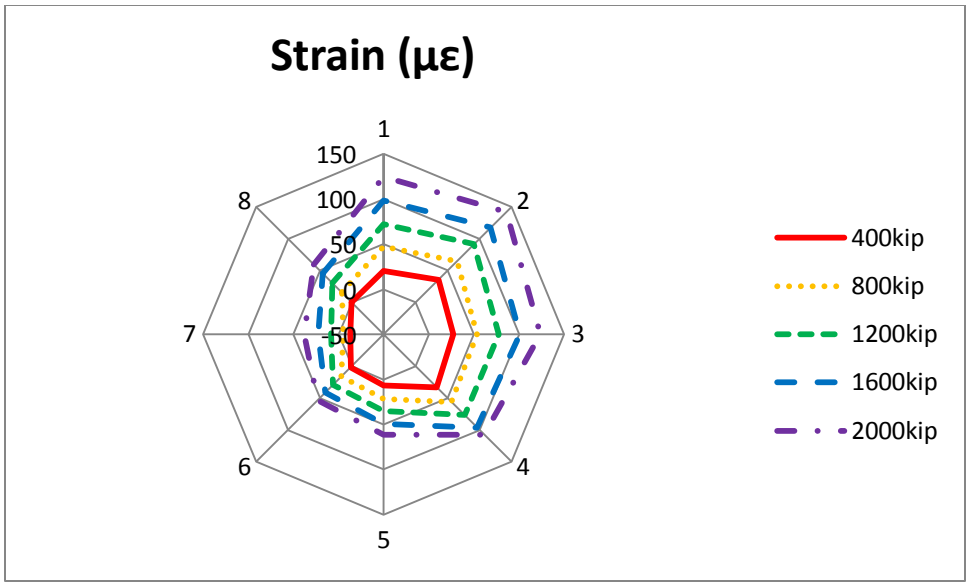

Figure A.23: LG2 radial strain eccentric 2 test

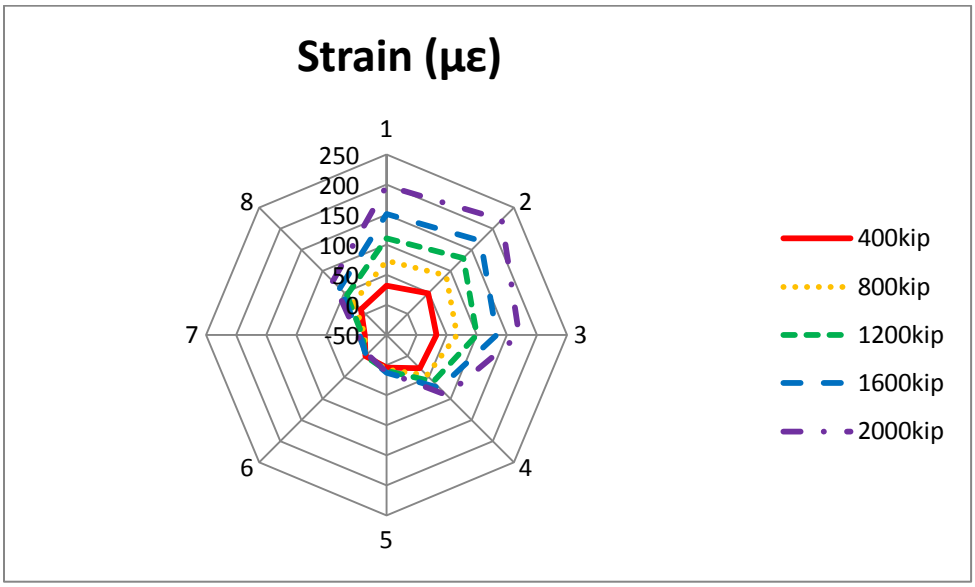

Figure A.24: LG2 radial strain eccentric 3 test

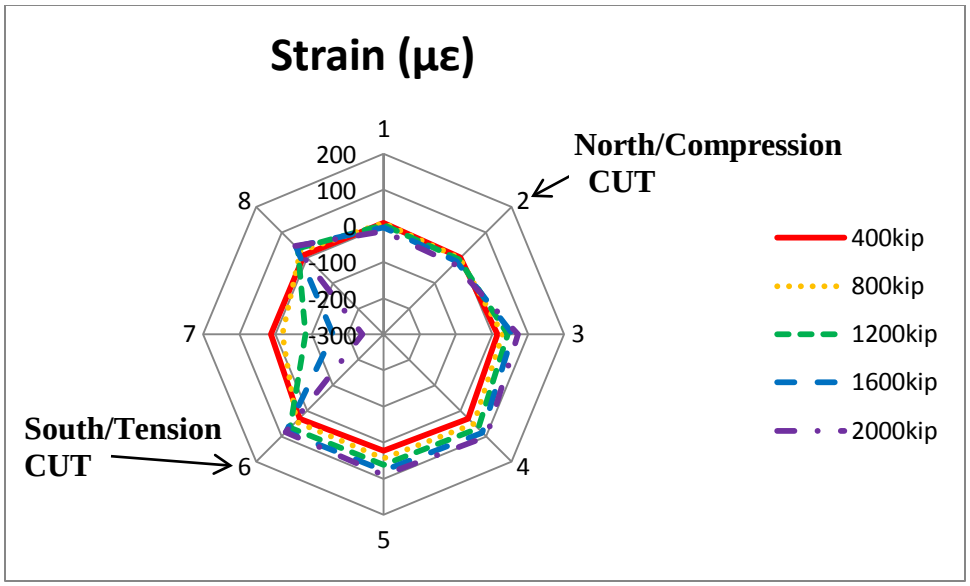

Figure A.25: LG2 radial strain cut concentric test

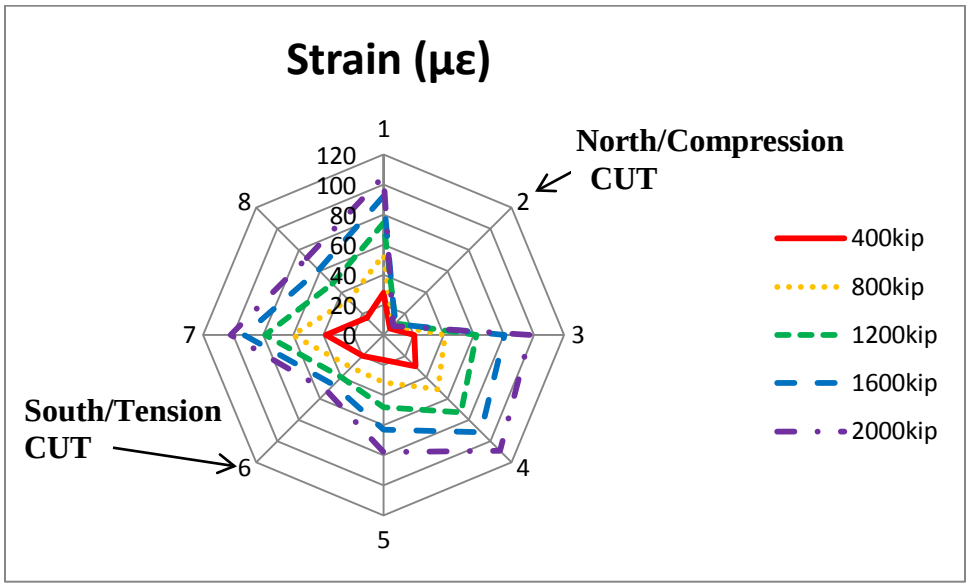

Figure A.26: LG2 radial strain cut eccentric 1 test

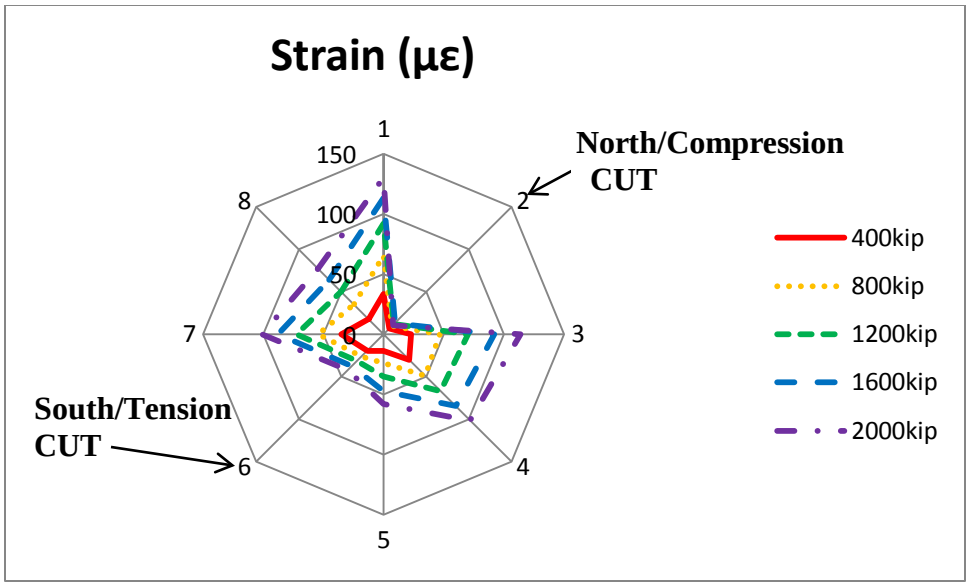

Figure A.27: LG2 radial strain cut eccentric 2 test

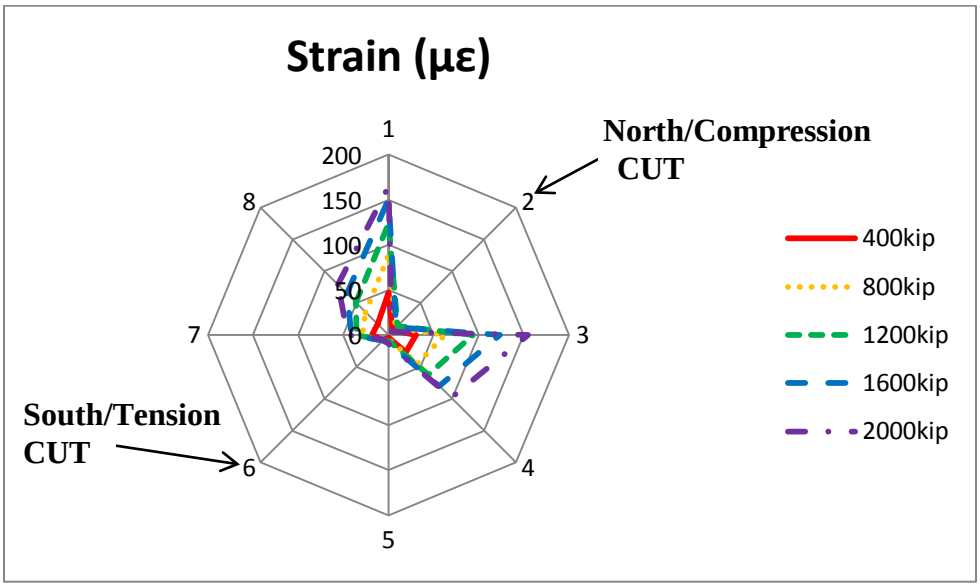

Figure A.28: LG2 radial strain cut eccentric 3 test

THIS PAGE INTENTIONALLY LEFT BLANK

REFERENCES

American Concrete Institute. (2008). *ACI 440.2R-08 Guide for the Design and Construction of Externally Bonded FRP Systems for Strengthening Concrete Structures.* Farmington Hills: American Concrete Institute.

Bae, S. W., and Belarbi, A. (2009). Effects of Corrosion of Steel Reinforcement on RC Columns Wrapped with FRP Sheets. *Journal of Performance of Constructed Facilities, 23*(1), 20-31.

Choo, C. C., Harik, I. E., and Gesund, H. (2006a). Minimum reinforcement ratio for fiber-reinforced polymer reinforced concrete rectangular columns. *Aci Structural Journal, 103*(3), 460-466.

Choo, C. C., Harik, I. E., and Gesund, H. (2006b). Strength of rectangular concrete columns reinforced with fiber-reinforced polymer bars. *Aci Structural Journal, 103*(3), 452-459.

Deitz, D. H., Hark, I. E., and Gesund, H. (2003). Physical properties of glass fiber reinforced polymer rebars in compression. *Journal of Composites for Construction, 7*(4), 363-366.

Lotfy, E. M. (2006). *Theoretical Analysis of Reinforced Concrete columns with GFRP Bars.*

Luca, A. D., Matta, F., and Nanni, A. (2010). Behavior of Full-Scale Glass Fiber-Reinforced Polymer Reinforced Concrete Columns Under Axial Load. *Aci Structural Journal, 107(5),* 589-596.

Mander, J. B., Priestley, M. J. N., and Park, R. (1988) "Theoretical Stress-Strain Model for Confined Concrete," *Journal of the Structural Division, ASCE,* Vol 114, No. 8, pp. 1804-1826.

Moran, D. A. and Pantelides, C. P. (2002). “Stress-strain model for fiber-reinforced polymer-confined concrete.” *J. Compos. Constr.,* 6(4), 233–240.

Pantazopoulou, S. J., Bonacci, J. F., Sheikh, S., Thomas, M. D. A., and Hearn, N. (2001). Repair of corrosion-damaged columns with FRP wraps. *Journal of Composites for Construction, 5*(1), 3-11.

Ranger, M., and Bisby, L. (2007). Effects of Load Eccentricities on Circular FRP-Confined Reinforced Concrete Columns. [Unknown].

Tastani, S. P., and Pantazopoulou, S. J. (2004). Experimental evaluation of FRP jackets in upgrading RC corroded columns with substandard detailing. *Engineering Structures*, *26*(6), 817-829.